2000

The Design and Construction of Novel Near -Infrared Time -Correlated Single Photon Counting Devices for the Identification of Analytes in Multiplexed Applications.

Emanuel Austin Waddell Jr
Louisiana State University and Agricultural & Mechanical College

INFORMATION TO USERS

This manuscript has been reproduced from the microfilm master. UMI films the text directly from the original or copy submitted. Thus, some thesis and dissertation copies are in typewriter face, while others may be from any type of computer printer.

The quality of this reproduction is dependent upon the quality of the copy submitted. Broken or indistinct print, colored or poor quality illustrations and photographs, print bleedthrough, substandard margins, and improper alignment can adversely affect reproduction.

In the unlikely event that the author did not send UMI a complete manuscript and there are missing pages, these will be noted. Also, if unauthorized copyright material had to be removed, a note will indicate the deletion.

Oversize materials (e.g., maps, drawings, charts) are reproduced by sectioning the original, beginning at the upper left-hand corner and continuing from left to right in equal sections with small overlaps.

Photographs included in the original manuscript have been reproduced xerographically in this copy. Higher quality 6" x 9" black and white photographic prints are available for any photographs or illustrations appearing in this copy for an additional charge. Contact UMI directly to order.

Bell & Howell Information and Learning
300 North Zeeb Road, Ann Arbor, MI 48106-1346 USA
800-521-0600

UMI®

THE DESIGN AND CONSTRUCTION OF NOVEL NEAR-INFRARED TIME-CORRELATED SINGLE PHOTON COUNTING DEVICES FOR THE IDENTIFICATION OF ANALYTES IN MULTIPLEXED APPLICATIONS

A Dissertation

Submitted to the Graduate Faculty of the
Louisiana State University and
Agricultural and Mechanical College
in partial fulfillment of the
requirements for the degree of
Doctor of Philosophy

in

The Department of Chemistry

by
Emanuel Austin Waddell, Jr,
I.B.S., Morehouse College, 1991
M.S., University of Rochester, 1995
August, 2000

Epigraph

To every *thing there is* a season, and a time to every purpose under heaven:

A time to be born, and a time to die; a time to plant, and a time to pluck up *that which is* planted;

A time to kill, and a time to heal; a time to break down, and a time to build up;

A time to weep, and a time to laugh; a time to mourn, and a time to dance;

A time to cast away stones, and a time to gather stones together; a time to embrace, and a time to refrain from embracing;

A time to get, and a time to lose; a time to keep, and a time to cast away;

A time to rend, and a time to sew; a time to keep silence, and a time to speak;

A time to love, and a time to hate; a time of ware, and a time of peace.

Ecclesiastes 3: 1-8

Acknowledgements

God has allowed me to arrive at this point of my academic career—be it deserved or undeserved. He has also given me the opportunity to interact with individuals who have enhanced my life in positive ways—regardless of whether I realized it at the time or not. It is somewhat overwhelming to remember all that the Lord has done for me and who he has blessed me with; so with all sincerity, love, appreciation, and gratitude I acknowledge the people who have gotten me to this point.

Thanks to "the Tribe" for putting up with me and keeping me honest. Thanks to Karol for carrying and bearing Austin, Khalil, and Kendyl and loving and supporting me in between. Thanks to "the Boys" for forcing me to create simple, correct answers for complex questions. Thanks to my mom-Evelyn Bedjane-- for instilling the spirit of curiosity in me. Thank you to my sister--Michelle Waddell—for pushing me, I'm always afraid you're going to catch up! Thanks to dad—"Buck" Waddell—for giving me the confidence to succeed. Much thanks to members of the extended family: Williamenia, Hamid, Marva, Sid, Keith, the Grahams, the Ramseys, and Dundee's Mom (Mary). "It's a family affair."

Professional Kudos and thanks to Dr. Steve "What time is it?" Soper for allowing me to join his research group and for demonstrating faith in me when no one else would. Thanks to Yolanda "See you in Gaithersburg!" Davidson, James Flanagan, Ben Legendre, and Daryl Williams for laying the path for me. Thanks to Sean "Anne" Ford, Suzanne "be back at six o'clock" Lassiter, Clyde "the NBA" Owens, Scott "don't send those people over here" McWhorter, Daniel "the chip has a leak in it" Qi, Wieslaw "just a few more minutes" Stryjewski, and Yichaun "I don't understand" Xu for

assisting me throughout. Special thanks to the National Institute of Health and FMC Corporation for financial support of this work. "This is DNA sequencing, not rocket science!"

"Shout outs" to Ken Brown, Derrick Butler, Jimmie Davis, Jesse Edwards, Kenneth Grimes, Ivan Guillory, David Jarmon, Damon Phillips, Keith Ramsey, Deric Scott, Victor Vandell, Dundee Wilson, and the countless other brothers who are "working it out". You guys force me to excel. Keep the faith. "Every brotha' man's life is like swingin' a dice right?"

I would be remiss not to thank Fayetteville St. Elementary School for laying an academic foundation that continues to propel me forward. Thanks, Dwight, David, Mark, and Courtland for the competition you gave me. I must give a special thanks to the North Carolina School of Science and Mathematics for challenging me when it counted and giving me a flavor of what real work is. Thanks to Morehouse College for placing the bar high above my head. Thanks to Dr. Robert Dixon and David Cook for mentoring me and a special acknowledgement to Dr. Mark Mitchell, of Clark Atlanta University, who served as my first research advisor. Special thanks to Coach Willie Hill for providing a framework in which to live my life; I learned more on the track than running. "No vision and you perish, no ideal and you are lost".

Finally, without negatives, we can never really appreciate the positives. Thanks to the Pitt County North Carolina School System and the University of Rochester for teaching me resilience, determination, perseverance, humbleness, and faith. "Duress builds character."

Table of Contents

List of Tables

List of Figures

Abstract

This manuscript details the design, construction, and application of novel near infrared time correlated single photon counting devices to the identification of analytes in analytical separations. The thrust of this research is to provide a simple, low cost technique for the high-speed identification of DNA sequencing bases that are labeled with a series of unique near infrared fluorophores. These fluorophores are unique because they possess the same emission and absorption maxima, but different fluorescence lifetimes. Consequently, they allow analytes to be discriminated by fluorescence lifetime as opposed to color.

The first goal of this dissertation research was to implement a time correlated single photon counting system with the use of single mode fiber optics. Utilizing a passively mode locked Ti:Sapphire Laser, a single photon avalanche diode, single mode fiber optics and a mechanical switch a fiber optic based time correlated single photon counting device with subnanosecond resolution was constructed. The experimental results showed that group velocity dispersion was low and that it was possible to perform multiple time correlated single photon counting experiments with a limited number of excitation sources and detectors. It was determined that the average instrumental response of each channel was 181 picoseconds. The fluorescence lifetime of a near infrared dye, aluminum tetrasulfonated naphthalocyanine was determined to be 3.08 nanoseconds.

The second phase of this doctoral research involved the construction and characterization of a near infrared time correlated single photon counting scanning device. This integrated device consisted of a pulsed diode laser, single photon

avalanche diode, and a time correlated single photon counting board. The instrument response function of this system was determined to be less than 300 ps. The sensitivity and ability to discriminate between various fluorophores was determined. In addition to its application for scanning solid surfaces such as DNA microarrays, the device was utilized to detect analytes in a micro-capillary electrophoresis separation. The fluorescence lifetimes of these analytes were determined on-line.

Chapter 1

Application of Near-Infrared Time Resolved Fluorescence Detection to Problems in Analytical Chemistry

1.1 Introduction

Analytical chemistry may be defined as a method for determining the chemical composition of samples of matter.[1] A subset of analytical chemistry is the instrumental method of analysis, which involves the exploitation of the physical properties of analytes-such as conductivity, light absorption, mass-to-charge ratio, fluorescence, and other properties-to gather quantitative and/or qualitative information about systems of interest. In this dissertation, spectroscopy-specifically time-correlated single photon counting (TCSPC) spectroscopy–is the primary method of instrumental analysis. In a broad sense, spectroscopy may be defined as the interaction of electromagnetic radiation and matter, which includes the absorption and emission of light by matter, the scattering of light by matter, and the rotation of the plane of polarization of polarized light by matter.[2] However, whereas analytical spectroscopy is capable of determining the chemical composition of matter it is not capable of separating solutions into individual components. For example, vibrational, mass, magnetic, or electronic spectroscopy may be utilized to identify the components that comprise the effluent of a sample stream from an industrial plant. However, none of these methods is capable of separating the effluent into toxic and non-toxic compounds. As a result, it is necessary to employ techniques that are capable of separating mixtures into its various components.

One of these instrumental methods of analysis is capillary electrophoresis (CE), which has become a viable method for the high speed separations of analytes such as

pharmaceutical compounds[3, 4], oligonucleotides[5-8], amino acids[9] and proteins[10-12]. A CE separation is performed by using a small column and subjecting it to a high electric field as depicted in Figure 1.1. Analytes are separated as a function of their mass and charge, with smaller fragments usually migrating at a faster rate than larger fragments. Since the advent of performing electrophoresis in small, glass capillaries with interior diameters of less than 100 μm, there have been increased demands on enhancing separation speeds and efficiencies.[13] Micro-CE has recently resulted in reduced column dimensions and higher electric field strengths. Consequently, more severe limits have been placed on detection strategies.

1.2. Fluorescence Lifetime Determinations in CE

New detection strategies in CE have been developed to handle this increased demand on sensitivity and the ability to perform multiplexed-type assays. For example, the general trend in electrophoresis is to reduce the dimensions of the column, with either smaller capillaries or the development of micro-CE systems using lithographic procedures.[14-16] The direct consequences of smaller columns are improved separation efficiencies and reduced separation times. However, reductions in the dimensions of the column place severe requirements on detection, because the loading volume is reduced as well. Furthermore, in many cases multiple targets (multiplexed applications) must be detected simultaneously, further complicating the detection process. An example is DNA sequencing, where one of four different probes must be detected and identified in a single electrophoresis run.[17-21]

Laser-induced fluorescence (LIF) is the common detection strategy used in many critical CE applications due to its superior limits of detection and the rather

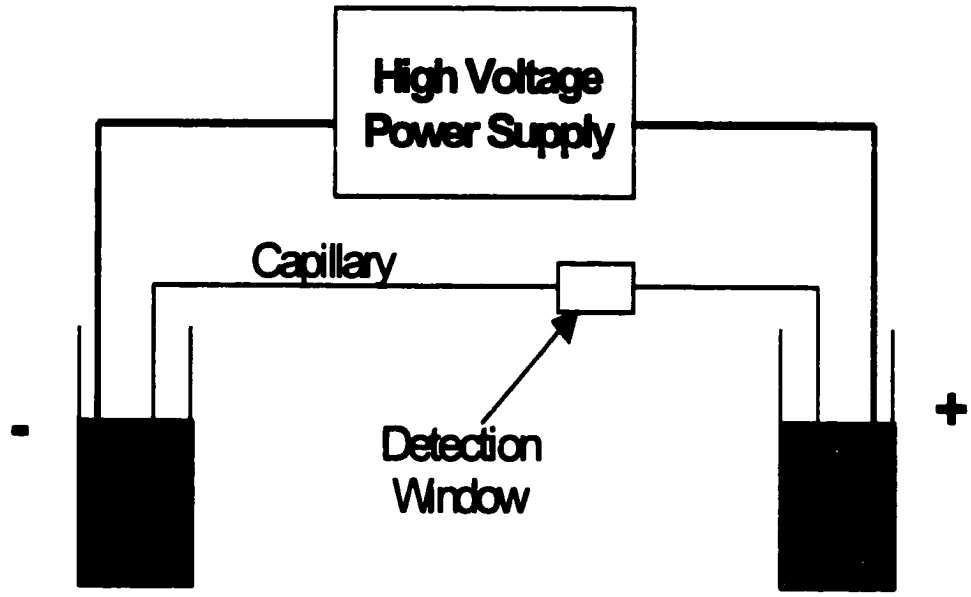

Figure 1.1. Basic Schematic of a Capillary Electrophoresis Device

simple instrumental requirements for its implementation.[22] In cases where multiple probes are used, the identification is typically carried out using spectral or wavelength discrimination. However, several groups have recently suggested the use of fluorescence lifetimes to discriminate amongst various probes in CE separations.[23-33] In fluorescence, the emission shows a time-dependent behavior, $I_f(t)$ which follows the general relation;

$$I_f(t) = \sum_{i=1}^{N} Ae^{-\frac{t}{\tau_f}}$$

where A is a pre-exponential factor which describes the percent contribution of component N to the overall decay; t is time; τ_f is the fluorescence lifetime and N is the number of components comprising the decay. The fluorescence lifetime (τ_f) is an intrinsic photophysical parameter of chromophores that measures the averaged time a chromophore resides in the excited state.

The fluorescence lifetime can be measured using either time-resolved or frequency-resolved techniques. In frequency-resolved methods, the excitation light is sinusoidally modulated, producing emission that is also sinusoidally modulated. The emission experiences a phase-shift with respect to the excitation and the magnitude of the shift is directly related to the lifetime of the chromophore. In the case of time-resolved fluorescence, the chromophore is excited using a light source that is pulsed with a time duration much shorter than the fluorescence lifetime being measured. Once excited, the time difference between excitation and emission is measured for single photons. The events are placed in appropriate time-bins and a resulting decay profile is constructed from which the lifetime can be extracted.

The measurement of fluorescence lifetimes on-line in analytical separations has made significant progress over the past few years, primarily due to advances in instrumentation. Two of these advances are the development of inexpensive excitation sources and improvements in detectors appropriate for lifetime measurements. Most time-resolved fluorescence measurements have been performed in the visible region of the electromagnetic spectrum (400 - 700 nm). This is due to a number of factors including, the commercial availability of light sources appropriate for time-resolved fluorescence applications in the visible, a wide selection of functional fluorophores that demonstrate excitation/emission in the visible wavelength range, and photon transducers that possess high quantum yields below 800 nm.

One of the first demonstrations of time-resolved fluorescence detection in CE applications was the work of Lytle and co-workers.[34] In this work, a "ratiogram" was constructed, in which the analyte was excited with a nanosecond pulsed nitrogen laser and the fluorescence emission monitored at two different times within the decay profile. This process allowed the removal of background photons from the measured signal, significantly improving the signal-to-noise ratio. One of the primary advantages to using time-resolved fluorescence is the potential improvement in the signal-to-noise ratio (SNR) during the separation. This is accomplished by discriminating against scattering photons or interferences with short lifetimes. In the analysis of a biological sample, time filtering was used to discriminate against short-lived interferences in CE.[35, 36]

The monitoring and identification of multiple dyes by lifetime discrimination during CE also allows for improved identification efficiency when compared to that of

spectral wavelength discrimination. For example, in DNA sequencing, the identity of a terminal nucleotide base during a separation can be accomplished by monitoring differences in spectral emission wavelengths associated with the fluorescent probes.[21] However, this identification method produces errors in the base call because of broad, overlapping emission profiles, which results in cross talk between detection channels. Lifetime discrimination, in which the nucleotide base is identified by monitoring the fluorescence lifetime of each fluorescent probe, can eliminate the problem of cross talk between detection channels.[27]

Several other advantages are associated with determining the fluorescence lifetimes of components in CE. These advantages include:[27]

(1) the calculated lifetime is relatively immune to concentration differences;

(2) the fluorescence lifetime can be determined with higher precision than fluorescence intensities;

(3) only one excitation source is required to efficiently excite the fluorescent probes and only one detection channel is needed to process the fluorescence for appropriately selected dyes.

However, several difficulties are associated with lifetime measurements in CE applications. The most serious is the poor photon statistics (limited number of photocounts) associated with the measurement. When the photon statistics are poor, the precision in the determination is reduced, adding error to the identification process. This results from the need to make a dynamic measurement (the chromophore is migrating through the excitation beam) and the low mass loading levels associated with CE. For example, consider a CE separation where the loading level of a 1 nM solution

is 1 nL. As a result, one attomole (1×10^{-18}) of molecules will be injected into the column. This is compounded by the detection volume, which may be less than 10 fL, making the detection efficiency (defined as the fraction of the analyte molecules that are sampled) as low as 0.01% when the electrophoretic separation is performed in 75-100 μm inner diameter capillaries. Now, consider the photophysical characteristics of a near-infrared (NIR) dye such as tetra-sulfonated aluminum 2, 3-naphthalocyanine that has a fluorescence quantum yield (Φ_f) of 0.34 and a molar absorption coefficient (ε) of 300,000 cm^{-1} M^{-1} (at 780 nm).[37] If such a molecule is injected into a column of 75 μm diameter and interrogated with a 5 mW-780 nm beam 5 μm in diameter- it will fluoresce at a rate (k_f) of 1.14×10^8 photons/sec. This is given by the relation;

$$k_f = \frac{3.8 \times 10^{-21} \varepsilon P}{\pi \omega^2}$$

where P is the power of the laser (photons/sec) and ω is the radius of the beam. Assuming an overall sampling efficiency of 0.01%, one will detect 1.14×10^4 photons/sec. However, this number is further degraded if one considers that the analyte is moving through the detection volume. The residence time in the beam may be less than a second. If a molecule is migrating at a rate of 100 μm per second, it remains in the excitation beam for 30 ms, resulting in a total fluorescence yield of 342 photons. Fortunately, there exist simple, non-intensive, computational techniques for the determination of fluorescence lifetimes on-line for cases where the photon statistics are poor.

Another potential problem that can surface when attempting to measure lifetimes in CE is the background, resulting from either impurity fluorescence or

scattering, which can degrade measurement precision, especially when the loading level of dye is low. These background problems can be particularly troublesome when monitoring fluorescence in the visible region of the spectrum. The sources of background may be chromophores that are an intrinsic part of the sample matrix and fluoresce upon excitation or Raman scattering from the matrix. To alleviate these problems, implementation of NIR fluorescence is very attractive because these background sources can be significantly reduced.[26]

Due to the increased availability of NIR diode lasers that can be operated in a pulsed mode as well as the development of efficient photon detectors that have a reasonable timing response and high single photon detection efficiency in the NIR, there has been increased interest in on-line fluorescence lifetime measurements for CE. Besides instrumental considerations, other advantages are associated with NIR fluorescence, the most important of which is the lower background level compared to visible fluorescence. This is because the scattering cross sections are reduced and fewer materials show intrinsic fluorescence in the NIR as compared to the visible. For example, there are a limited number of compounds which fluoresce in the NIR and Raman scattering cross sections are inversely dependent on the fourth power of the wavelength ($1/\lambda^4$); thus as the wavelength increases the Raman cross section decreases.

The first reported use of lifetime identification methods in CE was reported by Soper and co-workers, in which a conventional TCSPC instrument with a Ti:Sapphire laser system was used to acquire lifetimes on-line during the free solution separation of NIR fluorescent dyes.[26] The cationic (DTTCI, HITCI, IR-140, and IR-132) and anionic (IR-144 and IR-125) dyes were separated in a running buffer consisting of 95%

methanol and 5% triply distilled water set at a pH of 9.5. The inclusion of methanol was important to improve the fluorescence properties of the NIR dyes. Lifetimes were determined via the maximum likelihood estimator (MLE) method from decay profiles constructed over each electrophoretic band shown in Figure 1.2.[26] It was determined that the migration order, as determined by fluorescence lifetimes, agreed with the migration order evaluated from individual electrophoretic mobilities. Additionally the effects of neighboring components and background on the lifetime calculation were investigated. The inclusion of background and scattered photons into the calculation resulted in lifetimes biased towards shorter values. An inherent disadvantage of the MLE or rapid lifetime determination (RLD) techniques becomes evident with the inclusion of neighboring components (i.e., poorly resolved) into the calculation—the calculated value becomes a weighted average of the various components that constitute the decay.

One of the major applications for time-resolved fluorescence in CE has been in the area of DNA sequencing. Fluorescence identification of terminal bases used in traditional Sanger DNA sequencing strategies with capillary gel electrophoresis has been carried out using spectral discrimination by developing dyes with unique emission maxima. Lifetime discrimination offers some potentially unique advantages, including: (1) the elimination of cross talk between detection channels. In spectral discrimination techniques, the emission profiles of the fluorophore set are typically broad and therefore, spectral leakage on the four detection channels occurs, which must be corrected by software. For lifetime discrimination methods, cross talk does not occur, with the accuracy in the base call determined by the precision in the measurement.

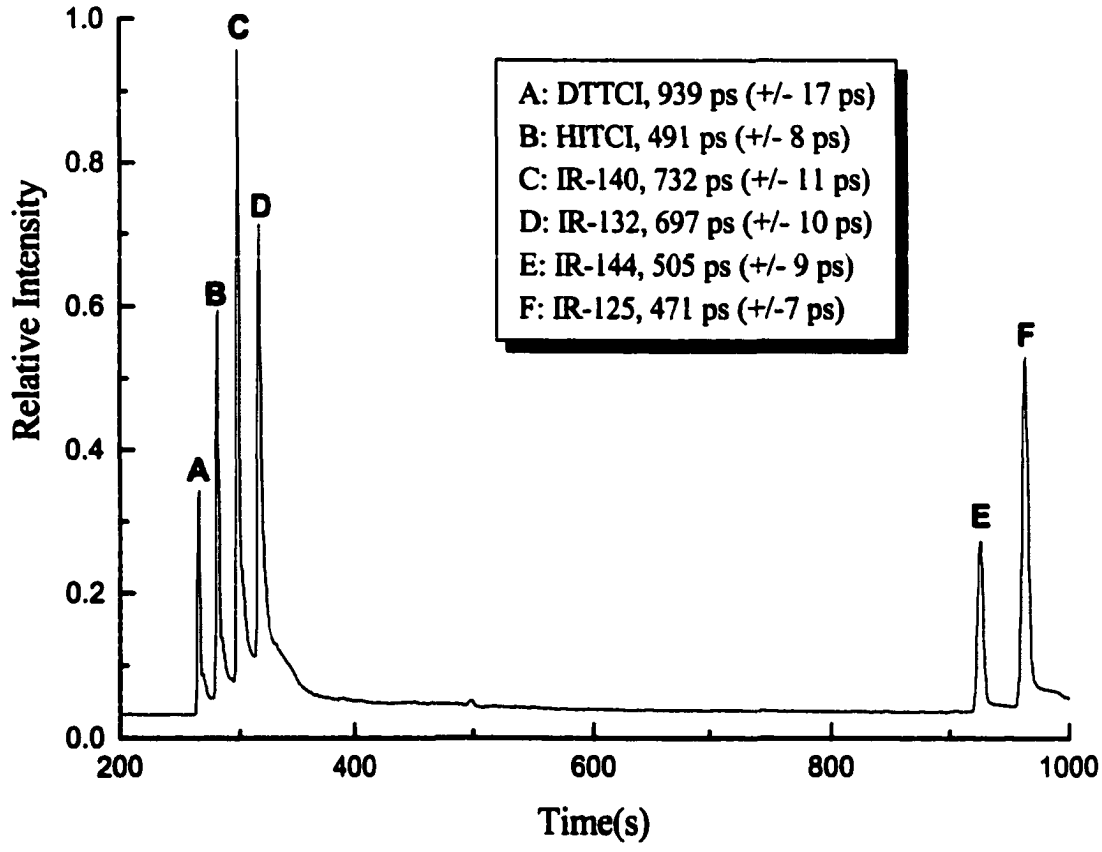

Figure 1.2. Six NIR dyes separated in a free solution capillary electrophoresis experiment. The cationic (DTTCI, HITCI, IR-140, and IR-132) and anionic (IR-144 and IR-125) dyes were separated in a running buffer of 95% methanol and 5% triply distilled water set at a pH of 9.5. The fluorescence lifetimes were determined via the MLE method from decay profiles constructed over each electrophoretic band shown.[26]

(2) The calculated lifetime is immune to concentration differences present within the electrophoretic peak. Therefore, dye terminators can be employed with a variety of polymerase enzymes to accommodate the particular sequencing application. Intensity variations in spectral discrimination methods have been shown to dramatically affect read length and as such, equalization of electrophoretic peak heights by altering the ddNTP to dNTP ratio during DNA polymerization becomes necessary. In addition, when terminator chemistry is implemented, the incorporation efficiency of the particular polymerase of the dye-labeled terminator can drop precipitously, requiring further alterations in the ddNTP to dNTP ratio. (3) It allows for the excitation of the fluorescence with one source and the processing of emission on one detection channel. If the dye set possesses similar absorption and emission maxima but distinct lifetimes, the hardware required for readout can be simplified. In addition, the duty cycle can be improved (elimination of filter wheels) during fluorescence readout, improving the signal-to-noise ratio. (4) Using the appropriate dye set, uniform electrophoretic mobilities can be obtained, eliminating the need for post-electrophoresis corrections. Most dyes do result in a mobility shift of the oligonucleotides to which they are tethered. The shift not only depends upon the identity of the dye, but also on the number of bases present in the oligonucleotides, complicating data processing (base calling).[32] (5) When using time-resolved techniques, time filtering can be simultaneously implemented to improve the signal-to-noise ratio in the measurement. By processing only late arriving photons with respect to the excitation pulse, scattering photons and photons produced by components with short lifetimes can be effectively removed from the fluorescence signal. This will be particularly attractive in gel

electrophoretic applications, where the gel matrix can produce high scattering backgrounds.

Soper and co-workers reported the first demonstration of time-resolved measurements in capillary gel electrophoresis (CGE).[26] A single NIR dye was labeled to a sequencing primer and a single base tract (Cytosine-terminated fragments) was fractionated in a gel column with the lifetimes of the electrophoretic bands determined using the MLE algorithm. No fluorescence was observed from the gel matrix when utilizing NIR excitation, which improved the efficiency (precision) in the measurement. Because of minimal fluorescent and scattering interferences contributing to the fluorescence decay profile, a high precision (± 4 ps) was obtained in determining the average fluorescence lifetime of components. In addition, the calculated lifetime (τ_f) was found to agree favorably to that determined in a static experiment.

Figure 1.3 presents an expanded view of the steady-state fluorescence intensity electropherogram for Adenine (A) and Cytosine (C)-terminated DNA sequencing fragments separated by CGE and their identification as determined by fluorescence lifetime discrimination.[28] (The Thymine (T) and Guanine (G) were unlabeled and were not fluorescently visible.) The average lifetime value determined for IRD40 A-terminated DNA fragments was 699 ps with a standard deviation of ±42 ps. The average lifetime of the IRD41 C-terminated DNA fragments was 528 ps with a standard deviation of ±68 ps. The standard deviations in these measurements were larger than expected based upon the average number of counts included into the determination. If the precision of the measurement was determined primarily by photon statistics, one

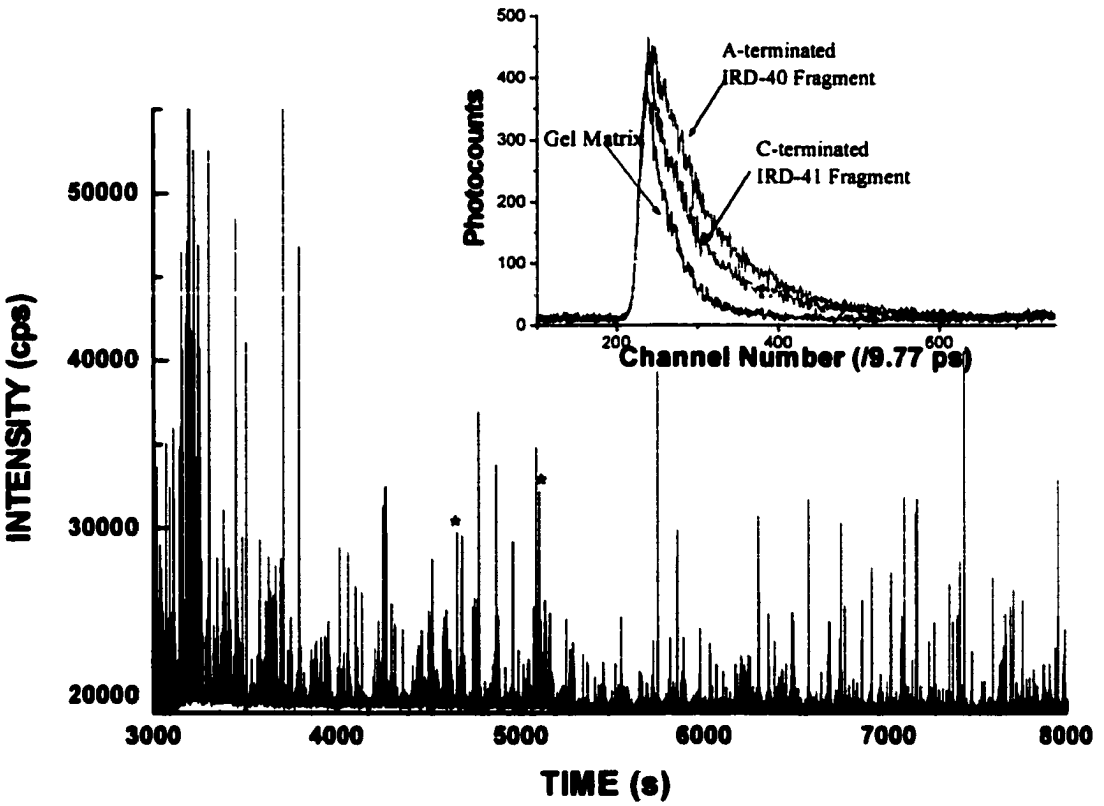

Figure 1.3. Steady-state fluorescence intensity electropherogram of A- and C-terminated DNA fragments separated by capillary gel electrophoresis. Inset shows time-resolved decay profiles from the gel matrix and two bands taken from the electropherogram, which are indicated with and asterisk.[28]

would expect standard deviations of ±5 and ±6 ps for adenine and cytosine terminated fragments, respectively. It was determined that the large standard deviation in these experiments was a result of the TCSPC electronics, which sequentially collected decay profiles over two second intervals during the electrophoresis. In some cases, the data accumulation time for construction of the decay profile was not aligned (in time) with the time interval over which the electrophoretic band was resident in the detection zone. This resulted in a decay profile that was constructed on the rising or falling edge of the electrophoretic band and inclusion of a disproportionately large amount of scattering photons, biasing the determination. In addition, if two bands were present in the detection zone during decay profile construction, the calculated lifetime would represent a weighted average of both dyes.

Wolfrum and co-workers have recently presented one-lane, four dye DNA sequencing data that is based on the time-resolved fluorescence identification method.[32] The multiplex dyes MR-200-1, JA169, JA242, and CY5 were utilized as fluorescent labels. Using a solid-state system composed of a laser diode, TCSPC board, and a home-built CE apparatus; a readlength of 660 bases was determined with 90% calling accuracy. Data analysis was achieved by the method of pattern recognition, in which fluorescence lifetimes were evaluated by comparison to pre-determined decay profiles. Due to different structural characteristics of the dyes employed, the coupling positions of the dyes to the oligonucleotides were varied. The variation in coupling position in conjunction with the addition of spacers allowed for the optimization of electrophoretic mobilities, in which dye-dependent shifts were equalized within the set.

In conclusion, time-resolved NIR fluorescence detection in CE is proving to be a viable technique for the identification of analytes. This technique may be applied to problems such as the identification of nucleotides during DNA sequencing, the characterization of environmental samples, and amino acid analysis. The method is also amenable to miniaturization due to the availability of laser diodes that can operate in a pulsed mode and the ability to mount time-correlated electronics inside personal computers. Advantages of time-resolved fluorescence include increased sensitivity; the ability to identify multiple analytes using one excitation source and one detector; and reduced cost—a direct result of the use of NIR fluorescence and a single detector channel. Additionally, the availability of multiplex NIR dyes and algorithms that allow for the rapid analysis of decay profiles on-line in CE will increase the attractiveness of this technique.

1.3. Research Focus

This manuscript details the design and construction of novel near-infrared time-correlated single photon counting devices for the identification of analytes in multiplex systems. The first area of research focuses on the design of a multichannel fiber optic based system for the performance of TCSPC spectroscopy. This system allows for the excitation and collection of fluorescence from multiple, remote sites simultaneously. The advantages of this system included its small size, and the ability to determine fluorescence lifetimes in the sub-nanosecond regime. The latter part of this doctoral research focuses on the construction and design of a compact, lightweight, and robust confocal scanning device. This device is also capable of determining fluorescence lifetimes in the subnanosecond regime. Additionally, the device has been applied to the

detection of near infrared dyes on a micro-CE chip as well as the identification of oligonucleotides in a DNA microarray.

Both of these devices are capable of being applied to multiplex applications in that more than one analyte may be monitored at one time with one excitation source, one filter set, and one detector. For example, the multichannel fiber optic based system is capable of monitoring twelve analytical separations simultaneously. In addition, the number of analytes that may be monitored in each separation is limited only by the number of fluorescent tags that satisfy the excitation and emission requirements of the laser source and filter set. The scanning system may be utilized to scan multiple capillaries either in an array or on a chip as well as an immunoassay or DNA microchip. Again, the number of analytes that may be studied is limited by the number of fluorescent tags available.

Both of these previously mentioned developments are essential towards the construction of "lab-on-a-chip" technology. Because of the ability to multiplex these detection systems, the multiplexing of multiple experiments on one experimental stage as well as multiple experiments in various locations has been demonstrated. This multiplexing capability allows for the detection of analytes in a high-throughput analytical system. The ability to excite molecules and detect their resulting fluorescence in multiple locations may also prove to be useful in industrial processes where multiple streams are monitored.

1.4 References

(1) Skoog, D. A.; Leary, J. J. *Principles of Instrumental Analysis*, Fourth ed.; Saunders College Publishing: New York, 1992.

(2) Levine, I. N. *Physical Chemistry*, Third ed.; McGraw-Hill, Inc.: New York, NY, 1988.

(3) Swartz, M. *Journal of Chromatography* **1993,** *640*, 441.

(4) Tsai, E. W.; Singh, M. M.; Lu, H. H.; Ip, D. P.; Brooks, M. A. *Journal of Chromatography* **1992,** *626*, 245.

(5) Luckey, J. A.; Drossman, H.; Kostichka, A.; Mead, D.; D'Chuna, J.; Swerdlow, H.; Gesteland, R. *Nucleic Acids Research* **1990,** *18*, 4417.

(6) Huang, X. C.; Quesada, M. A.; Mathies, R. A. *Analytical Chemistry* **1992,** *64*, 2149.

(7) Williams, D. C.; Soper, S. A. *Analytical Chemistry* **1995,** *67*, 3427-3432.

(8) Swerdlow, H. P.; Ahang, J. A.; Chen, D. Y.; Harke, H. R.; Grey, R.; Wu, S.; Dovichi, N. J. *Analytical Chemistry* **1991,** *63*.

(9) Soper, S. A.; Legendre, B. L.; Williams, D. C. *Experimental Technique of Physics* **1995,** *41*, 167-182.

(10) Legendre, B. L.; Soper, S. A. *Applied Spectroscopy* **1996,** *50*, 1196-1202.

(11) Mattusch, J.; Dittrich, K. J. *Journal of Chromatography: A* **1994,** *680*, 279.

(12) Schwartz, H. E.; Ulfelder, K. J.; Chen, F. A.; Pentoney, S. L. *Journal of Capillary Electrophoresis* **1994,** *1*, 36.

(13) Jorgenson, J. W.; Lukacs, K. D. *Analytical Chemistry* **1981,** *53*, 1298-1302.

(14) Soper, S. A.; Davidson, Y. Y.; Flanagan, J. H. J.; Legendre, B. L. J.; Owens, C.; Williams, D. C.; Hammer, R. P. *Proc. SPIE - Int. Soc. Opt. Eng.* **1996,** *2680*, 235-246.

(15) Woolley, A. T.; Mathies, R. A. *Analytical Chemistry* **1995,** *67*, 3676-3680.

(16) Haab, B. B.; Mathies, R. A. *Analytical Chemistry* **1999,** *71*, 5137-5145.

(17) Metzker, M. L.; Jing, L.; Gibbs, R. A. *Science* **1996,** *271*, 1420 - 1422.

(18) Ruiz-Martinez, M. C.; Berka, J.; Belenkii, A.; Foret, F.; Miller, A.; Karger, B. L. *Analytical Chemistry* **1993,** *65*, 2851-2858.

(19) Prober, G. M.; Trainor, G. L.; Dam, R. J.; Hobbs, F. W.; Robertson, C. W.; Zagursky, R. J.; Cocuzza, A. J.; Jensen, M. A.; Baumeister, K. *Science* **1987,** *238*, 336-341.

(20) Smith, L. M.; Z., S. J.; Kaiser, R. J.; Hughes, P.; Dodd, C.; Connell, C. R.; Heiner, C.; Kent, S. B. H.; Hood, L. *Nature* **1986,** *321*, 674-678.

(21) Trainor, G. L.; Hobbs, F. W.; Cocuzza, A. J.; Confalone, P. N. *Nucleic Acids Research* **1988,** 119-120.

(22) Gaussmann, E.; Kuo, J.; Zare, R. *Science* **1985,** *230*, 813-814.

(23) Bachteler, G.; Drexhage, K. H.; Ardenjacob, J.; Han, K. T.; Kollner, M.; Muller, R.; Sauer, M.; Seeger, S.; Wolfrum, J. *Journal of Luminescence* **1994,** *60-1*, 511-514.

(24) Bachteler, G.; Drexhage, K. H.; Ardenjacob, J.; Han, K. T.; Kollner, M.; Muller, R.; Sauer, M.; Seeger, S.; Wolfrum, J. *Journal of Luminescence* **1994,** *62*, 101-108.

(25) Sauer, M.; Ardenjacob, J.; Drexhage, K. H.; Marx, N. J.; Karger, A. E.; Lieberwirth, U.; Muller, M.; Neumann, M.; Nord, S.; Paulus, A.; Schulz, A.; Seeger, S.; Zander, C.; Wolfrum, J. *Biomedical Chromatography* **1997,** *11*, 81-82.

(26) Soper, S. A.; Legendre, B. L.; Williams, D. C. *Analytical Chemistry* **1995,** *67*, 4358-4365.

(27) Legendre, B. L.; Williams, D. C.; Soper, S. A.; Erdmann, R.; Ortmann, U.; Enderlein, J. *Review of Scientific Instruments* **1996,** *67*, 3984-3989.

(28) Legendre, B. L. Doctoral, Louisiana State University and Agricultural and Mechanical College, Baton Rouge, LA, 1997.

(29) Li, L. C.; McGown, L. B. *Analytical Chemistry* **1996,** *68*, 2737-2743.

(30) Li, L. C.; He, H.; Nunnally, B. K.; McGown, L. B. *Journal of Chromatography B* **1997,** *695*, 85-92.

(31) Nunnally, B. K.; He, H.; Li, L. C.; Tucker, S. A.; McGown, L. B. *Analytical Chemistry* **1997,** *69*, 2392-2397.

(32) Lieberwirth, U.; Arden-Jacob, J.; Drexhage, K. H.; Herten, D. P.; Muller, R.; Neumann, M.; Schulz, A.; Siebert, S.; Sagner, G.; Klingel, S.; Sauer, M.; Wolfrum, J. *Analytical Chemistry* **1998,** *70*, 4771-4779.

(33) Muller, R.; Zander, C.; Sauer, M.; Deimel, M.; Ko, D. S.; Siebert, S.; Ardenjacob, J.; Deltau, G.; Marx, N. J.; Drexhage, K. H.; Wolfrum, J. *Chemical Physics Letters* **1996,** *262*, 716-722.

(34) Desilets, D. J.; Kissinger, P. T.; Lytle, F. E. *Analytical Chemistry* **1987,** *59*, 1830-1834.

(35) Miller, K. J.; Leesong, I. K.; Bao, J. M.; Regnier, F. E.; Lytle, F. E. *Analytical Chemistry* **1993,** *65*, 3267-3270.

(36) Miller, K. J.; Lytle, F. E. *Journal of Chromatography* **1993,** *648*, 245-250.

(37) Casay, G. A.; Narayanan, N.; Evans III, L.; Czuppon, T.; Patonay, G. *Talanta* **1996,** *43*, 1997-2005.

Chapter 2

Time-Correlated Single Photon Counting

2.1. Introduction

Fluorescence spectroscopy has become the instrumental tool of choice for many analytical chemists. This is due to a number of reasons, the most prominent of which may be the negligible background as compared to absorbance. Additionally, fluorescence spectroscopy proves to be a valuable tool because it provides information about the excited state dynamics of a molecule. Because fluorescence lifetimes are sensitive to the electronic configuration of a molecule, it yields valuable information about the structure and dynamics of proteins, rotational diffusion in restricted environments, and excited state proton transfer reactions.

2.2. Fundamentals of Fluorescence

Fluorescence is a fundamental photophysical process, which involves the relaxation of the electronic excited state of a molecule to its electronic ground state by the emission of photons. This process typically occurs on a nanosecond time scale. On the other hand, absorption occurs on the femtosecond time scale. A semi-classical approach towards understanding this photophysical process is the Jablonski Diagram. As shown in Figure 2.1, the Jablonski diagram provides a schematic of the various processes that take place when a molecule is excited from the ground electronic state to an excited electronic state.

The absorption (ABS) of photons results in the excitation of a molecule from an electronic ground state to an electronic excited state. After absorption, the molecule may undergo internal conversion (IC), which involves the relaxation of the molecule to

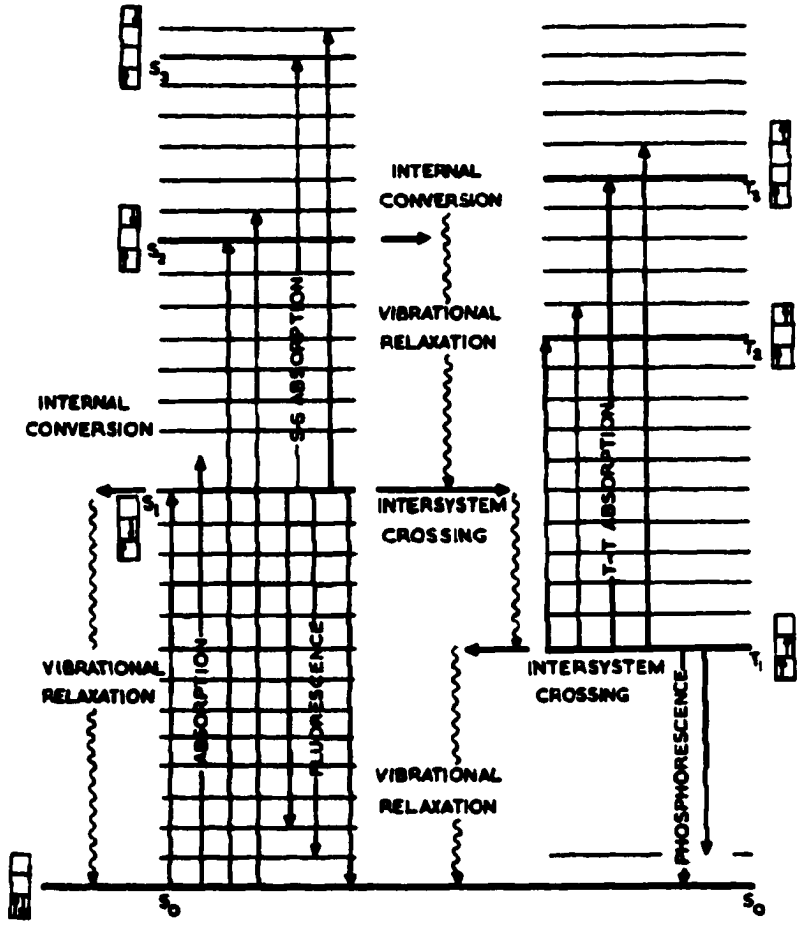

Figure 2.1. Jablonski Diagram illustrating radiative and nonradiative pathways of an excited polyatomic molecule.[1]

the lowest vibrational level of the excited state it resides. Internal conversion occurs on the picosecond time scale and is usually complete before the emission of photons. Fluorescence (FL) occurs when a molecule relaxes from an excited electronic state to the ground electronic state by the release of photons. Note that fluorescence is known as a "spin-allowed" transition because the molecules go from one singlet state to another singlet state. A singlet state is one in which all electrons have their spins matched-for every electron with a spin of +1/2 there exists an electron with a spin of −1/2. Finally, fluorescence photons are usually emitted at longer wavelengths than absorbing photons. This may be deduced from the Jablonski diagram in which the magnitude of the transition is typically lower for fluorescence than for absorbance, which is a direct result of vibrational relaxation.

In addition to internal conversion and fluorescence, molecules in the excited state may undergo intersystem crossing (ISC) from the excited singlet state to an excited triplet state. The emission of photons from this triplet state is referred to as phosphorescence (PH). This process usually occurs on a time scale of microseconds to seconds. However, since this is a forbidden process, the rate constant for phosphorescence is several orders of magnitude smaller than fluorescence.

The intensity of the steady-state fluorescence (I_f) is given by the following equation:

$$I_f = 2.303 I_0 b C \Phi_f F(\Theta) G(\lambda) \qquad (2.1)$$

where I_0 is the incident photon flux (photons/(cm^2 sec)), b is the path length of the sample cell in cm, C is the concentration of the fluorescent species (moles/L), Φ_f is the fluorescence quantum yield of the fluorescing species, ε is the molar absorptivity of the

chromophore (L cm^{-1} mol^{-1}), $F(\Theta)$ is the instrumental collection and transmission efficiencies of fluorescent photons through the detection system, and $G(\lambda)$ is the quantum efficiency of the detector at the observation wavelengths.

From a quantum mechanical point-of-view, fluorescence may be described as the transition of the electric dipole moment from an excited singlet state to ground singlet state. By utilizing the Born-Oppenheimer Principle and separating the nuclear and electronic wavefunctions, the probability of such a transition is proportional to R_{if}^2, where R_{if} is defined;

$$R_{if} = \int_{-\infty}^{+\infty} \psi_{ef} \hat{M} \psi_{ei} d\tau_e \int_{-\infty}^{+\infty} \psi_{nf} \psi_{ni} d\tau_n \qquad (2.2)$$

where $\hat{M}$ is the electronic dipole moment operator, i is the initial state, f is the final state, and ψ_e and ψ_n represent the electronic and nuclear wavefunctions, respectively. The electronic integral may be approximated to equal zero unless states i and f possess the same spin; which meets the requirement that allowed transitions occur from the excited singlet state to the ground singlet state. Note that this transition integral may also be used to define the absorption process, which also dictates that electronic absorption in most organic molecules occurs from the ground singlet state to the excited singlet state. Accordingly, the Franck-Condon Principle states that all electronic transitions are vertical, which results in the symmetric nature of absorption and emission spectra. This is commonly known as the mirror image rule.

Time-resolved fluorescence spectroscopy studies the rate associated with the fluorescence process. By listing simple, first order rate equations, we may define the total quantum yield of fluorescence:

$M + h\nu \rightarrow {}^1M^*$	I_a (absorption)	(2.3)
${}^1M^* + h\nu \rightarrow M + h\nu$	k_R (fluorescence)	(2.4)
${}^1M^* \rightarrow M$	k_{IC}(internal conversion)	(2.5)
${}^1M^* \rightarrow {}^3M^*$	k_{ISC}(intersystem crossing)	(2.6)
${}^1M^* \rightarrow$ products	k_D (dissociation)	(2.7)

The fluorescence quantum yield, ϕ_F, may be defined as;

$$\phi_F = \frac{k_R}{(k_R + k_{ISC} + k_{IC} + k_D)} \tag{2.8}$$

In addition, the fluorescence lifetime, τ_F, is the inverse of the sum of the rates that depopulate the excited state;

$$\tau_F = (k_R + k_{ISC} + k_{IC} + k_D)^{-1}. \tag{2.9}$$

Alternatively, this may be rewritten and expressed as;

$$\tau_F = \frac{1}{k_R + k_{NR}} \tag{2.10}$$

where k_R is the radiative rate constant and k_{NR} is the sum of the non-radiative rate constants.

2.3. Methods of determining the fluorescence lifetime

From an experimental viewpoint, fluorescence spectroscopy provides information about the electronic excited state and absorbance spectroscopy provides information about the electronic ground state. In addition to the processes mentioned previously, other non-radiative processes such as fluorescence quenching, solvent relaxation, and excited state reactions may occur. The fluorescence lifetime refers to the average amount of time that a molecule resides in the excited state. This physical

parameter is important because it is dependent upon a molecule's environment and provides valuable information about the electronic configuration of the excited state. However, in this treatment we are concerned with the determination of fluorescence lifetimes in analytical applications, such as capillary electrophoresis and microarrays for identification purposes.

2.3.1. Phase-Resolved Method

There are two predominate experimental methods for determining fluorescence lifetimes. Phase-resolved methods utilize a continuous excitation source that is modulated sinusoidally to excite the sample of interest. Since the fluorescence intensity is a direct result of the excitation intensity, the emission is also sinusoidally modulated. This may be explicitly expressed by the following equations for the sinusoidally excitation signal E(t) and the resulting modulated fluorescence signal, F(t);

$$E(t) = D_{EX} + A_{EX} \exp(i\omega t) \text{ and} \qquad (2.11)$$

$$F(t) = D_F + A_F \exp i(\omega t + \phi) \qquad (2.12)$$

where D_{EX} and D_F are the dc intensity component of the excitation beam and fluorescence signal, respectively; ϕ is the phase difference between excitation and emission; A_{EX} and D_{EX} are the amplitude of the excitation and fluorescence, respectively; and ω is the angular frequency which is given by;

$$\omega = 2\pi\upsilon \qquad (2.13)$$

and v is the frequency. However, the degree of fluorescence modulation is directly influenced by the fluorescence lifetime. The phase-resolved approach correlates the difference between the phase of excitation and fluorescence emission with the fluorescence lifetime. In addition to difference in phase, the relative amplitude of the

signals is important and is used to measure the demodulation factor, which is depicted in Figure 2.2. As Figure 2.2 shows, the demodulation factor is determined by taking the ratio of the relative amplitude of the emission to the relative amplitude of excitation. From Equation 2.11 and 2.12 this is mathematically determined by:

$$m = \frac{A_F D_{EX}}{A_{EX} D_F}. \qquad (2.14)$$

The demodulation factor is related to the phase (τ_p) and modulation (τ_m) lifetimes by the relations;

$$\tau_p = \omega^{-1} \tan\phi \qquad \text{and} \qquad (2.15)$$

$$\tau_m = \omega^{-1}\left[\left(1/m^2\right) - 1\right]^{1/2} \qquad (2.16)$$

where, ϕ is the phase difference between excitation and emission, and m is the demodulation factor. For a single exponential decay,

$$\tau_p = \tau_m = \tau_f. \qquad (2.17)$$

Thus, as the fluorescence lifetime of a molecule increases, its phase angle increases and the demodulation factor decreases.

However, an inherent problem with this approach is that small sources of error in determining the phase angle and demodulation factor leads to large errors in calculating the fluorescence lifetime. A 1% error in determining the demodulation factor can result in a 50% error in the calculated lifetime; in fact, the error in the measured value of the demodulation factor is likely to exceed 1%.[1]. Therefore, a 1% error in the measured value of the demodulation factor (a value of 0.993 or 0.973 instead of the correct value of 0.983) for a three-nanosecond lifetime will result in lifetime measurements of 1.9 and 3.8 ns. This is unacceptable in many multiplexed

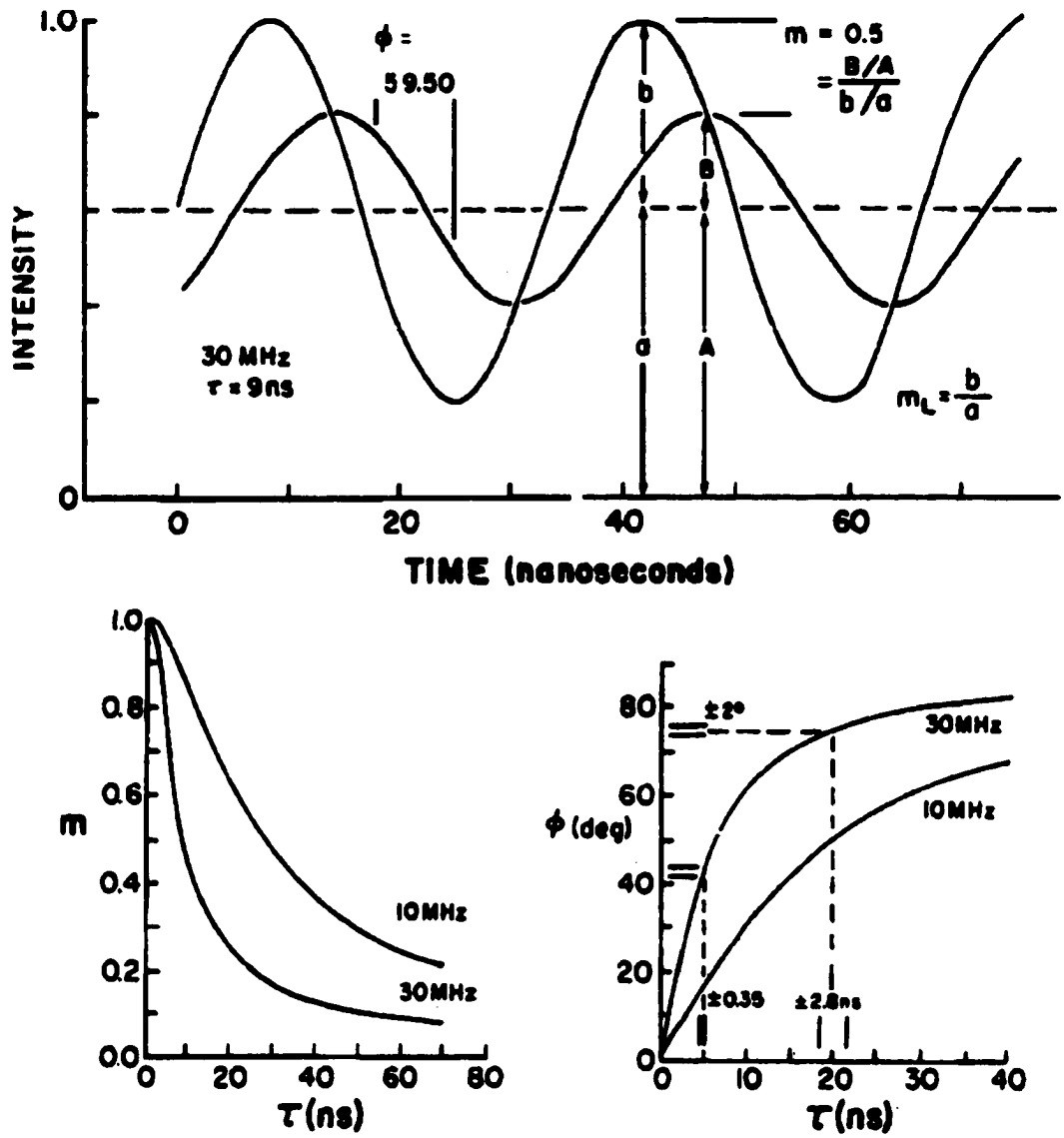

Figure 2.2. Schematic description of Phase and modulation lifetime measurements.[1]

applications where the difference in lifetimes may be as low as 35 ps.[2] As a result, an alternative method must be considered.

2.3.2. Time Correlated Single Photon Counting Method

An alternative to phase-resolved methods is pulsed methods, which directly records the time-evolution of the emission using a single excitation pulse. However, such a process is technically difficult because of the high gain and low response time required of the detection device. Multiple excitation pulses may be utilized if the delay between each pulse is longer than five fluorescence lifetimes in order to ensure that the fluorescence from one pulse does not interact with an incoming pulse. In the time correlated single photon counting method, the time between the excitation pulse and the arrival of the first fluorescence photon is measured. This process is repeated a number of times such that a histogram can be constructed that represents the decay kinetics of the excited electronic state. The fluorescence lifetime is determined by performing a deconvolution of the instrumental response function and the recorded decay spectra and comparing the profile to a calculated function. The timing resolution and the precision in determining the fluorescent lifetime is primarily a function of the reproducibility of the excitation pulse, its width, and the time response of the photon detector.

Figure 2.3 provides a detailed schematic of a standard TCSPC experimental setup. As with any system for the determination of fluorescence lifetimes, a number of standard elements are present. The excitation source is pulsed and is usually a flash lamp or a mode locked laser. This source is necessary to excite molecules from the electronic ground state to an excited electronic state. If a mode locked laser is used, the

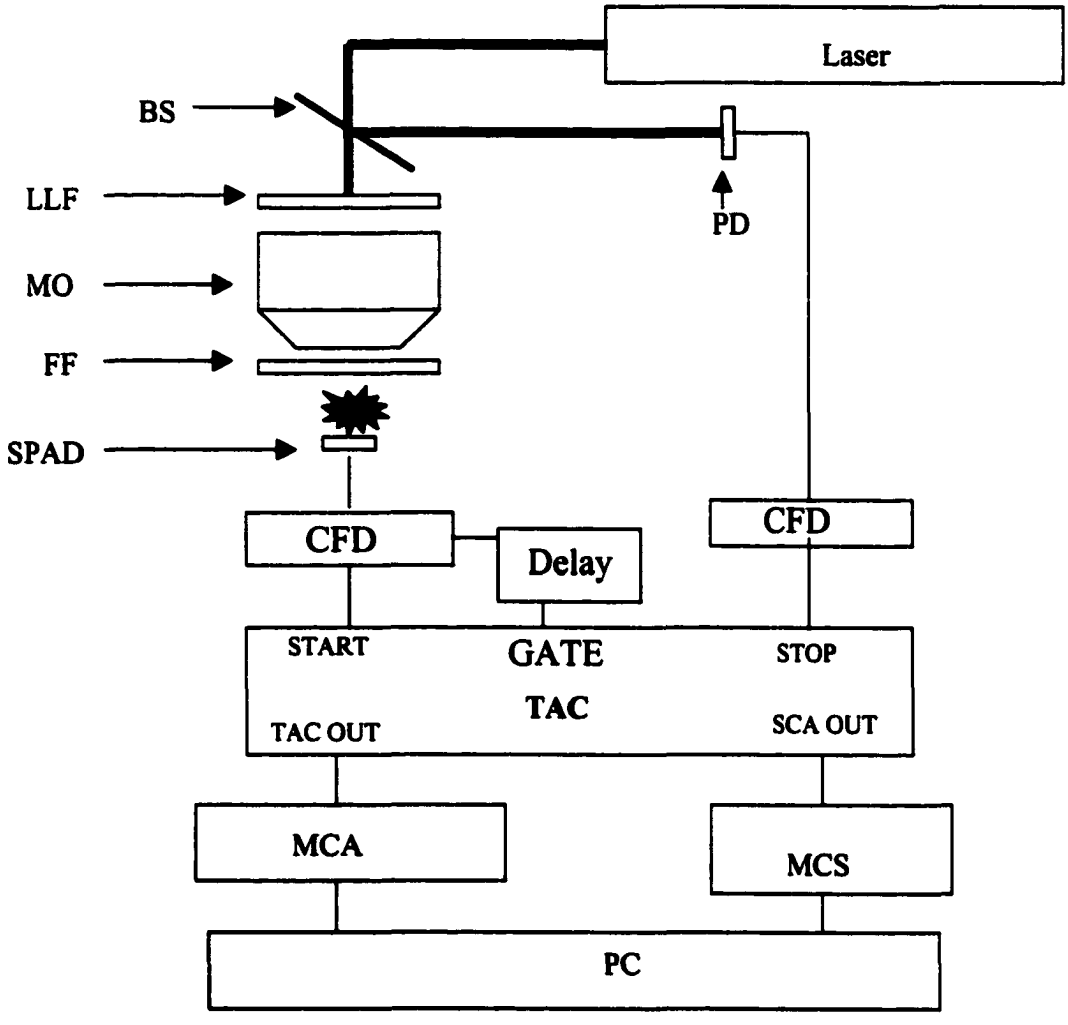

Figure 2.3. Typical time-correlated single photon counting (TCSPC) device. BS, Beam Splitter; LLF, Laser Line Filter; MO, Microscope Objective; FF, Fluorescence Filter; SPAD, Single Photon Avalanche Diode; CFD, Constant Fraction Discriminator; TAC, Time-to-amplitude Converter; SCA, Single Channel Analyzer; MCA, Multichannel Analyzer; and MCS, Multichannel Scaler.

pulse train may be monitored by an external fast photodiode that monitors a fraction of the excitation beam. The detector may be a photomultiplier tube, multichannel plate, or a single photon avalanche diode. The fluorescent photons are detected by the photon detector and subsequently amplified utilizing a fast amplifier. The electronic pulses from the excitation beam and the photon detector are then conditioned with the use of a discriminator, which is responsible for the elimination of any artifacts due to dark noise or multiple photon events. (Multiple photon events occur when more than one photon is detected.) The heart of a TCSPC system is the time-to-amplitude converter that is responsible for timing the duration between the excitation pulse and the arrival of the first fluorescent photon. This is accomplished by utilizing the excitation pulse as the electronic start and the pulse provided by the photon detector as the electronic stop. Each time measurement is placed in an appropriate time bin by a multichannel analyzer, from which a histogram is constructed.

One of the primary advantages of TCSPC versus phase resolved fluorescence lifetime determinations is that it is a digital technique as opposed to an analog technique. Consequently, intensity fluctuations in the excitation pulse become unimportant. Additionally, a digital technique allows the researcher to easily implement statistical tools such as non-linear least squares fitting methods. From a theoretical viewpoint, this statistical approach is based upon the assumption that following one excitation pulse; an average number of photons, z_i, impinge on the fluorescence detector during the time interval $t_{i-1/2}$ to $t_{i+1/2}$, corresponding to the time width of address i.[3] Therefore, the average number of electrons (w_i) that will be emitted from the cathode may be represented by;

$$w_i = qz_i, \tag{2.18}$$

where q is the quantum efficiency of the detector. Assuming a Poisson distribution for the probability of emission of l photoelectrons in the ith time interval ($p_l(i)$)[4]:

$$p_l(i) = \frac{(w_i)^l}{l!} e^{-w_i} \tag{2.19}$$

with the sum of the probabilities equal to unity. Solving the equation for l=0 and l=1, the value for l>1, which is the probability of at least one photoelectron being detected per excitation pulse, may be easily determined. This is written as:

$$p_{l>1}(i) = 1 - (1 + w_i)e^{-w_i} \tag{2.20}$$

At low excitation powers, w_i <<1 and

$$p_l(i) = w_i \tag{2.21}$$

and

$$p_{l>1}(i) = w_i^2 \langle\langle w_i . \tag{2.22}$$

Assuming a large number of excitation pulses (N_E), the number of anode pulses (detected number of photoelectrons, N_A) in the ith time interval may be written as:

$$N_A = N_E[p_l(i) + p_{l>1}(i)] \tag{2.23}$$

which upon substitution yields:

$$N_A = N_E q z_i . \tag{2.24}$$

Consequently, the probability of detecting a fluorescent photon in channel i is proportional to the fluorescence intensity at time, t_i. Moreover, the probability of

detecting two fluorescence photons per excitation pulse is low provided that;

$$\frac{S_P}{S_t} \leq 0.01 \qquad (2.25)$$

where S_P is the photodetector pulse due to fluorescence photons over all delay times and S_t is the repetition rate of the excitation source.[5] For pulsed excitation, the number of counts, N_i, accumulated in channel i after excitation, in a specified measurement time T is given by:

$$N_i = \alpha S_t T \frac{\Delta t}{\tau_f} e^{-i\Delta t/\tau_f} \qquad (2.26)$$

where τ_f is for a single exponential decay, α is a proportionality constant, and Δt is the time difference between the detected photon and the excitation pulse.[5]. Thus, the longer the measurement time, the greater the number of photons that accumulate within the decay profile.

2.4. Excitation Sources

2.4.1 Lamps

Before the advent of lasers, fluorescence lifetime studies utilized lamps as an excitation source. The most versatile of these is the high-pressure Xenon arc lamp, which provides a continuous light output from 270 to 700 nm, except for a number of sharp lines near 450 nm.[6] The high pressure Mercury lamp is more intense but only emits light at specific wavelengths. State of-the-art flash lamps are capable of providing pulse widths as low as two nanoseconds.[1] This is important because the time resolution in time-resolved fluorescence spectroscopy is a convolution of the pulse width of the excitation source and the response time of the detector, optics, and electronics. In 1960,

the first laser was constructed[7] and this advance as well as the continued improvement in solid state detectors has led to reduced time response of the instrument in TCSPC.

2.4.2. Lasers

The term laser is an acronym for Light Amplification by Stimulated Emission of Radiation. The output of a laser may be characterized as being coherent in that all of the emitted photons move in the same direction and are in phase with one another. Additionally, lasing may only occur at specific, quantum mechanically allowed, wavelengths. These wavelengths are defined by the lasing medium, which may be a gas, a solid-state crystal, an organic dye, or a semi-conducting material and the cavity length of the laser, which may range in length from sub millimeters to meters.

In order for lasing to occur, the lasing medium must be stimulated such that photons are emitted and amplified. At a basic level, this is achieved by moving (pumping) the majority of molecules from the ground state to a higher energy state, stimulating emission from the higher energy state to the lower energy state. Additionally, amplification must occur such that for every pumping photon, multiple "lasing" photons are emitted.

At room temperature, most molecules reside in the electronic ground state, with the distribution being best described by the Boltzmann distribution law;

$$\frac{N_e}{N_g} = \frac{g_e}{g_g} e^{-\frac{\Delta E}{kT}}, \qquad (2.27)$$

where k is the Boltzmann constant (k=1.38066 x 10^{-23} Joules·Kelvin^{-1}, ΔE is the difference in energy between the ground and excited state ($\Delta E = E_e - E_g$), T is the temperature in Kelvin, N_g and N_e are the number of molecules in the ground state and

excited state, respectively, and g_g and g_e are the degeneracies of the molecular energy levels. At room temperatures, the lower energy levels are more populated than the higher energy levels. In order to achieve lasing, a population inversion must be created such that the majority of molecules are in the excited state instead of the ground state. This is necessary in order to have the majority of molecules relaxing to the ground state by the release of photons. However, at room temperature, such a distribution would violate the Law of Boltzmann's distribution.

In 1958, Townes, Prochorov, and Basov[7] proposed that such a population inversion could be accomplished by utilizing a three level system. By 1960, the term laser had been created and the first laser was constructed. As Figure 2.4 illustrates, a three level system uses an intermediate level in which the electrons remain for a fixed period before relaxing back to the ground state. More precisely, the majority of molecules remain in the intermediate state as opposed to the ground state. This is accomplished because the intermediate state has a longer lifetime than the excited state and the transition from the excited state to the intermediate state is faster than the transition from the intermediate state to the ground state. After the population inversion is achieved, the intermediate state must be stimulated such that the molecules relax to the ground state by the release of photons.

Stimulated emission occurs when the molecules in the excited state relax back to the ground state under the influence of photons with the appropriate energy. As these molecules relax, photons in addition to the initial incident photon are released. In effect, the incident photon stimulates the release of additional photons and secondly, the direction in which the stimulated photons are released is in the same direction as the

incident photon. This directionality of emission results in the brightness usually associated with laser emission. Upon relaxation to the ground state, the molecules are pumped back to the upper state so that the process may be repeated again. Amplification occurs when an absorbed photon results in the stimulated emission of more than one photon. In addition to the stimulated emission from the intermediate state, there must also occur amplification of the emitted radiation (light). This is accomplished by passing light through the gain medium by reflecting it back and forth between two mirrors. Consequently, a gain is achieved each time the stimulated emission transverses the medium. The output of the laser is a small fraction of light that is transmitted through the output coupler.

The distance between these two mirrors defines the cavity length of the laser. With each pass through the gain medium, the light reinforces itself to form a standing wave with nodes at the surface of each mirror with a form of;

$$E_s = E_0 \cos \omega t \sin(ks) \qquad (2.28)$$

where E_0 is the maximum amplitude, ω is the angular frequency (radians/s) and is equal to $2\pi\nu$, where ν is the frequency, t is the time (s), and $k = \frac{2\pi}{\lambda}$ is the propagation constant. The points of maximum amplitude as well as the nodes between them do not move.

The laser cavity of length L supports longitudinal waves (modes) with an integral number of half wavelengths between the mirrors. This optical resonance will

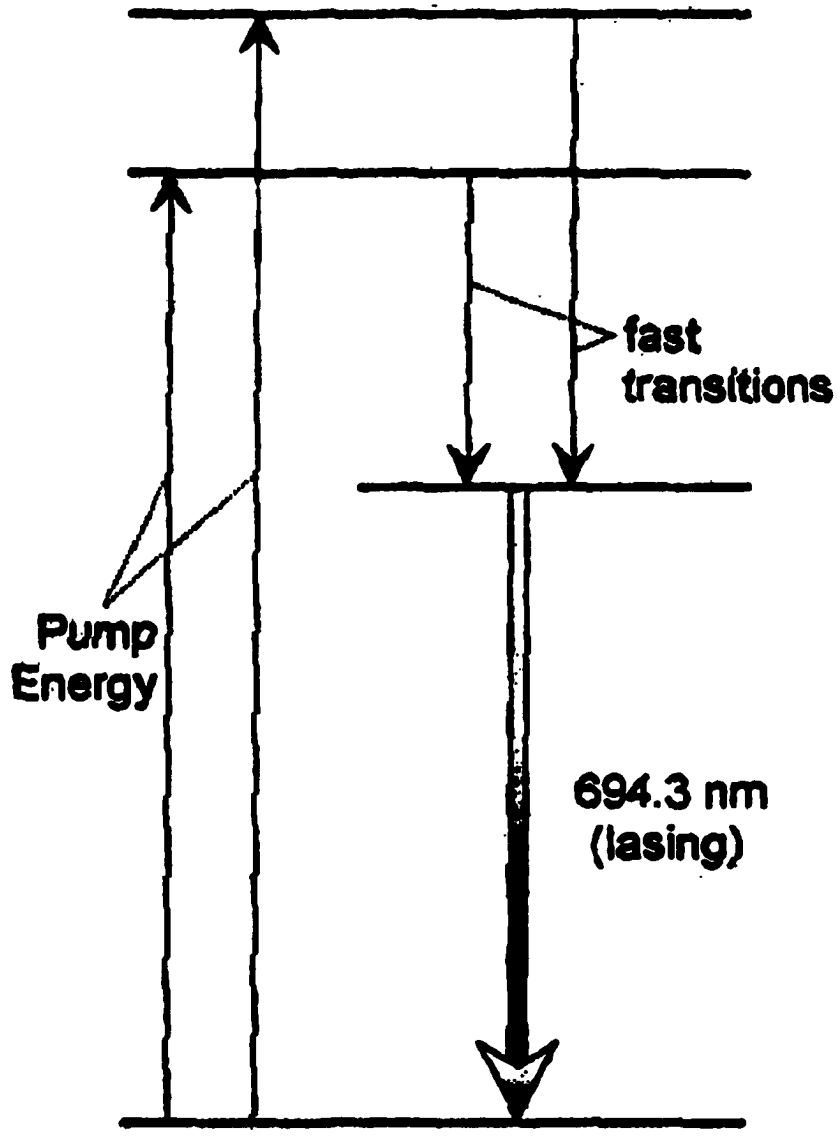

Figure 2.4 Energy levels of the three level ruby laser system. The population achieved by optical pumping of the ground electronic state to the upper electronic states is quickly depleted by fast transitions to the metastable state. Lasing at 694.3 nm occurs when a population inversion is created between the intermediate state and the ground state.[7]

occur at discrete wavelengths, λ_n, given by;

$$\lambda_n = 2L/n \tag{2.29}$$

where n is an integer.[5] This longitudinal resonance condition dictates that only those modes that satisfy equation 2.29 will be amplified in the laser cavity. Substituting frequency (v) for wavelength by utilizing the fundamental relation;

$$c = \lambda \nu \tag{2.30}$$

one obtains

$$\nu_n = nc/2L \tag{2.31}$$

and the frequency difference between the longitudinal modes is given by;

$$\Delta \nu = \nu_{n+1} - \nu_n = c/2L. \tag{2.32}$$

Typically, the greater the number of longitudinal modes a cavity supports, the narrower the pulse widths that can be obtained.

The majority of pulsed lasers consist of a three level system, with the molecules depopulating the intermediate level simultaneously and the ground state being pumped to propel the molecules back to the excited state. In Figure 2.4 is a schematic of the Ruby laser, which is a pulsed system.

The four-level laser system utilizes similar concepts, except there are two intermediate levels between the ground and excited state. In this instance, there is a rapid decay from the excited state to the first intermediate level and subsequent stimulated emission to the second intermediate level. The depopulation rate from the second intermediate level to the ground state is also high and therefore, most molecules

will reside in the first intermediate state. Because this is a cyclical process and the ground state is continually pumped; continuous lasing occurs.

2.4.2.1. Mode locked Lasers

A mode-locked laser is capable of providing short pulses of light that are essential to performing TCSPC. These pulses of light range in duration from nanoseconds to femtoseconds and occur at repetition rates from tens of hertz to the gigahertz range. Mode-locking may be achieved by modulating the light with a mechanical shutter and as a result the repetition rate of the laser is determined by the frequency of the modulator (shutter). However, in order to maintain lasing, the modulator must be readjusted to match the cavity or the cavity readjusted to match the modulator. Because of this continual readjustment, this method of mode locking is referred to as active mode locking. An alternative method of mode locking is referred to as passive mode locking and is dependent on the Optical Kerr Effect (OKE).

The OKE occurs in certain optical media when high intensity light produces an electric field, which distorts the material and alters its refractive index. In a passively mode locked laser, the material may be an organic dye or a crystal, which is opaque but becomes transparent when the intensity of light reaches a specific level. Consequently, high intensity light is transmitted, whereas low intensity light is not. In a mode locked system, this is a desired consequence because the high intensity light is in the form of mode locked pulses and the low intensity light in the form of continuous radiation. Also referred to as dynamic self-focusing or Kerr-Lens-Mode-Locking (KLM), the technique results in improved mode-locking when an aperture is placed in the cavity.[8]

The purpose of the aperture is to introduce losses for spatially large beams, which are typically continuous waves.

The Ti:Sapphire system utilized in these experiments works on the passively mode-locked principle mentioned in the previous paragraph. The beam diameter of the laser is large when the laser is operating in continuous wave (CW) mode and small in mode-locked operation. The addition of a slit with a certain width before the output coupler introduces a loss to the large diameter laser beam, which is associated with CW operation. Additionally, the mode-locked operation results in pulses that are nearly transform limited as described by the Heisenberg uncertainty principle which states that;

$$\Delta E \Delta t \approx h \tag{2.33}$$

where ΔE is the spectral bandwidth (nm) of the pulse which is expressed as Joules, Δt is the temporal bandwidth (s) of the laser pulse, and h is Planck's constant. The principle asserts that the greater the uncertainty in the energy of the pulse, the less uncertainty in the timing of the pulse. Using Fourier transform analysis for the Heisenberg uncertainty principle, the narrowest pulse that may be obtained from a perfectly mode-locked laser is limited by this Fourier transform relationship, and a pulse which approaches this fundamental limit is called transform limited. A pulse is nearly transform limited if the time-bandwidth product of the Heisenberg uncertainty principle is determined to be <0.4 (hyper secant-squared pulse shape).

2.4.2.2 Diode Lasers

Diode lasers are semi-conductor devices and have several unique advantages compared to solid-state, gas, and dye lasers. The most evident advantage is their small

size, which makes their use amenable to miniaturized devices. In addition to their small size, diode lasers have a long operating life, which may be as long as tens of thousands of hours and are simple to use as evidenced by their turnkey operation. Some of the more popular wavelengths are 680 nm, 780 nm, 850 nm, and 1550 nm.[9] Most of the available wavelengths are in the NIR region of the electromagnetic spectrum due the physical properties of the semi-conductor materials used in their construction. However, recent advances have led to the construction of diode lasers, which also lase in the visible region of the spectrum.[7, 10, 11] Output powers of the NIR lasers range from a few milliwatts to tens of milliwatts.

A semiconductor material possesses properties of both metals and insulators. Crystalline solids may be classified as a metal, semiconductor, or insulator dependent on the energy gap between their conduction and valence bands. The conduction band is comprised of unoccupied molecular orbitals and has a higher energy than the valence band, which is composed of partially or completely filled molecular orbitals. The energy gap in a metal is virtually non-existent and electrons move freely from the partially filled valence band to the conduction band upon the application of an electric field. An insulator has a large energy gap between the filled valence band and conduction band, which is too large for electrons to overcome and move to the unoccupied orbitals of the conduction band. For example, carbon in its diamond form has a band gap of ~6 electron Volts (eV). Electrons can not bridge this gap, either by thermal excitation or by the action of a strong electric field.[12]

A semiconductor has an intermediate band gap that allows for the movement of electrons from the filled valence band to the conduction band. However, a small

activation energy is required to propel the electrons across the band gap. This is a result of a small bandgap. Consider silicon, which has the same crystal structure as diamond but a gap width of ~1.1. eV.[12] The concentration of holes that is created in the valence band when electrons are promoted to the conduction band is denoted by n. The concentration of negative mobile electrons that have been promoted to the conduction band is denoted by p. At equilibrium, the values of p and n are usually small and nearly equal. However, a p-type semiconductor is created by adding a small amount of donor impurity (a material that has filled molecular orbitals) to the semiconductor material. Conversely, an n-type semiconductor may be created by doping a pure semiconductor with a small amount of acceptor material (a material that has unfilled molecular orbitals).

As illustrated in Figure 2.5, a semiconductor laser is constructed by mounting parallel layers of p-type and n-type semiconductors. As a result, a p-n junction (or active region) may be created. By applying a forward bias, which is a positive voltage at the p-type material and a negative voltage at the n-type material, a current is induced which transfers electrons from the conduction band to the valence band. The recombination of these mobile electrons from the n-type material with the holes present in the p-type material results in the release of photons with an energy equivalent to the band gap. Quantitatively, this wavelength may be determined by;

$$\lambda = \frac{hc}{E_g} \tag{2.34}$$

where λ is the wavelength of the emitted radiation, c is the speed of light, h is Planck's constant, and E_g is the band gap.

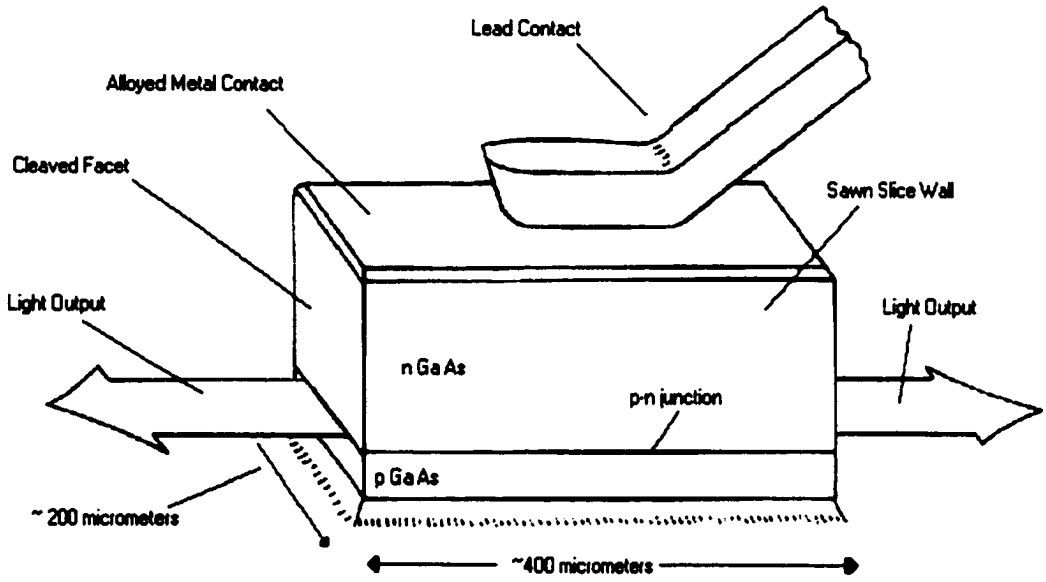

Figure 2.5. Schematic of a semiconductor laser constructed by mounting parallel layers of *p*-type and *n*-type semiconductors.[14]

A cavity is formed by polishing the ends of the semiconductor and placing materials with a lower refractive index next to the *p-n* junction. The required population inversion is maintained by applying a high forward bias and confining electrons and holes to the active region. This is accomplished by depositing layers of semiconductor material with higher band gaps than the *p-n* junction adjacent to the active region.[7]

These aforementioned semiconductor materials come from Groups III, IV, and V of the periodic table. Various semiconductor compositions and lasing wavelengths are given in Table 2.1.[9] The band gap of these semiconductor materials may be varied by manipulating the ratio of the semiconductors used, which has a direct bearing on the wavelength of light emitted.

Table 2.1. Semiconductor Composition and Wavelengths

Composition	Emitting Wavelength
AlGaInP	630, 670, 680, 690
AlGaAs	780, 830
InGaAs	980
InGaAsP	1310, 1480, 1550

Similar to gas and solid state lasers, diode lasers may also be actively or passively mode-locked.[13] Passive mode-locking functions on the same principle described for the Ti:Sapphire system. Once the pulse energy reaches a specific level in the saturable absorber, the absorber saturates, and the center of the pulse experiences net gain. As the pulse propagates, the saturation of the gain medium reduces the gain to below threshold and shuts off lasing.[13] One approach towards forming a saturable

absorber is to split the gain contact of the laser and reverse bias one segment to form an integrated saturable absorber. Active mode-locking is accomplished by externally applying the gain modulation of the laser. This may be easily achieved by modulating the electrical current, which is possible to very high frequencies. This is advantageous over other types of lasers, which do not respond as rapidly to a modulation of their pump supply.[14]

The PicoQuant GmbH pulsed-diode laser is an actively mode-locked diode laser. The diode head was driven by an electrical short pulse generator, which supplied high repetition rate picosecond current pulses.[5] The driver consisted of a variable radio frequency pulse generator, fast switching stage, coax line driver, and a pulse shaper stage.[15] Additionally, it is possible to adjust the pulse repetition rate from a single shot to 80 MHz at wavelengths from 635 nm to 1550 nm. This actively mode-locked scheme allows for higher output powers at the sacrifice of a broad bandwidth and higher pulsewidth in comparison to passively mode-locked diodes.[10]

Advantages of diode lasers include compact size, low cost, and ease of use. Typical wavelengths are in the NIR region of the spectrum but recent advances have led to emission in the visible region of electromagnetic spectrum. Additionally, whereas the useful life of gas (e.g., Argon Ion) or solid-state (e.g., Ti:Sapphire) lasers is typically measured in thousands of hours, that of carefully qualified diode lasers is measured in hundreds of years.[10] Unfortunately, the emission of light from diode lasers is not well collimated. This requires the use of external optics for increased collimation and focusing. Diode lasers may be applied to both the phase-resolved and time resolved techniques of fluorescence lifetime determinations.[9, 16-26]

2.5. Detection Sources

There are many choices for detectors in a fluorescence system. The ideal detector for ultrasensitive detection and spectroscopy experiments must exhibit single photon detection capability, high quantum efficiency, and low dark noise.[27] The choices include photomultiplier tubes, multichannel plates, and avalanche photodiodes. A coherent understanding of Einstein's photoelectric effect is essential in understanding the operational characteristics of photomultiplier tubes and microchannel plates; whereas the avalanche photodiode is a semiconductor device and functions on previously described principles for diode lasers.

The photoelectric effect rests on the principle that photons possess a characteristic energy, which is dependent on their wavelength. Additionally, bound electrons possess an intrinsic parameter that may be referred to as their work function. This is the amount of energy required to eject an electron from a surface and can be described using the relation;

$$E = h\upsilon = \phi + K_{max} \qquad (2.35)$$

where h is Planck's constant (6.63×10^{-34} J s), υ is the frequency of the light , ϕ is the work function of the emitting surface, demonstrates that the excess energy, $h\upsilon - \phi$, allows the electron to migrate from the surface. Thus, the photoelectric effect is the phenomenon that occurs when arriving photons transfer their energy to a surface and liberate bound electrons. In a photon detector, these liberated electrons in turn liberate other bound electrons in a cascading chain such that an electric current is produced. This cascading effect is typically quantified by the gain of the device, which is defined as the total number of electrons detected for each electron initially liberated.

2.5.1. Photomultiplier Tube

The photomultiplier tube is one of the most popular detection devices because of its high gain and low cost. The operating principle behind the PMT is that once a photon is detected, a cascade of photoelectrons is created, with the gain of a typical PMT being 10^6. This is accomplished by a photocathode, which is a thin sheet of metal placed inside the PMT and a series of dynodes that are held at a high negative potential. The potentials of the dynodes progress towards zero along the dynode chain and therefore the ejected electrons are accelerated down the dynode chain. As Figure 2.6 illustrates, the photocathode is held at negative one to two thousand volts, which reduces the spontaneous release of electrons. For each electron that impinges on the surface of the dynode, five to twenty additional electrons are released. Thus, in effect, the dynode chain acts as a gain medium, with the amplification determined by the voltage on the device. However, the PMT is most sensitive in the UV and visible region of the spectrum and rapidly falls off in the NIR.

2.5.2 Microchannel Plates

As Figure 2.7 details, a microchannel plate is similar to a PMT except that instead of dynodes, thin plates of leaded glass with an array of microscopic channels (10-25 μm inner diameter) bored through them. These capillaries are coated on the inside with an electron-emissive material that liberates multiple secondary electrons when struck by an energetic photon. A potential difference on the order of 1kV is placed across the plate, which causes the electrons to accelerate from one side of the plate to the other. Upon exiting the MCP, the secondary electrons typically enter a second and then a third MCP. For each incident electron, gains from 10^4 to 10^8 are

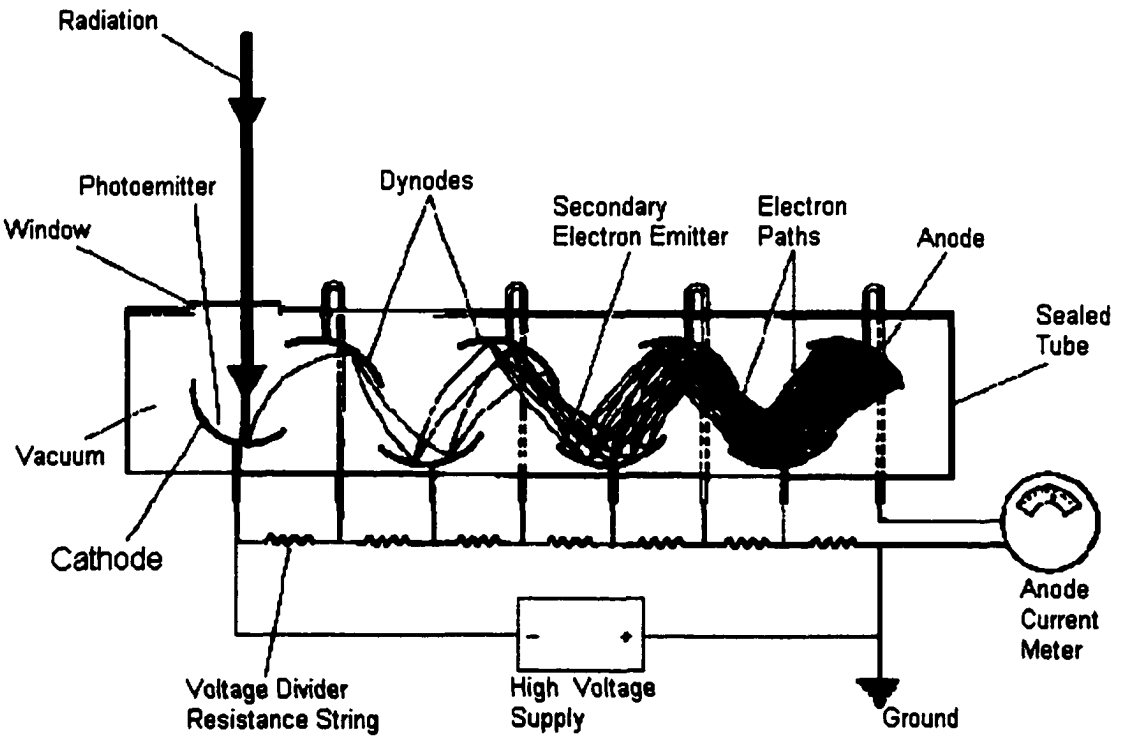

Figure 2.6. Schematic of a Photomultiplier Tube. Light typically impinges through a quartz window and undergoes a cascading photoelectric effect. The photocathode is held at negative one to two thousande volts, which reduces the spontaneous release of electrons.[1]

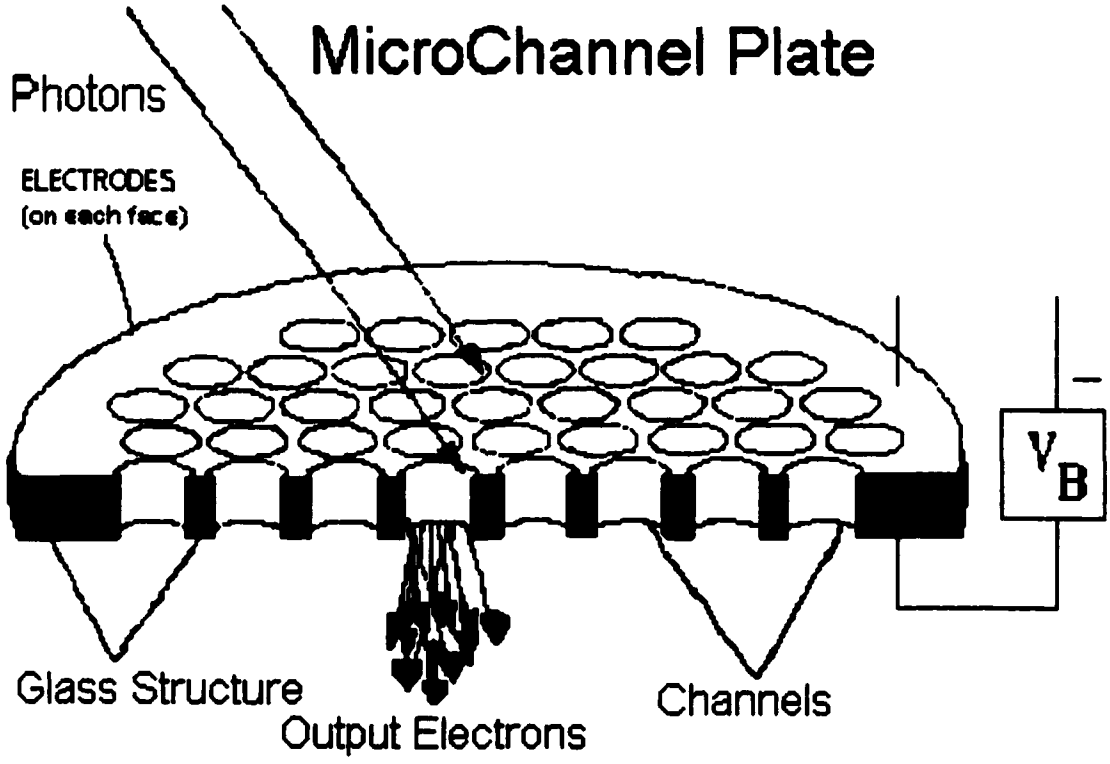

Figure 2.7. Schematic of a microchannel plate, which consists of thin plates of leaded glass with an array of microscopic channels bored through them. The potential difference on the order of 1kV is placed across the plate and causes the electrons to accelerate from one side of the plate to the other.[4]

realized. After passing through the last MCP, the electrons are collected at an anode to create a pulse of current.

2.5.3. Single Photon Avalanche Diodes

Single Photon Avalanche Photodiodes (SPADs) function on similar principles discussed earlier in that they are solid state semiconductors. In this instance, electrons are liberated from silicon after energy is transferred from incoming photons. These photogenerated carrier electrons trigger the flow of an avalanche current, which is sustained by the electric field of a p-n junction reverse biased above the breakdown voltage.[27] (This is in contrast to laser diodes, which are forward biased.) This Geiger mode of operation allows the detector current to remain zero until a carrier, such as a fluorescent photon, reaches the active layer of the p-n junction and triggers the cascade of electrons. This avalanche current continues until it is quenched by lowering the current below the latch current.

The quenching of the avalanche current may be accomplished by either an active or a passive circuit. In a passive situation, the SPAD quenches itself by generating a voltage pulse on a high load resistor (typically 100kΩ).[28] This results in a dead time on the order of a microsecond, which is the period of time the SPAD is unresponsive; as well as erratic operation immediately following the dead time, which may last for several more microseconds. In order to reduce the dead time, an active quenching circuit that applies a quenching pulse to the diode within 20 ns after the onset of the avalanche current, may be employed. The pulses have a magnitude of approximately 1V and when superimposed on the bias voltage shift the operating point above and

below the breakdown voltage. As a result, the dead time is well defined (on the order of 10 ns) and the detector operates under constant and well controlled parameters.[28]

SPADs have a number of advantages compared to PMTs, the most attractive of which is the high time resolution that is on the ps time scale.[29] In addition to this, the SPAD's resolution curve is free from the small secondary peaks observed with many PMTs and the wavelength range covered by their spectral sensitivity extends further into the NIR than PMTs. Their quantum efficiency is as high as 30% at 800 nm. For the applications discussed in this manuscript, SPADs are also attractive because the device is small and rugged. Additionally, the dark counting rate of these devices is low, which results in enhanced sensitivity.[30] One of the primary disadvantages of this type detector is the small active area, which places severe requirements on alignment and focusing.

One of the major advantages of utilizing a SPAD is the small transit time spread they exhibit. The transit time spread in the photon detector is probably the major contributing factor to temporal broadening in TCSPC.[31] The transit time is defined as the time interval between the arrival of a photon at the photocathode and the arrival time of the amplified pulse at the anode. The transit time spread is caused by the difference in the initial velocity, v, of photoelectrons as well as their initial trajectory, which results in different lengths of time for photoelectrons to arrive at the anode. The transit time spread in a SPAD is lower than that of a PMT because of the reduced detection area.

2.6. Timing Electronics

The associated timing electronics usually consist of a constant fraction discriminator (CFD), a multichannel analyzer (MCA), and a time-to-amplitude converter (TAC). As with all discriminators, the CFD eliminates noise associated with the detector. However, this method of discrimination is different from the familiar method of leading edge discrimination, because it samples a fixed fraction of the incoming pulse, inverts it and adds it to the original pulse. Therefore, a timing signal is generated that is independent of the amplitude of the input pulse, which is not the case for leading edge discrimination. The time measuring device is a time-to-amplitude converter (TAC), which calculates the time difference between the electronic start and fluorescence stop signals. The heart of this device is a capacitor that starts charging with the detection of the start pulse (generated from laser) and terminates the process when the electronic stop (generated from detector) is detected. The resulting charge is then converted to a voltage, which corresponds to a time difference between excitation and emission. The time (voltage) value is placed in an appropriate time bin from which a histogram is constructed. The MCA consists of an analog-to-digital converter (ADC) that converts analog signal to digital bits. This serves as the interface between the counting electrons and an oscilloscope or personal computer.

Because these modules (TAC, CFD, and MCA) are typically sold as nuclear instrumentation method (NIM) standards, traditional TCSPC setups required that these pieces of instrumentation be placed in a NIM bin. These NIM bins typically provide voltage at ±6, ±12, and ±24 volts. Additionally, the bins themselves allow multiple NIM modules to be inserted in various configurations that allow for tremendous

flexibility when designing experiments. Unfortunately, these NIM bins are heavy, not amenable to miniaturization, and intimidating to the novice user.

However, recent advances in technology have led to the migration of these electronics from the NIM bin to single TCSPC boards that plug directly into the bus of a standard PC.[26] For example, the set of electronics described in Chapter 4 allows for the collection of 128 sequential decay profiles with a timing resolution of 9.77 ps-per channel and more importantly, the electronics are transparent to the user. Controls such as the discrimination level, the upper and lower limit of the TAC (designates the range during which photons are counted), and the integration time are accessed through a Windows interface. This approach essentially eliminates the need for diagnostic electronics such as multimeters and oscilloscopes as well as the numerous cables required to interconnect the devices.

2.6.1. Discrimination

Discrimination is necessary in most analytical measurements in order to reduce the amount of noise present in the measurement and as a result, enhance the signal-to-noise ratio. In TCSPC, the analytical signal is the output from the fluorescence detector, which is a broad distribution of pulse heights. Because the discriminator determines the level at which noise is distinguished from signal, a reliable and consistent method must be utilized to distinguish between pulses generated by dark noise, single photon events, and multiple photon events. It is important that the discriminator provide pulses that are of constant amplitude and independent of the detector's pulse shape in order to maintain a consistent timing mechanism in the TAC.

Leading edge discrimination and constant fraction discrimination are two methods that may be applied in order to enhance signal-to-noise ratios.

As demonstrated in Figure 2.8, leading edge discrimination (LED) uses a user-defined voltage level to discriminate between noise and signal. However, this method leads to timing errors when applied to a broad distribution of pulse heights as those provided by a PMT. As Figure 2.9 shows, the photons in the pulse distribution of A and B have the same time origin but different pulse amplitudes; as a result, those photons in pulse A appear to arrive faster than the photons distributed in pulse B. Additionally, the timing error is dependent upon the threshold of the discrimination level. In order to counter these timing errors, a constant fraction discriminator may be employed.

As Figure 2.9 shows, a constant fraction discriminator times the pulses from a point on the leading edge that is a constant fraction of the pulse height.[3] This method results in pulses of similar shape but varying amplitude being timed from the same timing point. This is accomplished by feeding an incoming pulse with amplitude V_a into two separate paths and delaying one pulse by an amount δ and inverting it. The time delay, δ, is determined by determining the time difference between the maximum amplitude of the pulse and the amplitude at which timing is desired (point fV_a in Figure 2.10). The other pulse is attenuated to an amplitude fV_a and added to the first pulse to form a zero crossing signal as depicted in Figure 2.10(c). Only those pulses with amplitude greater than a user-defined threshold are timed.

2.6.2. Time-to-Amplitude Converter

As mentioned previously, the time-to-amplitude converter (TAC) measures the time difference between the excitation pulse and fluorescent photon. This is

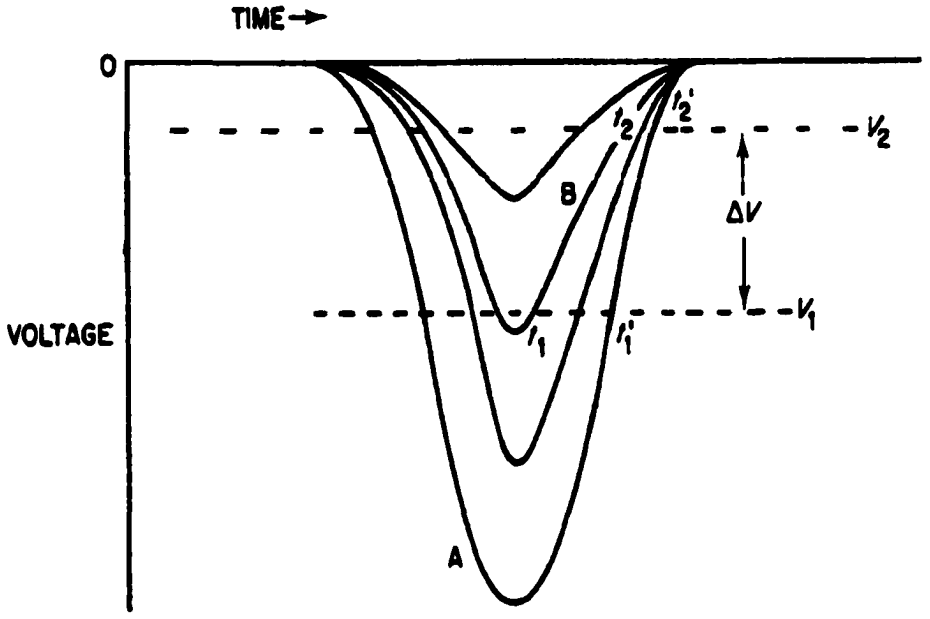

Figure 2.8. Schematic representation of timing errors associated with variable pulse amplitudes and leading edge discrimination. A, B, different amplitude pulses having the same time origin; $t_1 - t_1^1 = \Delta t_1$, timing error at high discriminator level, $-V_1$; $t_2 - t_2^1 = \Delta t_2$, smaller timing error at lower discriminator level, $-V_2$.[1]

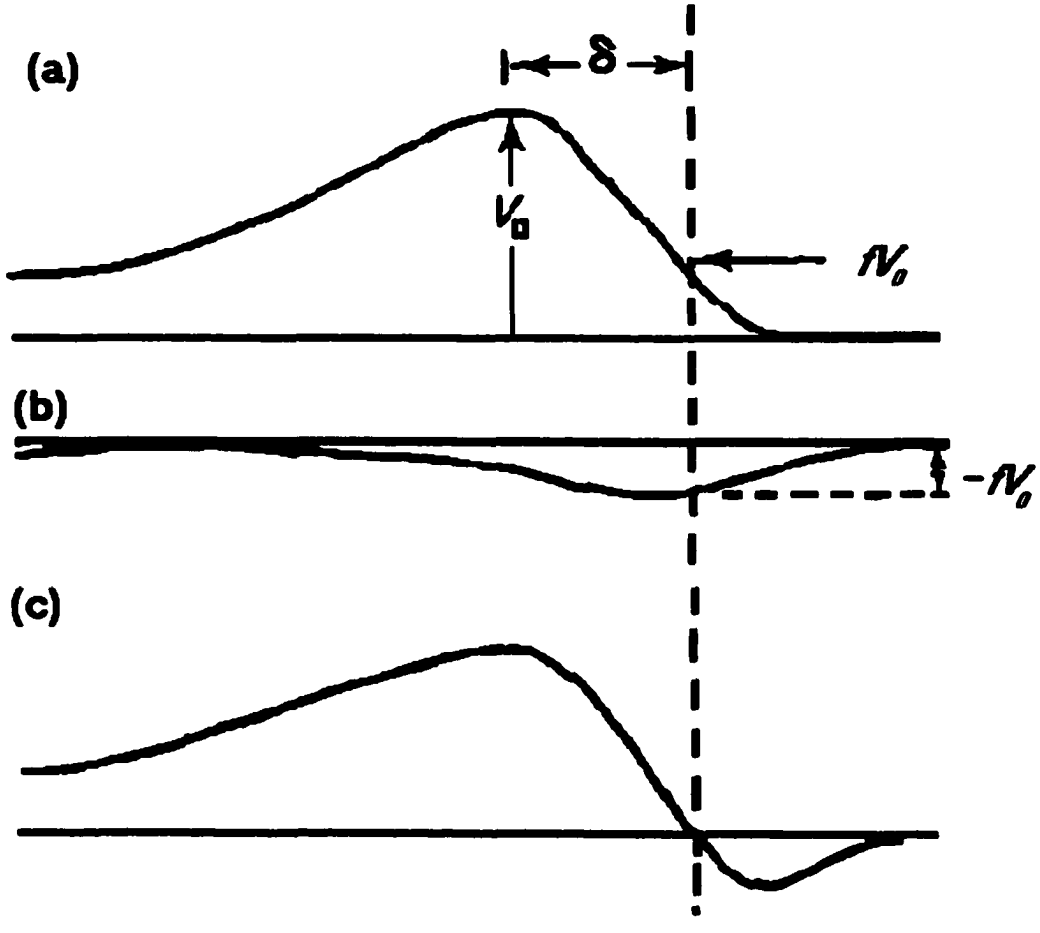

Figure 2.9. Schematic representation of constant fraction discrimination. Timing is from a position on the leading edge that is always a fixed fraction f of the input pulse height. Input pulse not shown. (a) Input pulse (amplitude $-V_a$) inverted and delayed by time δ. (b) Undelayed input pulse attenuated to maximum amplitude $-fV_a$. (c) Zero-crossing pulse (sum of (a) and (b)).[1]

accomplished by linearly charging a capacitor from a constant current source. The start signal from the laser pulse initiates the charging of the capacitor and the stop signal discontinues the charging. The stored charge generates an output pulse whose height is directly proportional to the time difference between the start and stop signals.

Mathematically, this may be expressed through a series of fundamental equations. The capacitance of a resistor is given by;

$$C = q/\Delta V \tag{2.36}$$

where C is the capacitance, q is the charge on the capacitor, and V is the voltage difference between t=0 and t=t_f. Recalling that voltage is defined by;

$$V = i \times R \tag{2.37}$$

where i is the current and R is the resistance and because current is the ratio of charge to time, equation 2.36 may be rewritten as;

$$t = \frac{q \times R}{\Delta V}. \tag{2.38}$$

Thus, the time is inversely proportional to the voltage difference.

2.6.3. Multichannel Analyzer

The multichannel analyzer (MCA) or pulse-height analyzer (PHA) consists of an analog-to-digital converter (ADC) and memory that stores a histogram. The ADC is responsible for measuring the maximum amplitude of an analog pulse and converting the value to a digital number. The digital outputs from the ADC are fed to a dedicated memory and sorted into a histogram that records the number of events counted for each pulse height. This histogram represents the distribution of input pulse heights.

In TCSPC spectroscopy, the MCA measures the output of the TAC and the histogram represents the time distribution of the arriving photons. The combination of the ADC, the histogram memory, and a display of the histogram form a multichannel analyzer (MCA). If a computer is employed to display the spectrum, then the combination of the ADC and the histogram memory is called a multichannel buffer (MCB).

2.7. Instrumental Response

The instrumental response function of a TCSPC system is a convolution of the pulse width of the excitation source, the uncertainty associated with the timing electronics such as the TAC and CFD, and the optical components of the system. This convolution is given by;

$$\Delta t \approx \left[\Delta t_e^2 + \sum_i \left(\Delta t_i^2 \right) \right]^{1/2}, \qquad (2.39)$$

where Δt_i is the full width half maximum (FWHM) of the impulse response of the i^{th} component (e.g., optics, discriminator, or detector), and Δt_e is the FWHM of the excitation pulse.

If the pulse width of the excitation source were infinitely narrow, and if the response were infinitely fast, the observed decay would represent the true decay, or δ-response, of the sample.[3] However, this true response ($G(t-t')$) is distorted by the previously mentioned factors and the fluorescence decay $F(t)$ can be analyzed because $F(t)$ may be expressed as;

$$F(t) = \int_0^t P(t')G(t-t')dt' \qquad (2.40)$$

where $P(t')$ is the convolution of the instrument response function and t' is the variable time delay of the infinitesimally small time widths dt' or channel widths of which $P(t)$ is composed.

2.8. Lifetime Analysis

2.8.1 Nonlinear Least Squares

A non-linear least squares approach is a typical method determining fluorescence lifetimes. In this method, a number of iterations are performed until a best fit is obtained. This is usually determined by evaluating the "goodness of fit" which is defined by χ^2.

Once the time-histograms are constructed, the lifetime must be extracted. This is typically done using a nonlinear least squares algorithm with deconvolution of the instrument response function (IRF). A time-histogram is constructed from a lifetime value and the calculated histogram compared to the experimental data. The comparison is made through a χ^2 value, where χ^2 is calculated from,

$$\chi^2 = \sum_{i=1}^{n} \omega_i \left[R(t) - R_c(t)\right]^2 \qquad (2.41)$$

where R(t) is the experimental data, n is the number of time bins, $R_c(t)$ represents the calculated values and ω_i is a weighting factor ($\omega_i = 1/R(t)$). The pre-exponential factor and the fluorescence lifetime, τ_f, are changed iteratively to best match the calculated decay to the experimental data. This process is continued until χ^2 reaches a minimum. In effect, the χ^2 value is the quantitative measure of the error between the actual data and the fitted function. Equation 2.41 may be recast as;

$$\chi^2 = \sum_N \left[\frac{Y(i) - F_Y(i)}{\sigma(i)} \right]^2 = \sum_N [W(i)]^2 \qquad (2.42)$$

where $Y(i)$ is the value of the fluorescence data point, $F_Y(i)$ is the value of the fitting function, $\sigma(i)$ is the statistical uncertainty of $Y(i)$, N is the number of total number of data points, and $W(i)$ is the weighted residual. Noting that the denominator of equation 2.42 represents the expected deviation from statistical considerations (noise) and the numerator represents the actual deviation between the experimental data point and the data point of the fitted function.[5] If the fitting function is a good match for the experimental data then the weighted residual is unity for each term of the sum and

$$\chi^2 = \text{number of data points (N).} \qquad (2.43)$$

However, one must also consider the number of fitted parameters, therefore, χ^2 may be more accurately represented by;

$$\chi^2 \approx (N - \nu) \qquad (2.45)$$

where ν is the number of fitted parameters. Additionally, a normalized expression for χ^2 would require the division of χ^2 by (N-ν) and χ^2=1 represents the "goodness of fit" mentioned earlier in this section. Unfortunately, the use of this algorithm is calculation intensive and produces large errors for cases where the photon statistics are poor.

2.8.2 Pattern Recognition

Wolfrum has employed a special pattern recognition technique, which is equivalent to the minimization of a log-likelihood ratio where fluorescent decay profiles serve as the pattern for identifying dyes based on lifetimes.[32] This technique utilizes all of the information present in the decay by comparing the measured fluorescence

decay curve to decay curves stored in a spectral database. For every measurement and pattern, the Kullback-Leibler minimum discrimination information;

$$I^*(j) = \sum_{i=1}^{k} n_i \ln\left(\frac{n_i}{Np_i(j)}\right) \tag{2.46}$$

where n_i is the number of counts in channel or bin i (i=1,...,k), for the measurement, k is the number of channels and $p_i(j)$ is the probability that or photon or count will fall in channel i if the molecules are of type j.[32] The $p_i(j)$ represents the experimental patterns and the sum of the counts ($N = \sum n_i$) represents the signal strength. $I^*(j)$ is the measure of the difference between the measurement and the calibration pattern, j. An error analysis of $I^*(j)$ using Cramer's inequality yields the probability to erroneously classify molecules as type h given molecules of type j is;

$$P(h \mid j) \leq \alpha_{hj}^{N}, \tag{2.47}$$

with

$$\alpha_{hj} = \min_{0<\vartheta<1} \sum_{i=1}^{k} p_i(h)^{\vartheta} p_i(j)^{1-\vartheta}, \tag{2.48}$$

where the $p_i(j)$ are the patterns defined above, α is symmetrical in h and j. Identical patterns have α = 1 and the predicted error probability approaches unity, whereas patterns that are different have α values that approach zero. However, qualitatively the error probability depends on the signal strength and as a result a small increase or loss in signal may largely change the error probability.[32] This large change in error probability would be unacceptable in situations where peak heights vary and thus an alternative method must be considered.

2.8.3. Maximum Likelihood Estimator

We have evaluated two simple algorithms for on-line fluorescence lifetime determinations in CE.[33] These methods assume monoexponential behavior and require small amounts of computational time. The first method is the maximum likelihood estimator (MLE) that calculates the lifetime via the following relation[34];

$$1+(e^{T/\tau f}-1)-m(e^{mT/\tau f}-1)^{-1}=N_t^{-1}\sum_{i-1}^{m} iN_i \qquad (2.49)$$

where m is the number of time bins within the decay profile, N_t is the number of photon counts in the decay spectrum, N_i is the number of photon counts in time bin i, and T is the time width of each bin. A table of values using the left-hand side (LHS) of the equation is calculated by setting m and T to experimental values and using lifetime values (τ_f) ranging over the anticipated values. The right-hand side (RHS) of the equation is constructed from CE decay data over the appropriate range of time bins. The fluorescence lifetime may then be determined by matching the value of the RHS obtained from the data with the table entry determined for the LHS of the MLE equation. The relative standard deviation in the MLE may be determined by using;

$$\frac{\sigma_{\tau_f}}{\tau_f}=N_t^{-\frac{1}{2}}\frac{1-e^{\frac{-T}{\tau_f}}}{\sqrt{\left(1-e^{\frac{-T}{\tau_f}}\right)^2-\left(\frac{T}{\tau_f}\right)^2 e^{\frac{-T}{\tau_f}}}} \qquad (2.50)$$

2.8.4. Rapid Lifetime Determination

Fluorescence lifetimes may also be calculated using the rapid lifetime determination (RLD) method, which is performed by integrating the number of counts within the decay profile over a specified time interval and using the following relationship[35];

$$\tau_f = \frac{-\Delta t}{\ln \frac{D_1}{D_0}} \tag{2.51}$$

where Δt is the time range over which the counts are integrated and D_0 is the integrated counts in the early time interval of the decay spectrum, while D_1 represents the integrated number of counts in the later time interval. The relative standard deviation may be calculated from;

$$\frac{\sigma_{\tau_f}}{\tau_f} = \frac{\sqrt{\frac{1}{D_0} + \frac{1}{D_1}}}{Log\left(\frac{D_0}{D_1}\right)} \tag{2.52}$$

where σ_{D_0} is the standard deviation in D_0 and σ_{D_1} is the standard deviation in D_1, determined by taking the square root of the total number of counts in D_1 or D_0.

Previous experimental results have indicated that the inclusion of scattering photons into the MLE or RLD method of lifetime determination results in values biased towards shorter lifetimes.[26] This problem may be overcome by one of two methods. The first technique is a software technique and involves shifting the start

of the calculation a prescribed number of time channels in order to eliminate the effects of scattering photons. Secondly, a hardware technique may be utilized in which the TAC is gated. This scenario involves using a time-gate, in which the TAC processes a prescribed number of channels so that scattering photons are eliminated and as a result never processed by the analog-to-digital converter (ADC). An inherent advantage of this hardware technique is the increased signal to noise ratios observed because of the elimination of background in the form of scattered photons.

It should be noted that when using on-line lifetime measurements in CE, one might also simultaneously acquire the normal intensity electropherogram as well. This is accomplished by binning together all photo-events accumulated into each decay profile for the appropriate integration time, yielding an intensity value. Therefore, the fluorescence intensity versus electrophoresis time can be plotted.

These techniques are important for determining fluorescence lifetimes on-line because of the limited time frame to determine the identity of a component. The primary disadvantage of these techniques is that they assume monoexponential decay and yield only one lifetime in the biexponential case. This becomes disadvantageous in situations where components overlap or a biexponential decay is encountered.

2.9 References

(1) Lakowicz, J. R. *Principles in Fluorescence Spectroscopy*; Plenum Press: New York, NY, 1983.

(2) Flanagan, J. H.; Owens, C. V.; Romero, S. E.; Waddell, E.; Kahn, S. H.; Hammer, R. P.; Soper, S. A. *Analytical Chemistry* 1998, *70*, 2676-2684.

(3) O'Connor, D. V.; Phillips, D. *Time-Correlated Single Photon Counting*; Academic Press (Harcourt Brace Jovanovich, Publishers): New York, 1984.

(4) Mandel, L.; Wolf, E. *Review of Modern Physics* 1965, *37*, 231-287.

(5) Legendre, J., B.L. Doctoral Dissertation, Louisiana State University and Agricultural and Mechanical College, Baton Rouge, LA, 1997.

(6) Lakowicz, J. R. *Topics in Fluorescence Spectroscopy*; Plenum Press: New York, 1992.

(7) Van Hecke, G. R.; Karukstis, K. K. *A Guide to Lasers in Chemistry*; Jones and Bartlett Publishers: Boston, MA, 1998.

(8) Ippen, E. *Applied Physics: B* 1994, *58*, 159-170.

(9) Imasaka, T. *Talanta* 1999, *48*, 305-320.

(10) Coldren, L. A.; Corzine, S. W. *Diode Lasers and Photonic Integrated Circuits*; John Wiley and Sons, Inc.: New York, NY, 1995.

(11) Imasaka, T.; Tsukamoto, A.; Ishibashi, N. *Analytical Chemistry* 1989, *61*, 2285-2288.

(12) Halliday, D.; Resnick, R. *Fundamentals of Physics*, Second ed.; John Wiley and Sons: New York, NY, 1986.

(13) Helkey, R.; Bowers, J. In *SemiConductor Lasers: Past, Present, and Future*; Agrawal, G. P., Ed.; American Institute of Physics: Woodbury, NY, 1995.

(14) Thompson, G. *Physics of Semiconductor Lasers*; John Wiley and Sons: New York, NY, 1980.

(15) Soper, S. A.; Flanagan, J. H.; Legendre, B. L.; Williams, D. C.; Hammer, R. P. *IEEE Journal of Selected Topics in Quantum Electronics* 1996, *2*, 1129-1139.

(16) Bachteler, G.; Drexhage, K. H.; Ardenjacob, J.; Han, K. T.; Kollner, M.; Muller, R.; Sauer, M.; Seeger, S.; Wolfrum, J. *Journal of Luminscence* 1994, *62*, 101-108.

(17) Bachteler, G.; Drexhage, K. H.; Ardenjacob, J.; Han, K. T.; Kollner, M.; Muller, R.; Sauer, M.; Seeger, S.; Wolfrum, J. *Journal of Luminescence* 1994, *60-1*, 511-514.

(18) Imasaka, T.; Yoshitake, A.; Hirata, K.; Kawabata, Y.; Ishibashi, N. *Anaytical Chemistry* 1985, *57*, 947-949.

(19) Zhang, Y. L.; Soper, S. A.; Middendorf, L. R.; Wurm, J. A.; Erdmann, R.; Wahl, M. *Applied Spectroscopy* 1999, *53*, 497-504.

(20) Muller, R.; Zander, C.; Sauer, M.; Deimel, M.; Ko, D. S.; Siebert, S.; Ardenjacob, J.; Deltau, G.; Marx, N. J.; Drexhage, K. H.; Wolfrum, J. *Chemical Physics Letters* 1996, *262*, 716-722.

(21) Imasaka, T.; Yoshitake, A.; Ishibashi, N. *Analytical Chemistry* 1984, *56*, 1077-1079.

(22) Lieberwirth, U.; Arden-Jacob, J.; Drexhage, K. H.; Herten, D. P.; Muller, R.; Neumann, M.; Schulz, A.; Siebert, S.; Sagner, G.; Klingel, S.; Sauer, M.; Wolfrum, J. *Analytical Chemistry* 1998, *70*, 4771-4779.

(23) Muller, R.; Herten, D. P.; Lieberwirth, U.; Neumann, M.; Sauer, M.; Schulz, A.; Siebert, S.; Drexhage, K. H.; Wolfrum, J. *Chemical Physics Letters* 1997, *279*, 282-288.

(24) Sauer, M.; Ardenjacob, J.; Drexhage, K. H.; Marx, N. J.; Karger, A. E.; Lieberwirth, U.; Muller, M.; Neumann, M.; Nord, S.; Paulus, A.; Schulz, A.; Seeger, S.; Zander, C.; Wolfrum, J. *Biomedical Chromatography* 1997, *11*, 81-82.

(25) Soper, S. A.; Legendre, B. L.; Williams, D. C. *Analytical Chemistry* 1995, *67*, 4358-4365.

(26) Legendre, B. L.; Williams, D. C.; Soper, S. A.; Erdmann, R.; Ortmann, U.; Enderlein, J. *Review of Scientific Instruments* 1996, *67*, 3984-3989.

(27) Li, L.-Q.; Davis, L. *Review of Scientific Instruments* 1993, *64*, 1524-1529.

(28) Cova, S.; Longoni, A.; Ripamonti, G. *IEEE Transactions on Nuclear Science* 1982, *NS-29*, 599-601.

(29) Cova, S.; Longoni, A.; Andreoni, A.; Cubeddu, R. *IEEE Journal of Quantum Electronics* 1983, *QE-19*, 630-634.

(30) Cova, S.; Lacaita, A.; Zappa, F.; Lovati, P. *SPIE Proceedings: Advances in Fluorescence Sensing Technology II* 1995, *2388*.

(31) Bebelaar, D. *Review of Scientific Instruments* 1986, *57*, 1116-1125.

(32) Kollner, M.; Fischer, A.; Ardenjacob, J.; Drexhage, K. H.; Muller, R.; Seeger, S.; Wolfrum, J. *Chemical Physics Letters* 1996, *250*, 355-360.

(33) Soper, S. A.; Legendre, B. L. *Applied Spectroscopy* 1994, *48*, 400-405.

(34) Hall, P.; Selinger, B. J. *Physical Chemistry* 1981, *85*, 2941-2946.

(35) Ballew, R. M.; Demas, J. N. *Analytical Chemistry* 1989, *61*, 30-33.

Chapter 3

A Fiber Optic Based Multichannel Time-Correlated Single Photon Counting Device with Subnanosecond Resolution

3.1. Introduction

Time-Correlated Single Photon Counting (TCSPC) is a powerful technique that allows one to probe the excited states of molecules as well as the molecule's environment and has been used in a variety of photophysical and biophysical studies, such as molecular associations, protein dynamics and excited-state reactions.[1-5] In addition, time-resolved fluorescence measurements can be used to identify chromophores in analytical applications. The power of TCSPC results from its broad dynamic range, single photon sensitivity and favorable time resolution that can be achieved when appropriate instrumental components are used. In most cases, the instrument response function (IRF) of the measuring device must be less than the upper state lifetime of the chromophoric system under investigation. The instrumental components which primarily determine the time resolution (formal width at half maximum of IRF) are the light sources used for excitation and the photon transducer. In many TCSPC experiments, the excitation source is a mode-locked laser that can produce picosecond to sub-picosecond light pulses at high repetition rates. In terms of the detector, it must produce low transit time spreads and operate in a photon counting mode with high quantum efficiencies at the monitored wavelengths. The detectors that typically meet these criteria are microchannel plate PMs, photomultiplier tubes and single photon avalanche diodes (SPADs).

In most cases, TCSPC is done with a single channel, in which the time-resolved fluorescence is excited with a single source and processed on a single detection channel.

However, in many cases, it would be advantageous to conduct TCSPC experiments in a multichannel format. One example where a multichannel lifetime-based measurement system would be advantageous includes imaging applications. Time-resolved imaging systems developed to date typically employ resistive anode microchannel plates in which the time-resolved data is imaged onto a two-dimensional resistive plate in order to obtain spatial information with the time-resolved data processed in a conventional fashion.[6-8] Recently, Birch described a sixteen-channel lifetime imaging camera which used TCSPC to process time-resolved data.[6] In this work, the investigators developed an application specific integrated circuit used in conjunction with a multianode multichannel plate photomultiplier (MCP-PM). The spatial distribution of fluorescence lifetime contours of a strongly self-absorbing sample was observed. Courtney described a multichannel device in which 1024 decays were collected simultaneously on 1024 spectral channels.[8] One thousand twenty-four fluorescence decays as a function of emission wavelength were recorded for one sample using a resistive anode array (RAD) coupled to one constant fraction discriminator (CFD) and one time-to-amplitude converter (TAC). These imaging systems are particularly appropriate for microscopy applications, where the high spatial resolution required can be easily decoded from the information obtained from the resistive anode plate without sacrificing timing resolution afforded by the microchannel plate.

In some applications, it is beneficial to have the ability to monitor various experiments simultaneously and independently of one another in order to increase sample throughput when lifetime-based measurements are used for detection. For example, in sensing applications using fluorescence lifetimes for transduction, the fluorochrome, which in the ideal case monitors one specific target, is immobilized onto the end of a fiber optic

(F/O).[9-18] If multiple targets would need to be screened in a single sample, it would be necessary to simultaneously monitor the output of multiple fiber sensors. While the resistive anode array detectors could be configured in such a manner to monitor multiple F/O based time-correlated single photon counting experiments, it would require special attention to the imaging optics. A resistive anode array would also require a confined arrangement of the multiple experiments being monitored (i.e., reduced flexibility). The ideal multichannel TCSPC system for this application would permit expandability and spatial flexibility in that additional experiments could easily be added and the measurements could be performed on multiple samples in any type of platform.

In another example, several groups have suggested that lifetime-based identification methods can be used for calling bases in DNA sequencing applications.[19-27] In this format, the oligonucleotides prepared using standard Sanger chain termination methods are labeled with fluorochromes that possess unique fluorescence lifetimes. Since the sequencing process requires an identification of one of the four constituent bases comprising the oligonucleotide, four unique lifetime probes are needed. The lifetime measurement can then be made during the electromigration of these unique-sized oligonucleotides through a fractionating gel matrix. While fluorescence lifetime-based systems have been developed for identification of bases in single channel experiments, for high throughput applications it will be necessary to scale up the experiment to monitor many sequencing lanes running in parallel. One approach is to develop a scanning system in which the laser and collection optics are rastered over a series of fractionating channels.[28] However, the difficulty associated with this approach is that losses in signal can result due to lowering of the duty cycle. This problem is compounded in lifetime-

based applications, since the precision in the lifetime measurement requires high counting statistics (high numbers of photocounts in the decay profile).[29]

Near-infrared fluorescence monitoring can be particularly attractive for lifetime-based applications where high sensitivity is necessary. This is because interference's in the form of scattering and impurity fluorescence are minimal in the near infrared. The reduction of this interference leads to dramatic improvements in the precision and accuracy of a lifetime-based measurement, especially when dealing with low photon numbers (poor statistics).[30, 31] In addition, the instrumentation that can be implemented in the near infrared can be much simpler than that used in the visible excitation. This is because solid state diode lasers can potentially be used for excitation in place of mode-locked ion or YAG lasers.[23, 25] The diode laser can be operated in a pulsed mode by seeding the diode with a current source that generates temporally narrow current pulses. Unfortunately, in the near infrared, microchannel plates are difficult to use due to their low quantum efficiencies when monitoring wavelengths above 800 nm. As such, multichannel TCSPC experiments using resistive anode array microchannel plates would be difficult.

In this chapter, the development and operational characteristics of a multichannel, time-resolved instrument using single mode F/Os will be discussed. The system to be described consists of 12 separate channels, which use single mode F/Os to carry the laser light from a single source to 12 channels via F/O splitters. The time-resolved emission is collected by another series of twelve single mode fibers. The light is processed on three separate single photon avalanche diodes after demultiplexing using three single mode mechanical switch boxes. Therefore, the system is a composite of a multichannel format (three detectors) to improve the duty cycle (higher signal-to-noise ratio) and a multiplexed

system, in order to increase system throughput without significantly adding instrumental complexity to the TCSPC device. In addition, the source used for excitation is a passively mode-locked Ti:Sapphire laser that produces transform limited pulses at high repetition rates and average powers of approximately 1 W in the near-infrared. Since the pulses are transform limited, special attention was focused on analyzing the time evolution of these transform limited pulses after traveling through relatively long distances of single mode fibers and its affect on the timing resolution of the device. The optical design of this 12 channel system, the electronics required to process the fluorescence and the operational characteristics of this novel multi-channel, fiber-optic-based TCSPC instrument will be discussed.

3.2 Instrumentation

The excitation source consisted of a mode-locked Ti:sapphire laser which was pumped by the multiple line output of a small frame Argon Ion laser (Mira-900F and Innova 310, respectively; Coherent Lasers, Palo Alto, CA). The Ti:sapphire laser operated at a repetition rate of 76 MHz generating nearly transform-limited pulses with a temporal width of 148 fs (autocorrelation trace) and a bandwidth of 12.9 nm. The light was vertically polarized with a tunable output from 760 to 1100 nm with the appropriate optics set installed into the laser cavity.

3.2.1 Fiber Delivery System

The output of the pulsed laser source was split into three beams of equal intensity by first passing the light through a 70/30 beam splitter and subsequently passing the seventy percent beam through a 50/50 splitter (see Figure 3.1). A quarter-wave and half-wave plate were used to rotate the beams to achieve the best possible coupling efficiency

into each of three single mode fiber couplers and to equalize the power into each of the three beam legs. The single mode fiber couplers were obtained from Optics for Research (Model PAF-X-780, Caldwell, NJ). These couplers consisted of a fish eye lens (aspheric) mounted with a magnet and leaf spring to optimize the alignment of the beam spot onto the face of the single mode fiber by using simple precision setscrews. On the back end of each coupler, a single mode fiber was attached with the use of an SMA connector, which allowed one to easily change fibers with minimal set-up time and loss in coupling efficiencies. The bare end of each fiber was attached to the input of a one-by-four single mode F/O splitter, which equally split the light into four fibers (Metro-Tek Industries, Elmsford, NY). The connection of the bare fiber (from laser) to bare fiber (splitter) was accomplished using a reusable single mode fiber-to-fiber mechanical splice (Metro-Tek Industries, Inc.) This device consisted of a small diameter capillary filled with optical coupling gel. Each fiber was cleaved using a fiber cleaver (MR1, Photon Kinetics, Inc., Beaverton, OR) and then inspected under a stereomicroscope to assure the ends were blunt, which was required to achieve optimal coupling efficiency. This procedure effectively produced twelve identical light sources from one solid state laser. Similarly, fluorescence emission was collected by a series of twelve, bare end single mode fibers, each of which was fed into one of three single mode F/O mechanical switches (model MFSW-1 x 4, E-Tek Dynamics, Inc., San Jose, CA) which possessed one output fiber and allowed rapid demultiplexing of the time-resolved signals and directing the output onto one of three photon transducers. The single mode F/O mechanical switch consisted of a prism whose positioning was controlled by a solenoid and allowed rapid switching between the four F/O input lines. The switch would operate at a maximum switching rate of approximately 10

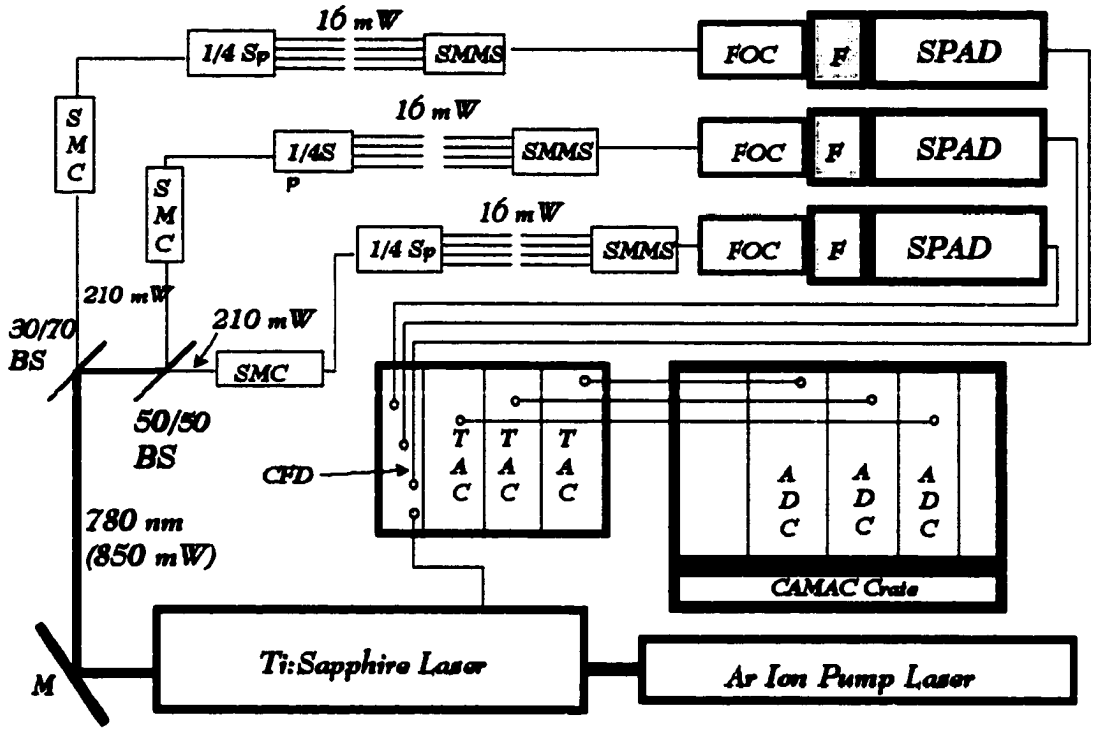

Figure 3.1. Optical System for a multichannel, fiber optic based time-correlated single photon counting system. TAC, time-to-amplitude converter; SMC, single mode coupler; FOC, fiber optic coupler; ADC, analog-to-digital converter; F, filter; CFD, constant fraction discriminator; BS, beam splitter.

Hz with a transition time of ~10 ms. The output emission from each switch was then collimated with the use of a single mode fiber coupler purchased from Newport Corporation (Mountain View, CA). The coupler consisted of a F/O chuck mounted on a two-way stage and a 20X microscope objective to gather and collimate the output of the F/O. The collimated light was then passed through a set of spectral filters in order to reduce the amount of background generated from scattered light coincident with the laser wavelength. This filter set consisted of a dielectric interference bandpass filter (Omega Optical, Brattleboro, VT) possessing a center wavelength of 830 nm and a half-bandwidth of 15 nm, and a longpass filter with a cutoff wavelength of 820 nm. The light was then passed through a 12X microscope objective to focus the emission onto the 150 μm diameter active area of a single photon avalanche diode (SPAD, EG&G Optoelectronics Canada, Vaudreuil, Canada). The 12X microscope objective in conjunction with the 20X objective used for beam collimation produced a beam waist of less than 20 μm at the face of the SPAD. The small size of the imaged radiation onto the face of the photoactive area of the SPAD is necessary in order to optimize the timing response of the device.[32]

3.2.2 Electronic System

The layout of the electronic system for processing the time-resolved data is shown in Figure 3.2. In this device, the start (synchronization) pulse for each of three, single channel time-to-amplitude converters (TAC, Tennelec TC 863, Oak Ridge, TN) was generated by an external cavity photodiode monitoring the pulse train of the Ti:sapphire laser and conditioned by one channel of a four-channel constant fraction discriminator (CFD, Tennelec TC 754, Oak Ridge, TN). The synchronization pulse was fed into a NIM-bin-based logic fan in/fan out that generated three NIM pulses from the input pulse, which

were subsequently fed into the start input of each TAC. The output pulses from the three SPADs were conditioned by the CFD and sent into the gate and stop inputs of the appropriate TAC. The TAC was operated in a gated-mode of operation, in that the conversion rate was set by the photon counting rate.[33]

The program for data acquisition and experimental control was written in C using National Instruments LabWindows/CVI for the SUN workstation (Austin, TX). The program was run on a workstation SUN Sparc IPC running under SunOS™4.1.1 and OpenWindows™ Version 2 (Mountain View, CA). Except for the drivers used for interfacing the workstation to the Computer Automated Measurement and Control (CAMAC) crate (KineticSystems Corporation, Lockport, IL), the program is fully portable to other computer platforms under the LabWindows environment. A graphical user interface (GUI) allowed easy access to all experimental parameters such as integration time, length of experiment, and F/O switching rate. The CAMAC modules used for data processing consisted of two, two channel ADCs (Jorway model S32, Spring Valley, NY), a twelve channel counter (LeCroy model 2551, Spring Valley, NY), three List Sequencers (Kinetic Systems model 3982) and the SCSI crate controller (Kinetic Systems 3929). The List Sequencers served as temporary storage devices (FIFO registers) and allowed storage of up to 16K bytes of information. In addition, a short list of instructions could be loaded into each of the List Sequencers. The use of these particular modules allowed processing of higher photon counting rates and faster data transfer rates. In these experiments, four channels were monitored sequentially for a period of 250 ms. The TAC output was converted to a digital signal using the 12 bit analog-to-digital converters (ADCs) in the

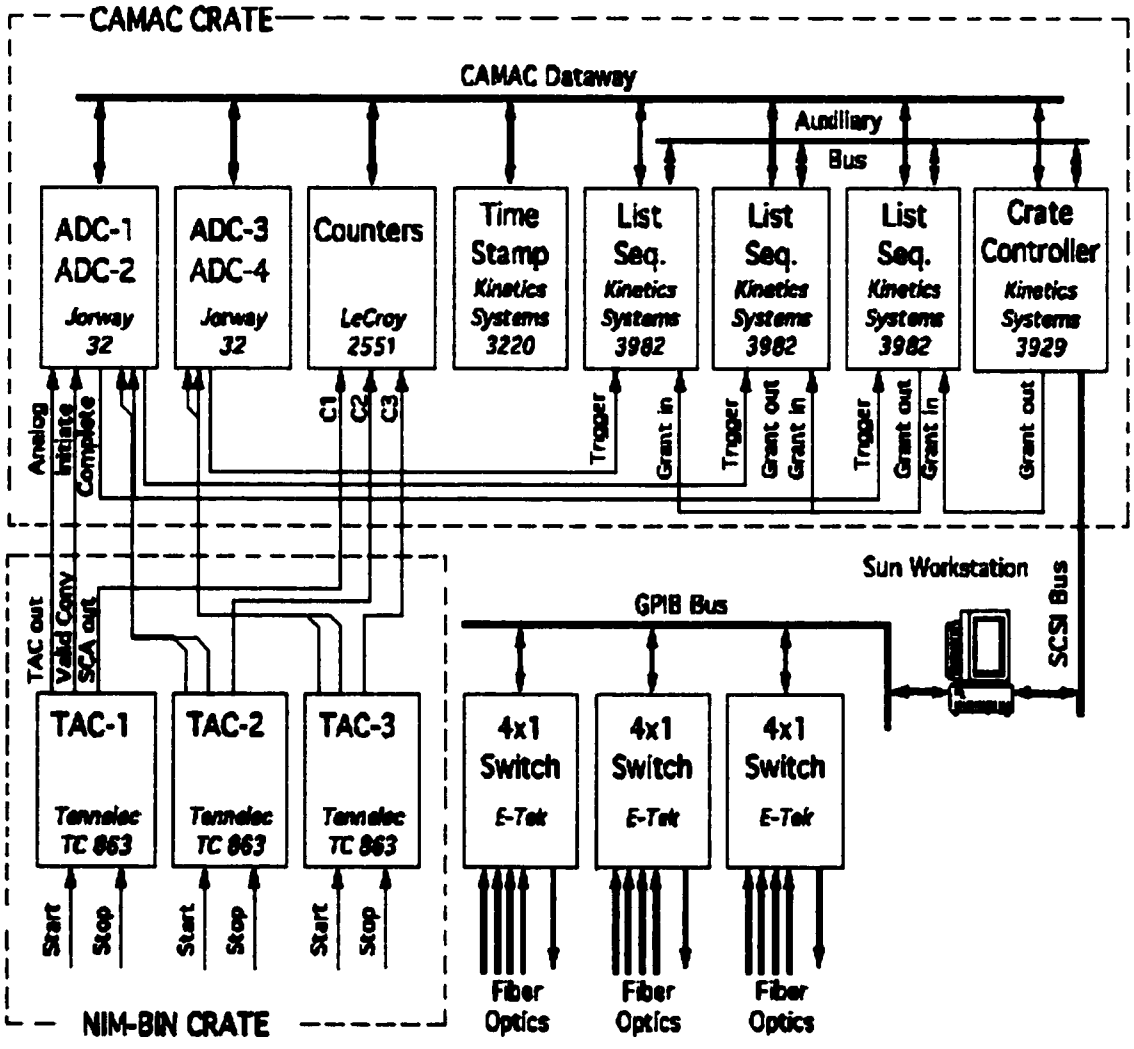

Figure 3.2. Electronic layout for multichannel, fiber-optic-based time correlated single photon counting (TCSPC) device. The output pulses from the three SPADs are processed on the multichannel electronic system above and the data analyzed by the SUN workstation. ADC, analog-to-digital converter; TAC, time-to-amplitude converter; SCA, single channel analyzer; SCSI, small computer system interface

CAMAC crate. The ADCs were triggered by the valid conversion output of the TAC. The ADC conversion of the TAC occurred within the 250 ms time frame whereupon the conversion was added to previously accumulated values within the appropriate time bin for the particular decay being constructed and was determined by the position of the F/O switch. The switching of the F/O mechanical switch was controlled by the SUN workstation through the GPIB interface. This configuration allowed up to 50,000 events per second of data per detection channel to be collected without loss. At the beginning of the experiment, all counters were cleared, the 16 KB FIFO registers in each List Sequencer were emptied, and short NAF lists (instructions) were sent to each List Sequencer. These instructions were carried out each time a valid photon was detected. Auxiliary bus control in the CAMAC crate and grant out/grant in chain commands eliminated the dataway access collisions. Once the FIFO registers were filled, the blocks of FIFO data were streamed through the CAMAC dataway and to the hard drive of the workstation via the SCSI port.

3.2.3. Autocorrelation

The temporal width of the transformed-limited laser pulses were evaluated using an autocorrelator obtained from Clark Instruments (Model AC-1, Pittsford, NY). In these measurements, a 1 m length of single mode polarization preserving fiber was used since the autocorrelation signal was obtained from the second harmonic signal generated from a $LiIO_3$ crystal. The light emanating from the fiber was collimated and directed into the autocorrelator via steering mirrors. The spectral content of the laser pulses was measured by feeding the laser pulses into a spectrograph (Jobin-Yvon, CP200, Cedex, France) and imaging the dispersed spectrum onto a linear diode array (EG&G, RC1000, Sunnyvale, CA). The spectral resolution was determined by the linear dispersion of the spectrograph

and the pixel size of the diode array (25 μm). In both the temporal and spectral measurements, the analog output was read from a digital oscilloscope (Tektronix, Model TDS 520, Beaverton, OR).

3.3. Results and Discussion

3.3.1 Temporal and Spectral Width of Laser Pulses Traveling in Single Mode Fibers

The Ti:sapphire was used as the excitation source for this instrument due to the solid-state nature of the laser, the ability to produce reasonably high average powers in the NIR and also, the tunability of the laser across a wide range of wavelengths in the NIR. Since the Ti:sapphire laser produces pulses that are sub-picosecond in width and have a broad spectral content, it was necessary to evaluate the ability to transport these laser pulses through extended lengths of optical fibers and to determine the degree of pulse broadening that could result. Two prominent factors that can broaden these pulses are group velocity dispersion (GVD, linear effect) and self phase modulation (SPM, nonlinear effect).[34] GVD results from the wavelength dependent refractive index associated with the glass fibers used for transporting the pulses. The temporal width (T_1) of a pulse traveling in a fiber of length Z can be calculated from the simple relation;

$$T_1 = T_0\{1 + (2Z / L_d)\}/2 \qquad (3.1)$$

where T_o is the initial pulse width and L_d is the dispersion length determined from T_o^2/β_2, where β_2 is the dispersion factor (ps^2/cm).[34] For fused silica fibers transporting light at 800 nm, the value of β_2 is 30 ps^2/km, where the positive sign indicates that the dispersion is normal (red wavelengths travel faster than blue wavelengths). For a 1 m length of fiber and

an initial pulse width of 148 fs, pulses would be expected to possess a width of approximately 350 fs using equation (1) and the values cited above. In Figure 3.3A is shown the autocorrelation trace for the Ti:sapphire laser pulses traveling through no fiber and 1 m of polarization preserving fiber. As can be seen, the pulse width was 198 fs (FWHM), less than that predicted using equation 1 and the dispersion factor for fused silica fiber at 800 nm. The observed result likely arises from the fact that the laser pulse produced from the Ti:sapphire laser is chirped due to non-equal GVD compensation produced by the prism pair found within the laser cavity used to correct for this effect. If the laser pulse is chirped, then the time-bandwidth product would be greater than its theoretical value for a purely transform limited pulse. The time-bandwidth for a packet of light with a temporal pulse width (τ_P) and a spectral bandwidth ($\Delta\upsilon$) is given by;

$$\text{time-bandwidth product} = TB = \tau_P \, x \, \Delta\upsilon. \qquad (3.2)$$

For a transform limited pulse with a hyper-secant squared shape, the time-bandwidth product should be 0.32. Calculation of the time-bandwidth product for the Ti:sapphire laser yielded a value of 0.79, consistent with a slight frequency chirp. In the absence of this frequency chirp, the pulse would be expected to broaden more. Therefore, sacrificing laser pulse width by introduction of a frequency chirp will help to maintain the temporal characteristics of the laser pulse after being transported through extended lengths of optical fiber.

The spectral content of the laser pulse before and after being transported in the single mode fiber was then measured. Figure 3.3B shows the spectral content in both cases and as can be seen, very little spectral broadening was observed. In the no fiber case, the spectral content was 12.9 nm (FWHM) while for the fiber the value was 13.1 nm (FWHM).

Significant spectral broadening for propagating ultrashort pulses in optical fibers typically results from SPM, which is produced by the intensity-dependent nature of the refractive index of the medium and is a nonlinear process which depends on the third order susceptibility of the medium ($\chi^{(3)}$).[34] The extent of SPM can be calculated from the expression;

$$L_{nl} = \frac{1}{\rho P_0} \qquad (3.3)$$

where L_{nl} is the nonlinear length, P_0 is the peak power of the laser pulse and ρ is related to the nonlinear-index coefficient n_2 and has a value of approximately 3 W^{-1} km^{-1}. In the present case, approximately 1 mW of average laser power was launched into the single mode fiber. Therefore, at the pulse repetition rate of the Ti:sapphire laser (76MHz) and a pulse width of 148 fs (P_0=88 W), L_{nl} = 4 m. In this case the fiber length (Z) was 1 m and since $Z < L_{nl}$, little SPM would be expected, consistent with our observed results (minimal spectral broadening). As stated above, the time-bandwidth product of the pulses produced by our Ti:sapphire laser was found to be 0.79. For the case where the pulses were launched into the polarization-preserving fiber, the time-bandwidth product was determined to be 0.97. While some distortion of the pulse was observed, it was minimal and should not affect the timing response of the multichannel TCSPC instrument to any appreciable extent. The timing resolution would be expected to be limited by the transit time spread associated with the photon transducer.

The coupling and transport efficiency of the various components used in the multichannel, F/O-based TCSPC instrument is summarized in Table 3.1. In order to couple

(A)

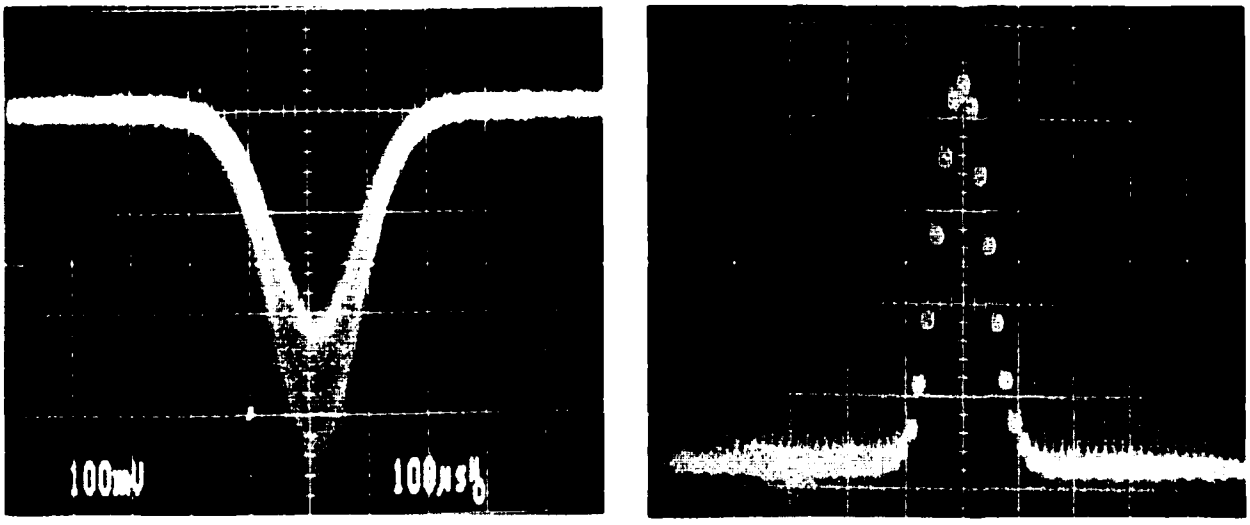

(B)

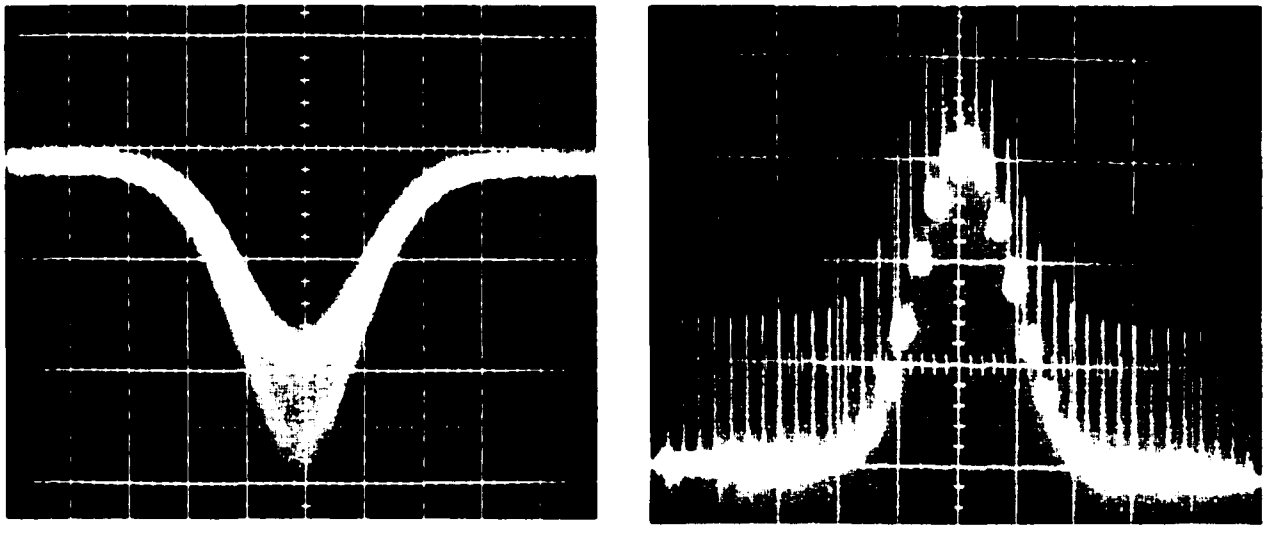

Figure 3.3. (A) Oscilloscope traces of temporal widths of Ti:Sapphire laser pulses traveling through no fiber (161.3 fs) and spectral images from a linear diode array showing the spectral content of the direct output(12.9 nm). The traces represent the direct output of the autocorrelator. (B) Oscilloscope traces of temporal widths of Ti:Sapphire laser pulses traveling through 1 m of polarization preserving fiber (198.3 fs) and spectral images from a linear diode array after traveling through 1 m of polarization preserving fiber(13.1 nm).

the light from the Ti-Sapphire laser into three separate legs, a series of turning mirrors, beam splitters, and polarizers in conjunction with simple alignment F/O ports was utilized. These ports rely on a single fish eye lens held in place by a magnet to focus light onto the 8 μm core of the single mode optical fiber. Due to the interdependent nature of our F/O system, coupling ratios of 5-6 dB were typically observed at this interface.[35] The power loss in dB is determined by;

$$dB = 10 \log \frac{P_{in}}{P_{out}}, \qquad (3.4)$$

where P_{in} is the input power and P_{out} is the output power. It was possible to achieve coupling ratios as low as 3 dB in one coupler at the sacrifice of the other two (ratios rose to 10 dB). The transmission of 800 nm light through the one-by-four F/O splitter was determined to be 0.45 dB. This was a composite of coupling a single mode fiber used to transport the laser light to the bare silica fiber associated with the splitter as well as the transmission efficiency of this splitter. The insertion loss for the two ends of the bare silica fiber was estimated to be 0.04 dB and it was concluded that the majority of this loss is associated with the splitter. The output splitting efficiency of this device was determined and it was found that the light was split equally (within experimental error) between the four fiber outputs.

TABLE 3.1. Coupling and transmission efficiencies of various components used in the NIR, F/O time correlated single photon counting device.

Component	Coupling/Transmission Efficiency
Fiber Port (Laser-to-Fiber)	5-6 dB
Single Mode Fiber-to-Fiber Splicer	0.04 dB (insertion loss)
1 x 4 Single Mode Mechanical Switch	0.45 dB
1 x 4 Single Mode Splitter	1.24 dB (overall loss)

The next set of F/Os used in the system are the terminal ends of the mechanical switch fibers, which serve as the fluorescence collection fibers used in the time-resolved luminescence measurement. The one-by-four F/O switch consists of four single mode optical fiber inputs that are switched sequentially to one common fiber output. The return loss through this device was stated to be >30 dB[35] with an overall transmission loss of <1.24 dB. In addition, no crosstalk was observed between the four input optical lines. The switching time (dead time) associated with this F/O switch when the switch was operated at 5.5 Hz was measured. It was determined that the switch could change between the various input fibers with a dead time of ~10 ms. Therefore, the duty cycle in this case was determined to be 24%, close to the limit of 25% for a 4 channel device. This dead time was independent of the measurement time.

3.3.2. Instrument Response Function of Device

The instrument response function of the system was determined using a series of three SPAD detectors and scattering produced from the laser with excitation and collection fibers arranged in a 180° configuration. The IRF is typically a convolution of the pulse width of the laser and response time of the electronics, detectors, and optics. In these series of experiments, the excitation fibers had a total length of 10 m and the collection fibers a length of approximately 1.5 m. In addition, the light traveled through the 1 x 4 F/O splitter, and the 1 x 4 F/O mechanical switch. In Figure 3.4 is shown a series of IRF functions collected from the 12-channel F/O system. As can be seen, the average IRF time width was 181 ps (FWHM) with a standard deviation of +/- 3.0 ps. Also apparent from Figure 3.4 is that the position of the prompt peak within the function was shifted between the various channels of the device. This is a result of the different length of fibers that the

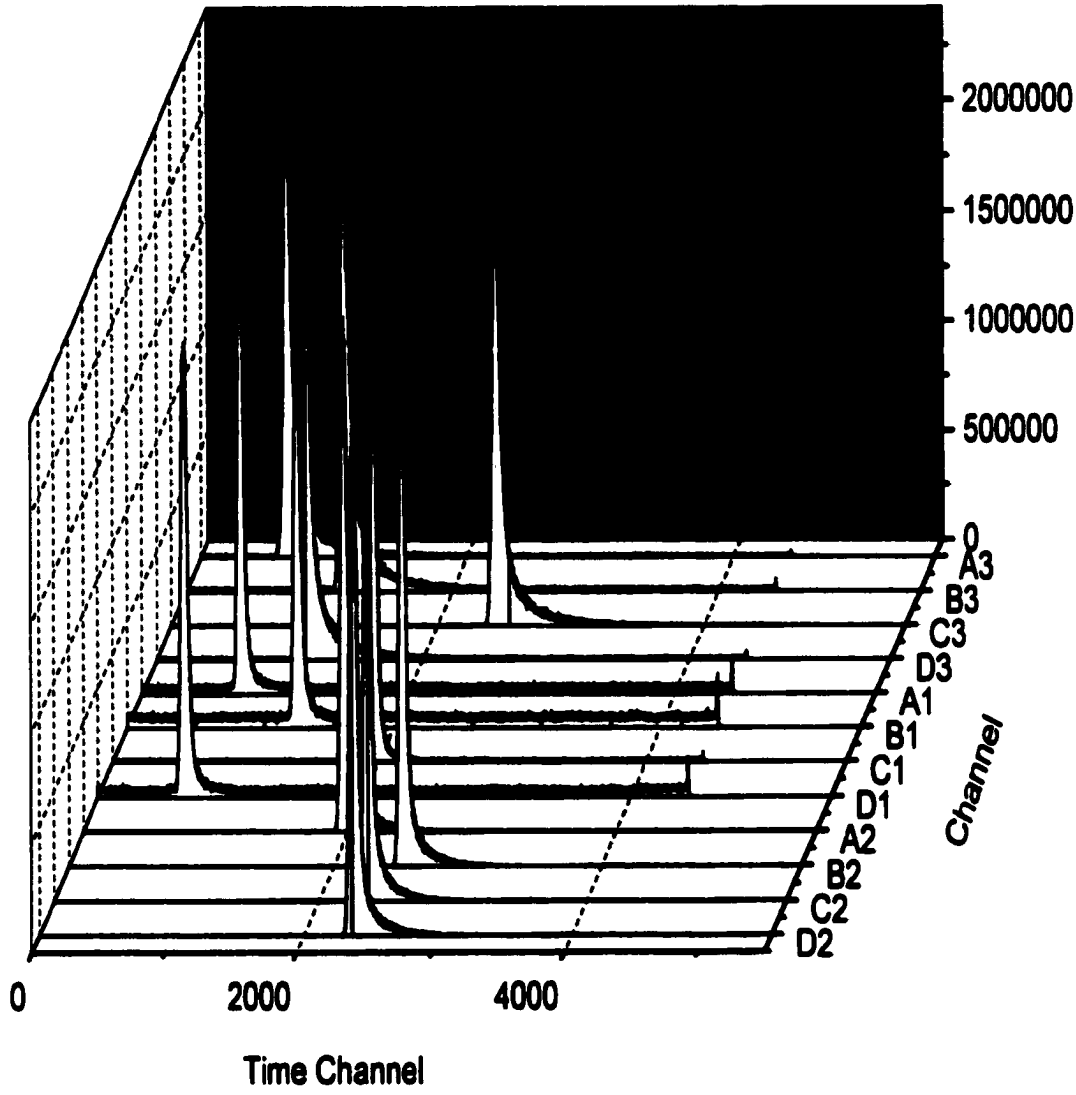

Figure 3.4 Instrument response functions for 12-channel, fiber optic NIR time correlated single photon counting device. The average lifetime of these 12 functions was found to be 181 ps ± 3.0 ps.

light traversed for each channel. The IRF of this system (single channel) when both the excitation and scattered light did not travel through the fibers was measured and determined to be 176 ps (+/- 1.4 ps). Therefore, although pulse broadening produced by the optical fibers for both the laser and scattered radiation is expected, the transit time spread produced by the detector is the major factor contributing to the observed IRF temporal width since the fiber and no-fiber IRFs possessed similar FWHM.

3.3.3 Fluorescence Lifetime Measurement Determination of Aluminum 2,3-Tetrasulfonated Naphthalocyanine

The measurement of the fluorescence lifetime of a NIR fluorochrome was carried out using the fiber-optic-based TCSPC instrument. In this experiment, the lifetime of the fluorochrome, Al-tetrasulfonated naphthalocyanine, was determined in DMSO by inserting both F/Os (excitation and emission fibers) into a drop of liquid containing the fluorochrome at a concentration of 1 μm. The fibers were oriented at 90° with respect to each other by placing each fiber in a magnetic fiber holder (Newport Instruments). The fiber used for collection was mounted on a three-axis microtranslation stage in order to situate it as close as possible to the excitation fiber. A drop of the dye solution was suspended at the end of a 1 ml syringe and slowly moved into the intersection of the collection and excitation fibers. In Figure 3.5 the IRF function of the DMSO blank is shown along with the resulting decay. Inspection of Figure 3.5 reveals that a significant amount of scatter was observed in the resulting decay, even at this relatively high dye concentration. This is attributed to the significant amount of excitation and scattered light trapped inside the droplet and the limited amount of fluorescence that was collected due to misalignment of the excitation and

(A)

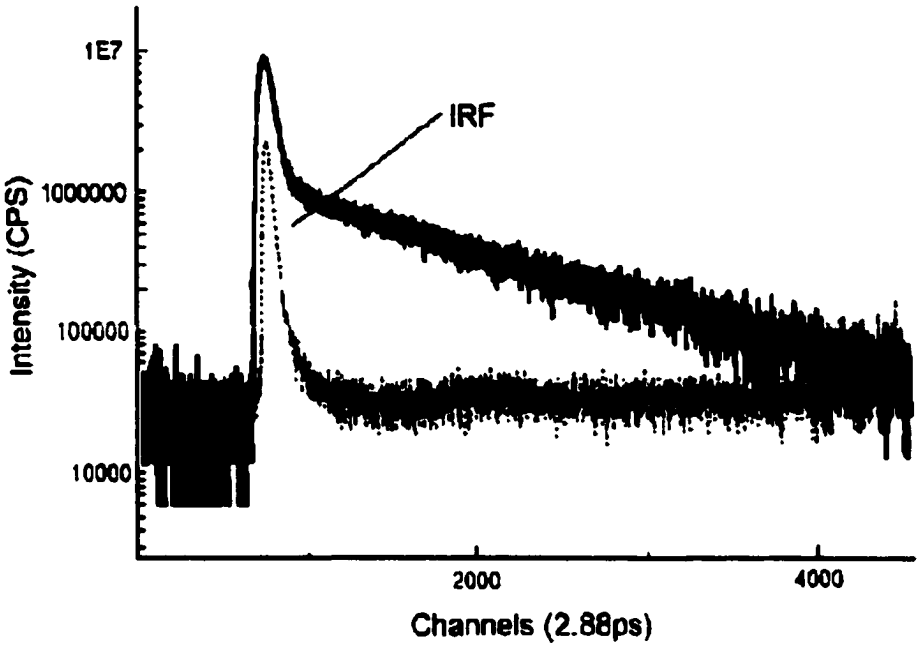

(B)

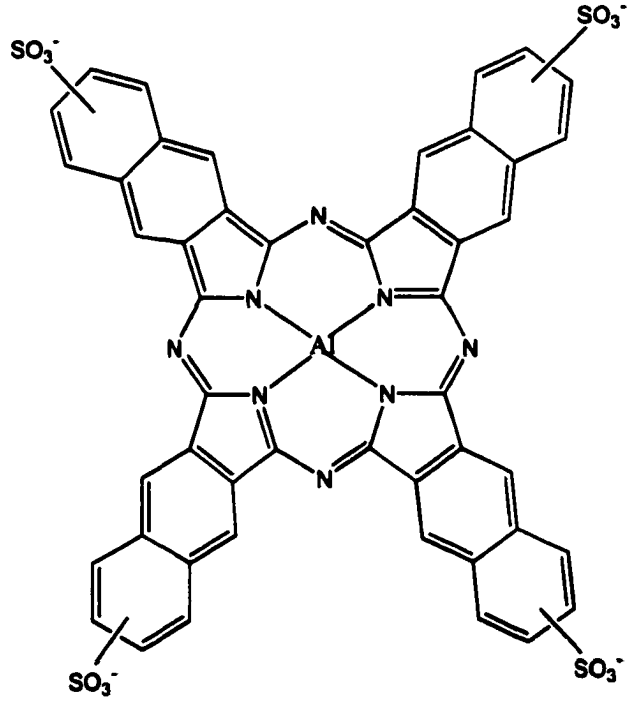

Figure 3.5. (A) Fluorescence Decay Profile of (B) Aluminum Tetrasulfonated Naphthalocyanine dye. The decay profile was obtained with the use of single mode excitation and collection fibers. The dye solution was at a concentration of 1μM in DMSO. The fluorescence lifetime was determined to be 3.08 ns.

emission fibers. The caclulated lifetime found was found to be 3.08 ns when the data was fit to a single exponential function utilizing the maximum likelihood estimator (see equation 2.42). This value compares favorably to the published value of 2.5 ns in methanol.[36]

3.4. Conclusions

A 12 channel fiber-optic based TCSPC instrument has been constructed. The device uses single mode fibers for directing the excitation light to the appropriate experiment and then another series of 12 single mode fiber optics to collect the resulting emission and direct it to one of three SPAD detectors. The device was developed to operate in the NIR, with excitation provided by a passively mode-locked Ti:sapphire laser. Transport of transform limited pulses produced by the Ti:sapphire laser indicated that even in fibers with lengths greater than 10 m, the IRF was primarily determined by the transient time spread in the SPADs and not GVD effects. The IRFs of the 12 channel instrument was found to be 181 ps (FWHM), comparable to the case where no fibers were used in the instrumental arrangement (176 ps). Collection and analysis of a decay profile by the dual fiber arrangement was investigated by interrogating a drop of liquid containing a NIR chromophore. The lifetime value was determined to be 3.08 ns, but a significant amount of scattered radiation was observed in the decay profile due to poor alignment of the excitation and emission fibers.

3.5 References

(1) De Schryver, F. C. *Pure and Applied Chemistry* **1998**, *70*, 2147-2150.

(2) Deschryver, F. C.; Boens, N.; Vanderauweraer, M.; Viaene, L.; Reekmans, S.; Hermans, B.; Vanstam, J.; Gehlen, M.; Berghmans, H.; Berghmans, M.; Ameloot, M. *Pure and Applied Chemistry* **1995**, *67*, 157-165.

(3) Reid, P. J.; Higgins, D. A.; Barbara, P. F. *Journal of Physical Chemistry* **1996,** *100,* 3892-3899.

(4) VanStam, J.; DeSchryver, F. C.; Boens, N.; Hermans, B.; Jerome, R.; Trossaert, G.; Goethals, E.; Schacht, E. *Macromolecules* **1997,** *30,* 5582-5590.

(5) Xie, X. S.; Dunn, R. C. *Science* **1994,** *265,* 361-364.

(6) Mcloskey, D.; Birch, D. J. S.; Sanderson, A.; Suhling, K.; Welch, E.; Hicks, P. J. *Review of Scientific Instruments* **1996,** *67,* 2228-2237.

(7) Suhling, K.; Mcloskey, D.; Birch, D. J. S. *Review of Scientific Instruments* **1996,** *67,* 2238-2246.

(8) Becker, W.; Stiel, H.; Klose, E. *Review of Scientific Instruments* **1991,** *62,* 2991-2996.

(9) Thompson, R. B.; Ge, Z. F.; Patchan, M.; Huang, C. C.; Fierke, C. A. *Biosensors & Bioelectronics* **1996,** *11,* 557-564.

(10) Thompson, R. B.; Lakowicz, J. R. *Analytical Chemistry* **1993,** *65,* 853-856.

(11) Campiglia, A. D.; Vodinh, T. *Talanta* **1996,** *43,* 1805-1814.

(12) Chudobova, I.; Vrbova, E. *Chemicke Listy* **1996,** *90,* 295-306.

(13) Patonay, G.; Casay, G.; Meadows, F.; Daniels, N.; Roberson, A. *Spectroscopy Letters* **1995,** *28,* 301-326.

(14) Wang, F.; Christian, G. D.; Fuh, M.-R. S.; Burgess, L. W.; Hirschfeld, T. *Analyst* **1987,** *112,* 1159-1163.

(15) Bublitz, J.; Dickenhausen, M.; Gratz, M.; Todt, S.; Schade, W. *Applied Optics* **1995,** *34,* 3223-3233.

(16) Zen, J.-M.; Patonay, G. *Analytical Chemistry* **1991,** *63,* 2934-2938.

(17) Schade, W.; Bublitz, J. *Environmental Science & Technology* **1996,** *30,* 1451-1458.

(18) Schubert, F.; Wang, F.; Rinneberg, H. *Mikrochemica Acta* **1995,** *121,* 237-247.

(19) Davis, L. M.; Fairfield, F. R.; Harger, C. A.; Jett, J. H.; Keller, R. A.; Hahn, J. H.; Krakowski, L. A.; Marrone, B. L.; Martin, J. C.; Nutter, H. L.; Ratliff, R. L.; Shera,

E. B.; Simpson, D. J.; Soper, S. A. *Genetic Analysis-Biomolecular Engineering* **1991,** *8*, 1-7.

(20) Hemmingsen, S. L.; McGown, L. B. *Applied Spectroscopy* **1997,** *51*, 921-929.

(21) Nunnally, B. K.; He, H.; Li, L. C.; Tucker, S. A.; McGown, L. B. *Analytical Chemistry* **1997,** *69*, 2392-2397.

(22) Li, L. C.; He, H.; Nunnally, B. K.; McGown, L. B. *Journal of Chromatography B* **1997,** *695*, 85-92.

(23) Legendre, B. L.; Williams, D. C.; Soper, S. A.; Erdmann, R.; Ortmann, U.; Enderlein, J. *Review of Scientific Instruments* **1996,** *67*, 3984-3989.

(24) Muller, R.; Zander, C.; Sauer, M.; Deimel, M.; Ko, D. S.; Siebert, S.; Ardenjacob, J.; Deltau, G.; Marx, N. J.; Drexhage, K. H.; Wolfrum, J. *Chemical Physics Letters* **1996,** *262*, 716-722.

(25) Muller, R.; Herten, D. P.; Lieberwirth, U.; Neumann, M.; Sauer, M.; Schulz, A.; Siebert, S.; Drexhage, K. H.; Wolfrum, J. *Chemical Physics Letters* **1997,** *279*, 282-288.

(26) Han, K. T.; Sauer, M.; Schulz, A.; Seeger, S.; Wolfrum, J. *Berichte der Bunsen Gesellschaft fur Physikalische Chemie-An International Journal of Physical Chemistry* **1993,** *97*, 1728-1730.

(27) Sauer, M.; Ardenjacob, J.; Drexhage, K. H.; Marx, N. J.; Karger, A. E.; Lieberwirth, U.; Muller, M.; Neumann, M.; Nord, S.; Paulus, A.; Schulz, A.; Seeger, S.; Zander, C.; Wolfrum, J. *Biomedical Chromatography* **1997,** *11*, 81-82.

(28) Huang, X. C.; Quesada, M. A.; Mathies, R. A. *Analytical Chemistry* **1992,** *64*, 2149.

(29) Lakowicz, J. r. *Principles in Fluorescence Spectroscopy*; Plenum Press: New York, NY, 1983.

(30) Tellinghulsen, J.; Goodwin, P. M.; Ambrose, W. P.; Martin, J. C.; Keller, R. A. *Analytical Chemistry* **1994,** *66*, 64-72.

(31) Soper, S. A.; Legendre, B. L. *Applied Spectroscopy* **1994,** *48*, 400-405.

(32) Li, L.-Q.; Davis, L. *Review of Scientific Instruments* **1993,** *64*, 1524-1529.

(33) Soper, S. A.; Mattingly, Q. L.; Vegunta, P. *Analytical Chemistry* **1993,** *65*, 740-747.

(34) Agrawal, G. P. *Nonlinear fiber optics*, 2nd ed.; Academic Press: San Diego, 1995.

(35) E-Tek Dynamics, I. ; E-Tek Dynamics Inc.

(36) Casay, G. A.; Narayanan, N.; Evans III, L.; Czuppon, T.; Patonay, G. *Talanta* **1996**, *43*, 1997-2005.

Chapter 4

A Near-Infrared Scanning Device for Time Resolved Measurements

4.1. Introduction

Microarrays are rapidly becoming a ubiquitous tool for the analysis of chemical, biological, and environmental systems.[1-3] The general protocol for the technique involves depositing materials onto a solid support and subsequently exposing the surface to analytical probes, which undergo some specific molecular interaction with the tethered material. Typically, the analytical probes contain a reporter molecule, such as a fluorescent dye. After exposure to the probes, the support is washed to remove unassociated probes and then interrogated for the signal of interest. Many times, these assays are run in a multiplexed format, in which more than one distinguishable reporter molecule is used to label the analytical probes, allowing simultaneous monitoring of the targets in one assay. The microarray format has been applied to several different types of applications, such as immunoassays, in which antibodies are immobilized to a solid support and the antigens serve as the analytical probes or for the determination of metallic species (environmental), which are adsorbed to the surface and probed by chelating agents.[4]

Recently, microarrays have been utilized in DNA applications and have assumed immense popularity for both research and clinical applications due to the highly parallel nature in which they are constructed and operated.[5] In most DNA microarrays, the material that is tethered to the solid support can be a short oligonucleotide probe (<100 nt, Format II) or an intact DNA target (>100nt, Format I).

The applications that have been targeted for DNA microarrays included expression profiling[6], de novo sequencing[7], and DNA variation on a genome wide scale.[8]

When short oligonucleotides are immobilized to the solid support, the attachment and/or construction of the probes can be accomplished using one of two methods. In the first, a photolithographic method is used to perform solid-phase DNA synthesis with phosphoramidite chemistry and photochemical deprotecting groups.[6] Using this light generated synthesis method, high density arrays (pixel size ~ 2 μm) can be generated using minimal synthetic steps (number of steps = 4 X N, where N is the length of the synthetic DNA probe). In the second method, inkjet technology is used to actually "print" specific oligonucleotide probes, which have been pre-synthesized and purified using standard procedures, at different locations and are tethered covalently to the support.[9] When intact DNAs are immobilized onto the solid support, various types of substrates are used to allow covalent types of interactions with the DNA to the support material following UV exposure of the pre-spotted DNA target. Examples of materials used in these applications include poly-lysine coated glass slides and nylon membranes.

In most cases, the common support material that is used for high density microarrays is glass. The properties of glass that make it an attractive substrate for DNA microarrays include;

(1) its impermeability which speeds up the kinetics of hybridization by keeping the hybridization volume small;

(2) its high rigidity making it easy to image;

(3) robust immobilization chemistries to allow covalent linkage of

(4) robust immobilization chemistries to allow covalent linkage of oligonucleotides to the solid-support and

(5) the low background fluorescence level it generates when high intensity lasers are focused onto its surface, improving the signal-to-noise in the measurement when fluorescence is used for readout.

Unfortunately, there are some severe limitations when incorporating glass as the substrate material for microarrays, namely the limited surface density of material for interrogation due to its impermeability (2-dimensional measurement). For example, in glass, the surface concentration of the tethered oligonucleotides is determined by the surface concentrations of the functional groups (silanol groups), which is $\sim 10^{-10}$ moles/cm^2. Due to steric considerations (low loading of tethered oligos to the surface) and the inefficiency of hybridization, the surface concentration of accessible oligonucleotides is one molecule/500Å^2, resulting in a detection level of ~6500 molecules/μm^2.[9] The situation is even more severe in cDNA arrays due to further steric considerations (extremely poor hybridization efficiency), producing on average 12 fluors/100 μm^2 spot size from each probe attached to the glass substrate.

Radiometric, enzymometric, amperometric or fluorometric detection methods have been effectively applied to reading microarrays.[4] The commonality in these approaches is the need for labeling the probe or reverse transcribed DNA with a reporter molecule to interrogate the microarray. However, there have recently been reported detection protocols for monitoring hybridization events that do not require direct labeling, such as surface plasmon resonance (SPR)[10-12], quartz crystal microbalance[13], Brewster angle reflectometry[14], and the grating coupler[15]. The most commonly used

transduction mode for reading microarrays is fluorescence due to its superior limit of detection and the ability to monitor multiple reporter molecules simultaneously (multiplexed applications). In the case of fluorescence, a dye is either covalently attached to the 5' end of the probe used to interrogate the array or to dUTP analogs incorporated during reverse transcription, which are then hybridized to bound DNA clones tethered to substrate material. Absolute intensity may then be used to determine whether selective binding of the probe to the immobilized target occurred. The common dyes that are used for interrogating DNA microarrays include Cy3 (λ_{ex}=514 nm) and Cy5 (λ_{ex}=632 nm).[16] The choice of these dyes is due to their favorable photochemical stabilities and quantum yields, well-resolved emission profiles and the fact that the dUTP analogs are readily incorporated during reverse transcription.

In many applications, in particular Format I-type hybridization assays, it becomes necessary to screen for multiple probes hybridizing to a single target tethered to the substrate. In addition, differential expression assays, which report on the relative abundance of particular genes in different cell lines, require dual labeling of reverse transcribed DNA labeled with unique reporter molecules. In these cases, it is necessary to use wavelength-discrimination methods to effectively identify whether the probe(s) hybridized to the target DNA found at a specific location on the array. However, the number of probes that can be effectively identified is limited by the broad emission profiles associated with most chromophores.

Recently, fluorescence lifetimes have been proposed as an alternative to wavelength discrimination in multiplexed applications, especially in DNA sequencing.[17-28] Implementation of lifetime discrimination into a multiplexed application

could potentially allow for the use of one readout channel (one laser and one photodetector) but still possess the ability to monitor many different fluorescent reporters when the reporters have similar absorption and emission profiles, but distinguishable fluorescence lifetimes.[19, 26, 28, 29] The common approach for acquiring lifetimes of fluorophores, especially in the limit of poor photon statistics, has been the use of time-correlated single photon counting (TCSPC), which uses a pulsed laser and the appropriate electronics. The advantages of TCSPC are its broad dynamic range, single photon sensitivity and favorable time resolution that can be achieved when appropriate instrumental components are used.[30] Additionally, because TCSPC is a time-resolved method, it is possible to eliminate background in the form of scatter by time-gating, which processes only those photons that are produced during a pre-selected time window set by the hardware. Therefore scattering photons that are coincident with the laser pulse can be gated out of the observed signal improving the signal-to-noise ratio in the measurement.[31-35]

Near-infrared (NIR) fluorescence monitoring can be particularly attractive for lifetime-based applications where high sensitivity is required.[22, 31, 36, 37] The advantages of NIR fluorescence include the minimal amount of background, in terms of both scattering and impurity fluorescence, generated from the sample matrix compared to visible fluorescence. The reduction of such sources of background improves the precision and accuracy in a lifetime measurement.[36,37] In addition, the instrumentation that can be implemented in the NIR can be much simpler that that required for visible time-resolved fluorescence measurements.[21] This is because solid-state diode lasers can be used for excitation and avalanche photodiodes, operated in a single photon

counting mode, for time-resolved photon transduction.[40] In addition, the simplification of the ancillary signal processing electronics further reduces the instrumental demands placed on TCSPC. Therefore, robust and simple TCSPC devices can be fabricated when using NIR fluorescence that exhibit high sensitivity, are capable of simple operation, and can be configured in a footprint that can be easily scanned for imaging applications.

In this chapter, the use of time-resolved NIR fluorescence for reading fluorescence signatures from microarrays will be discussed. The fluorescence produced from two representative NIR dyes, NN382 (tricarbocyanine) and aluminum tetrasulfonated naphthalocyanine (see Table 4.1), was evaluated following deposition of the material onto different substrates appropriate for microarray applications. In addition, to obtain the time-resolved fluorescence, a high resolution (spatial and temporal) NIR TCSPC scanner was developed and the operational characteristics of this device will be reported. Finally, the application of NIR time-resolved confocal imaging for reading both steady-state and time-resolved fluorescence from DNA microarrays will be discussed.

4.2 Experimental

4.2.1 Chemicals and Substrates

All chemicals and solvents were purchased from Aldrich (Milwaukee, WI) and used as received. The oligonucleotides used for hybridization assays were purchased from Midland Certified Reagent Company (Midland, TX) and consisted of a 5'amino modified end with a sequence of 5'$H_2N(CH_2)_6$-TTTTTTTTTTTTTTTGTCGTTTTACAAACGTCGTG-3'. The complementary

strand, which contained a near-IR label (IRD-800, LiCor, Lincoln, NE) had the following sequence; IR800-5'CACGACGTTGTAAAACGAC-3'.

Poly(methyl methacrylate) (PMMA) was obtained from Goodfellow (Berwyn, PA). Precleaned glass microscope slides and microscope cover slides were obtained from Fisher Scientific (Pittsburgh, PA). Glass slides coated with poly-L-lysine were obtained from Sigma Diagnostics (St. Louis, MO). The glass and PMMA slides were washed with methanol and dried with lens tissue (Kodak, Rochester, NY) before use. The poly-L-lysine coated slides were used as received.

4.2.2. Instrumentation

Previously, we described a scanner for time-resolved NIR fluorescence which utilized an avalanche photodiode (APD) in conjunction with a 780 nm pulsed diode laser. This system was configured such that the laser was positioned at Brewster's angle with respect to the collection lens.[41] The scanner was reported to have subnanosecond timing resolution but had a relatively large spot size of (15 μm along the short axis and 20 μm along the long axis). In addition, the large f/# resulted in minimal collection of the fluorescence. However, this scanner was not appropriate for the present application due to the large spot size of the laser and the poor collection efficiency of the relay optics. Therefore, we constructed a confocal imager with time-resolved capabilities.

Time-correlated single photon counting measurements made from solid surfaces were performed with a device built in-house which consisted of a pulsed diode laser, with subnanosecond pulses (PicoQuant GmbH, Model 800, Berlin, Germany), a time-correlated single photon counting board (PicoQuant GmbH, Model SPC 430, Berlin,

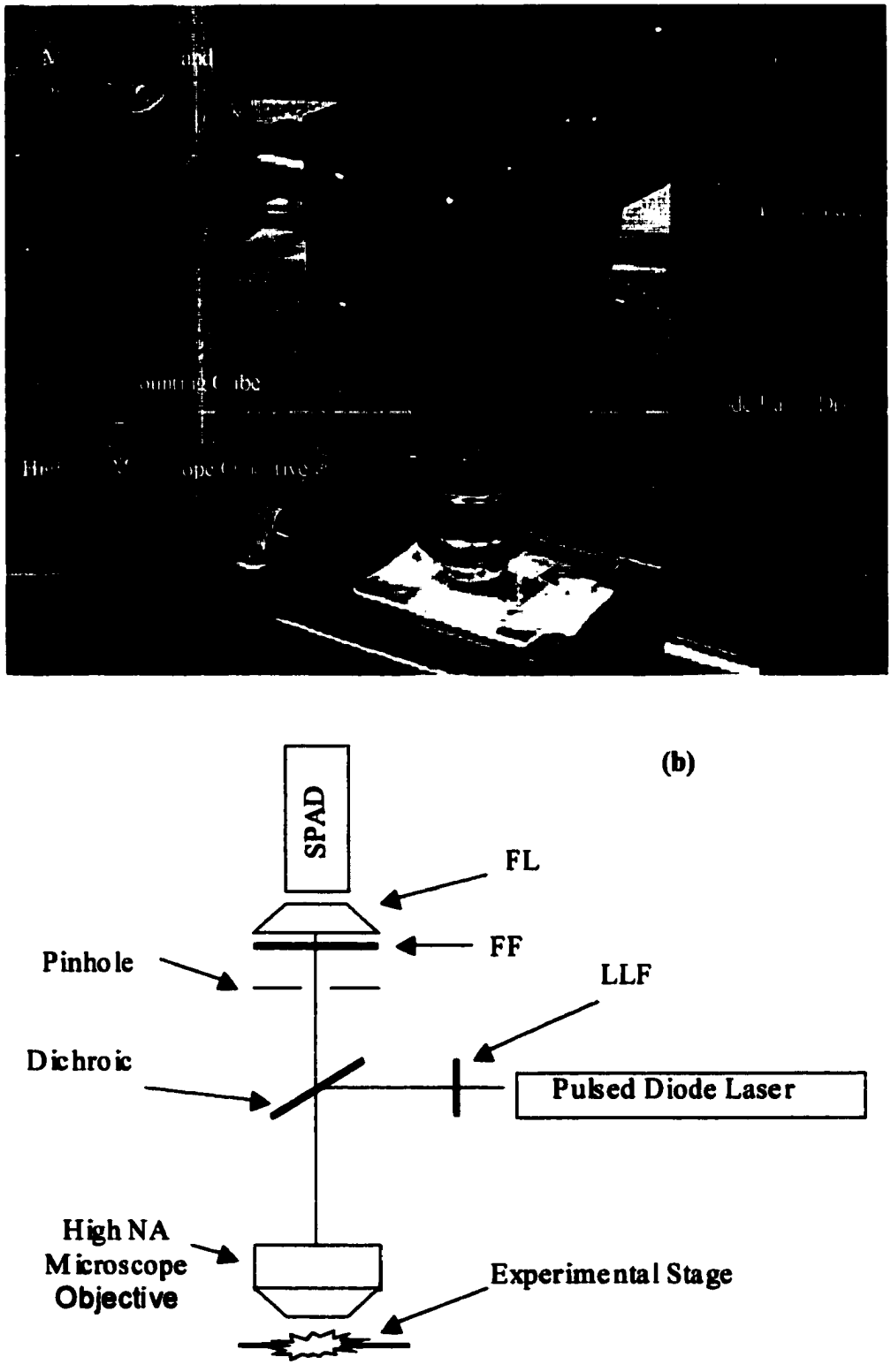

Figure 4.1. (a) Picture of NIR scanning time-correlated single photon counting (NIR-TCSPC)device. (b) Schematic of the optical system for a NIR-TCSPC device. LLF, laser line filter; FF, fluorescence filter; and FL, focusing lens.

Germany), and a single photon avalanche diode (SPAD, EG&G Optoelectronics, Model SPCM-AQ, Vaudreuil, Canada). As Figure 4.1 depicts, the components were mounted with the aid of a mounting cube and lens tubes purchased from ThorLabs (Newton, NJ), allowing the optics to be configured in an epi-illumination format. In addition, a circular aperture was placed in the secondary image plane of the objective to allow implementation of confocal imaging when required.

The pulsed diode laser operated at a wavelength of 780 nm and the repetition rate was adjustable from single shot to 80 MHz with a temporal pulse width of approximately 50 ps. An integrated optics set was provided with the laser that produced a collimated output. The laser excitation beam was passed through a 780 nm line filter (Omega Optical, 780DF10, Brattleboro, VT) and then reflected by a dichroic filter (Omega Optical, 795DRLP, Brattleboro, VT) and focused onto the array surface using a 40X high numerical aperture (NA) microscope objective (Nikon, Natick, MA, NA=0.85). The $1/e^2$ spot size was measured to be 3 μm on the minor axis and 5 μm on the major axis (the laser beam was elliptical). The fluorescence excitation was collected by the same microscope objective, transmitted through the dichroic, the aperture, and finally onto the appropriate filter stack. The filter stack consisted of a bandpass filter centered at 825 nm (825RDF30, Omega Optical, Brattleboro, VT) and a longpass filter with a cut-on wavelength of 830 nm (FSQ-RG830, Newport Corporation, Irvine, CA). After passing through the filter stack the fluorescence was passed through a condensing lens (01LAG111/076, Melles Griot) and focused onto the SPAD. The passively quenched SPAD possessed a small photoactive area of approximately 180 μm in

diameter, which resulted in decreased transit times and therefore, better timing resolution.[42]

The scanning stage consisted of a three-axis translational stage purchased from Newport Corporation (Model 461-XYZ) and an open loop DC motorized actuator (Model 860A-05, Newport Corporation). The slide was mounted with the use of an adjustable lens holder (07-LHC-003, Melles Griot), which prevented unintended movement. It was possible to adjust the rate of movement with the use of a hand-held single-axis open-loop controller (Model 861, Newport Corporation).

The TCSPC electronics were mounted on a board to fit into an ISA slot of a personal computer (SPC400 TCSPC Module, PicoQuanT GmbH, Berlin, Germany). These electronics included the constant fraction discriminator (CFD), time-to-amplitude converter (TAC), and analog-to-digital converter, which performed time-resolved measurements in a reverse start-stop format. The electronics were controlled by a software package that allowed the user to manipulate settings such as the discrimination level, the timing range of the TAC and integration time. The start (synchronization) pulse for the TAC was generated by monitoring the electrical driver for the pulsed diode laser and conditioned by the onboard CFD. The output pulse from the SPAD was also conditioned by the CFD and sent into the stop input of the TAC. The instrument response function of the device was determined to be 275 ps (FWHM), sufficient for the determination of lifetimes in the subnanosecond domain. The counting board consisted of 1024 channels with a timing resolution of 9.77 ps per channel. Additionally, the module was capable of taking 128 sequential measurements prior to requiring dumping to memory. Consequentially it was possible to scan an array in a semiautomatic format-

the integration time for each data point was set and the user moved the scanning stage in the forward or reverse direction. This resulted in a two-dimensional picture of fluorescence lifetime versus position on the microarray.

Steady state fluorescence measurements were performed at 488 nm and 780 nm on a PMMA slide, a poly-L-lysine-coated slide, and a glass slide. In the 488 nm case, an air-cooled Argon Ion Laser (OmniChrome Model 532, Chino, CA) was used for excitation. The setup was similar to that of the NIR case in that the excitation beam was passed through a dichroic filter (495DRLP, Omega Optical) and focused onto the solid substrate with a 40X high numerical aperture (NA) microscope objective (Nikon, Natick, MA, NA=. 85). A bandpass filter with a center wavelength of 515 nm (515DF10, Omega Optical) was used to block out any stray light or scatter. Measurements were performed with the use of a Tennelec Nucleus software package that resided in a PC. The pulses from the SPAD were amplified with a fast amplifier (Model 6954, Phillips Scientific, Mahwah, NJ). The amplified nuclear instrumentation module (NIM) pulses were passed through a level adapter (Model 688AL, Lecroy Instruments, Chestnut Ridge, NY), which converted it to a transistor-transistor logic (TTL) pulse. The TTL pulses were passed to a 12 bit multi-channel scaler (MCS, Tennelec,) that displayed a plot of fluorescence intensity versus time.

4.2.3. Fluorescence Measurements of Spotted Dyes

Fluorescence measurements were performed by manually spotting NN382 and Aluminum Naphthalocyanine ($AlNc(SO_3^-)_4$) on the surface of the appropriate substrate. This was accomplished by drawing a 1 cm by 1 cm grid and placing it under the transparent substrate surface. Each element of the grid measured 2 mm x 2 mm (5 x 5

array). The dyes were dissolved in DMSO and spotted onto the surface with the use of a 25 μm i.d. capillary or a .5-10 μL Pipette Tip (Fisher Scientific) using an Eppendorf pipette. After spotting, the slides were either allowed to dry (in the dark) under a stream of N_2 or covered with a cover slip.

4.2.4. Hybridization of Oligonucleotide to PMMA

The covalent attachment of the oligonucleotides to PMMA was accomplished using the procedure depicted in Scheme 1.[43] Oligonucleotide hybridization experiments were performed on PMMA sheets cut into 20 mm x 50 mm rectangles. Before preparation, the PMMA slides were soaked in a 10% methanol solution (v/v) for thirty minutes, rinsed with triply deionized water and dried with compressed air. A lithium ethylenediamine solution was prepared by agitating n-butyl-lithium, tetrahydrofuran (THF), and ethylenediamine in a vortex mixer for thirty minutes. The cleaned PMMA sheets were then agitated with the lithium ethylenediamine solution and THF, which resulted in the attachment of the diamine to the PMMA surface through the formation of an amide bond. After washing with deionized water, the PMMA slide was placed in a 5% glutaraldehyde-phosphate buffer ($H_2PO^-_4/HPO_4^{2-}$) solution for five hours at a pH of 7.0. After washing with deionized water, the PMMA was then placed over a grid as described above. In each element, 1 μL of a 5 mM amino linker-oligonucleotide in phosphate buffer solution was allowed to incubate at 37°C for 90 minutes. After derivitization, the sheet was washed once with 1% ammonium and immediately rinsed with deionized H_2O. This final step was followed by drying with compressed air and placing the sheet under a vacuum until use.

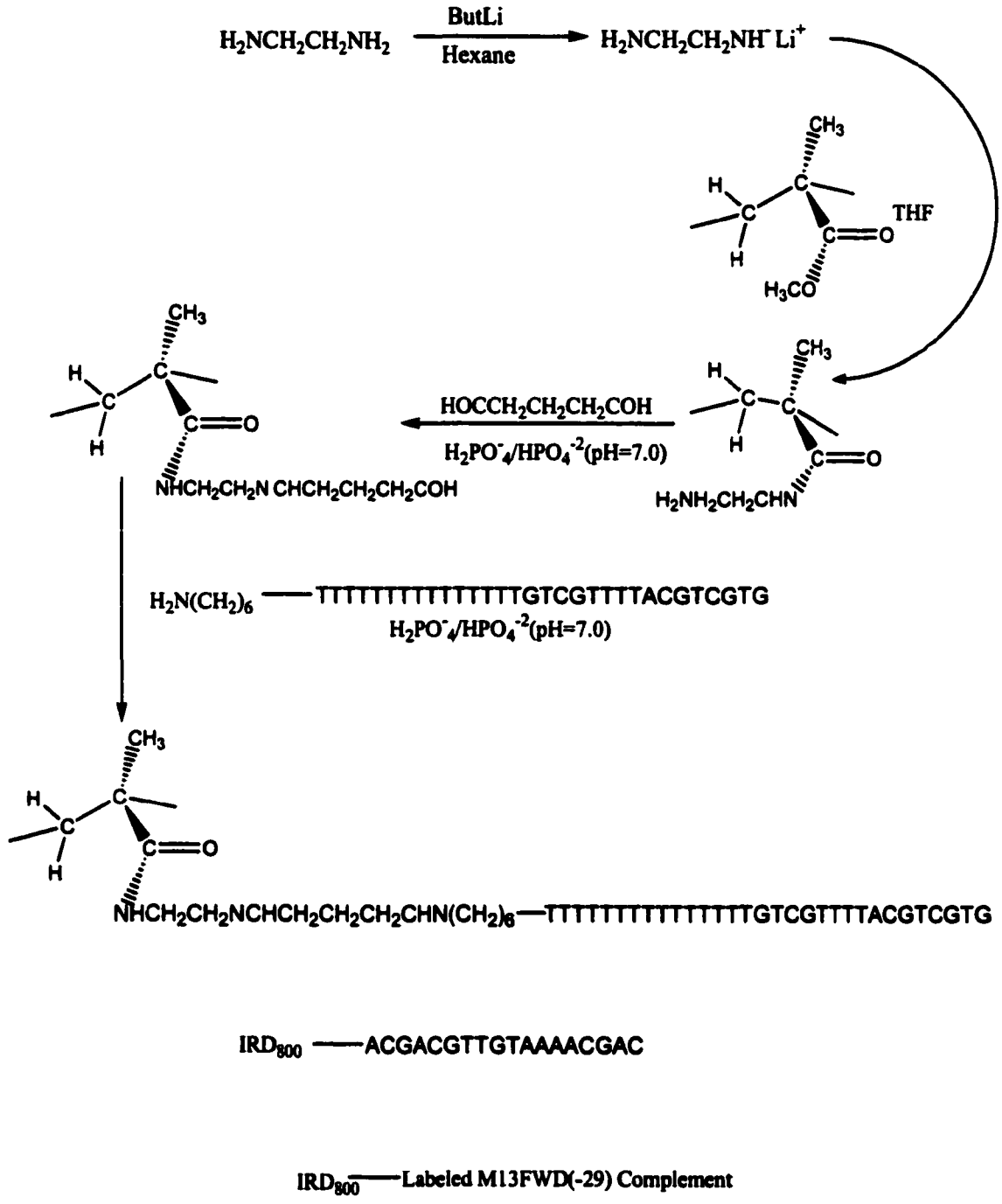

Scheme 4.1. Reaction Scheme for attachment of oligonucleotide to PMMA

Following the preparation of the derivatized PMMA sheets; a 100 nM solution of IRD800 labeled complementary probe, 5X Saline-sodium-phosphate-EDTA (SSPE), and 0.5% Sodium Dodecyl Sulfate (SDS), was placed on a specific element of the PMMA by utilizing the previously described grid. Hybridization was allowed to occur for thirty minutes in the dark at 30°C. Following the hybridization, the PMMA was washed with 5X SSPE-0.5% SDS solution for 15 minutes.

4.3 Results and Discussion

One of the more common approaches towards increasing sensitivity in an analytical measurement is to reduce the amount of background. In fluorescence, this may be achieved by implementing the use of spectral filters to reject stray light or the use of time-gating to discriminate against Rayleigh and Raman scatter. A simpler and at times overlooked approach is to reduce the number of fluorescent impurities in the sample matrix or to excite in a region where the number of fluorescent impurities is low. In this instance, the matrix was a solid substrate on which fluorescent samples of interest were placed. Three substrates were studied in order to quantify the amount background observed from each material as a function of excitation wavelength.

As depicted in Table 4.1, the glass slide yielded the least amount of background (76,000 counts per second (cps)) at 488 nm. Glass slides coated with poly-L-lysine, a widely used substrate in molecular biology because of its cationic nature and its resulting ability to bind DNA efficiently[44], yielded the highest background (135,000 cps). PMMA yielded 103,000 counts per second. Due to its intrinsically low background, these results indicate that glass should be the substrate of choice when using visible excitation. The same three substrates were then scanned under the same

(a)

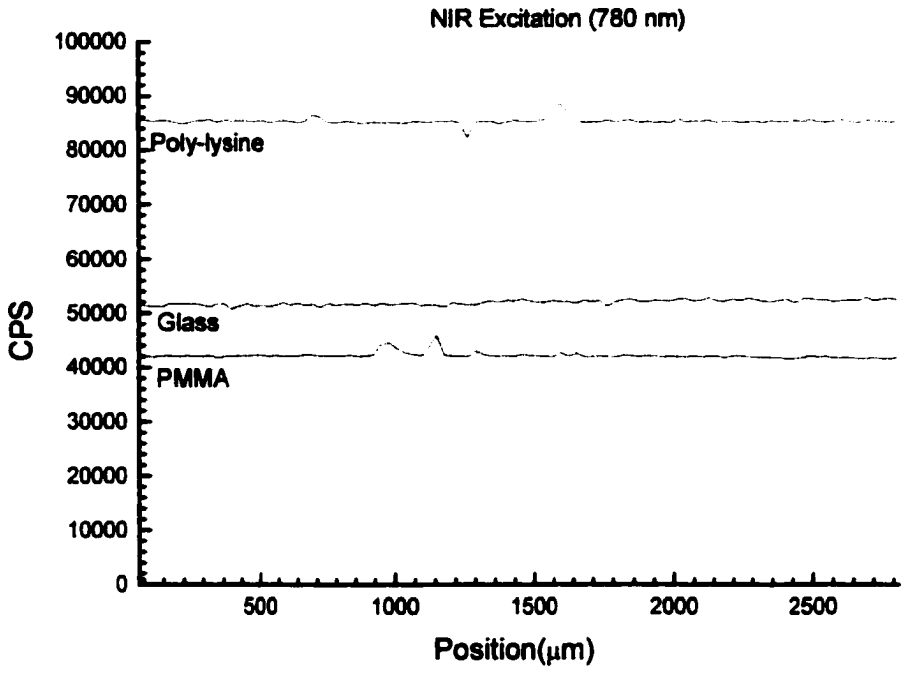

(b)

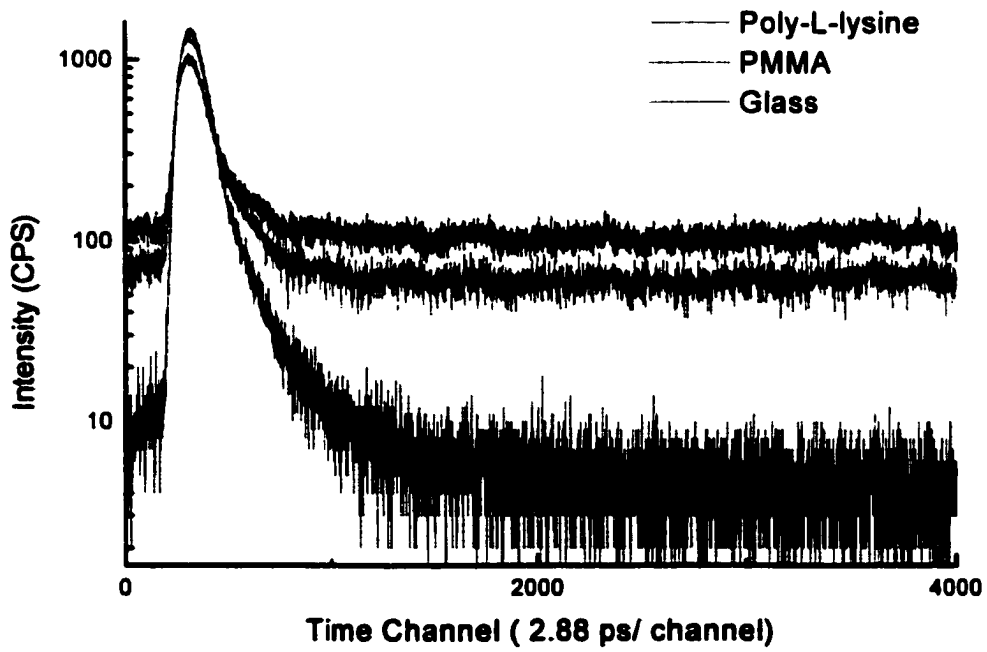

Figure 4.2. (a) Intensity profile of PMMA, glass, and poly-L-lysine coated slide. Excited at 780 nm. (b) Decay profiles from glass, poly-L-lysine, PMMA, and a mirror.

conditions, but at 780 nm excitation. Figure 4.2 (a) shows that at 780 nm the amount of light coupled back into the system was significantly lower in all cases as compared to visible excitation. The lowered background was because of the limited number of fluorophores that fluoresce in the NIR as well as the reduced amount of scattering photons produced due to the smaller Raman cross sections, which is a direct result of working in the NIR region.[45] In addition, PMMA yielded the least amount of background with a value of 42,000 counts per second. The poly-L-lysine yielded the highest amount of background signal of 84,000 counts per second. We also considered the sensitivity of the SPAD in different regions of the electromagnetic spectrum, since both imagers used the SPAD for photon transduction. The specifications supplied by the manufacturer indicated that the single photon detection efficiency is 50% at 515 nm and 825 nm (the respective center wavelength of the bandpass filter placed in front of the SPAD for the visible and NIR case). Consequently, the SPAD does not favor one wavelength over another.

Table 4.1. Amount of background scatter coupled into NIR TCSPC scanning device from various substrates at 488 nm and 780 nm excitation wavelengths. The center wavelength of the bandpass filters placed in front of the SPAD was 515 nm and 825 nm respectively.

Material	488 nm Excitation	780 nm Excitation
PMMA	103000	42000
Glass	76000	51000
Poly-L-lysine	135000	84000

Because we were interested in measuring fluorescence lifetimes on these substrates, decay profiles for each substrate was then acquired at 780 nm excitation to determine if any residual fluorescence was produced by the substrate that would affect

the lifetime measurement. Figure 4.2(b) depicts the decay profiles of PMMA, glass, and poly-l-lysine. The decay profile of the PMMA was measured to be 275 ps at its full width half maximum (FWHM). In addition, it was noticed that the scattering peak observed in the decay profiles for glass and poly-l-lysine was superimposed on a relatively large and flat background, while this was not seen in the case of PMMA. This background was believed to arise from some long-lived luminescent species present in glass that could be excited at 780 nm, but absent in PMMA. Therefore, PMMA not only resulted in a lower absolute intensity in the observed background, but also the photon distribution in the decay indicated that their origination was predominantly from scattering effects. This is an important result, since it will allow the effective implementation of a time-gate to improve the SNR in the measurement and improve the precision and accuracy in the fluorescence lifetime measurement.[20, 33, 34, 46-48]

In order to determine the analytical figures of merit for NIR fluorophores spotted on PMMA, 100 nM $AlNc(SO_3^-)_4$ in DMSO was spotted onto a PMMA slide in a gridded pattern. The spots were placed on the surface by manually pipetting 1 μL of solution onto the surface. The spots, which averaged approximately 2 mm in diameter, were allowed to dry prior to acquiring the fluorescence. The steady state fluorescence was collected as the scanner was rastered over the surface at a speed of ~70 μm per second. As Figure 4.3 shows, the background fluorescence from the PMMA was low and consistent across the scan range. However, as evidenced by Figure 4.2, the back right corner of the pattern is missing. This is due to a spotting error in which the dye was placed out of alignment with the checkerboard pattern. The irregularity in the

(a)

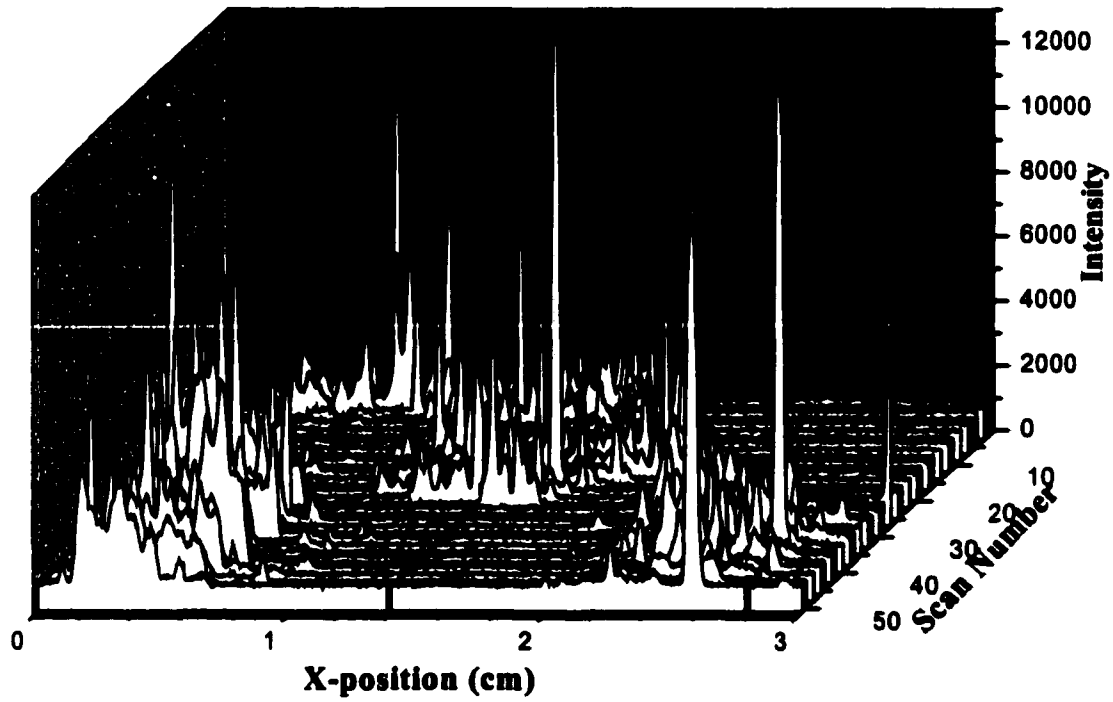

(b)

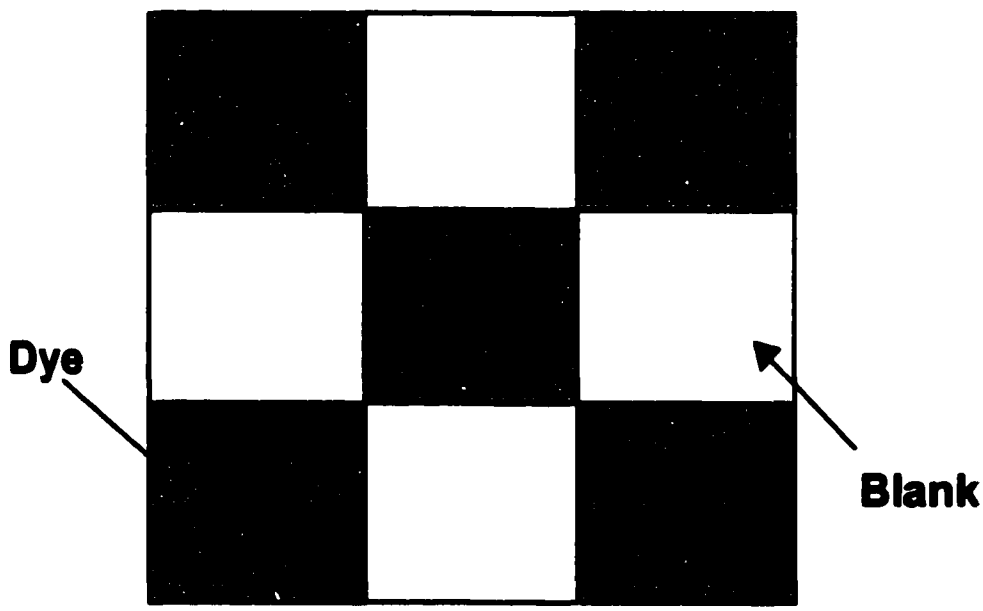

Figure 4.3. (a) Fluorescence Intensity pattern from gridded array. 10 μL drops of 100 nM NN382 were placed on PMMA in a checkerboard pattern (b) and scanned with the NIR-TCSPC scanning device. Right rear spot is not present due to misalignment of scanning device and/or misplacement of dye.

fluorescence intensity across each spot was most likely due to the manual method of spotting the dye and the non-covalent nature of the deposition process. When spotted, the dye spreads across the surface with the amount of spreading determined by the rate of evaporation, the surface tension of the liquid (DMSO), and the hydrophobicity of the solution and substrate. In addition, it is reasonable to suspect that some dye-stacking may be occurring as well. In this case, the dimers would be expected to produce a much lower level of fluorescence due to reduced quantum yields compared to monomers.[36, 49, 50]

We next looked at the fluorescence properties of two different NIR fluorescent dyes deposited onto the PMMA surface. A comparative analysis of the photophysical characteristics of tricarbocyanine versus naphthalocyanine dyes is presented in Table 4.2.

Table 4.2. Photophysical Characteristics of Aluminum Naphthalocyanine and NN382.

Photophysical Parameter	($AlNc(SO_3^-)_4$)	NN382
Absorption Maximum	781 nm (MeOH)[51]	778 nm (MeOH)[29]
Emission Maximum	784 nm (MeOH)[51]	802 nm (MeOH)[29]
Quantum Yield(ϕ_f)	0.25 (H_2O)[52]	0.05 (DMSO)[29]
Fluorescence Lifetime (τ_f)	2.9 ns (MeOH)[51] 2.5 ns (Aqueous Buffer)[53]	0.87 ns (MeOH)[29]
Photochemical Stability (ϕ_d)	3.0×10^{-3} (Aqueous Buffer)[53]	7.0×10^{-3} (H_2O/DMSO)[54]
Photon Yield per Molecule (ϕ_f/ϕ_d)	83	7.1

The photon yield per molecule, which is determined by calculating the ratio of the quantum yield to the photodestruction yield per molecule, is an important property to assess since it determines the magnitude of the analytical signal, especially when high

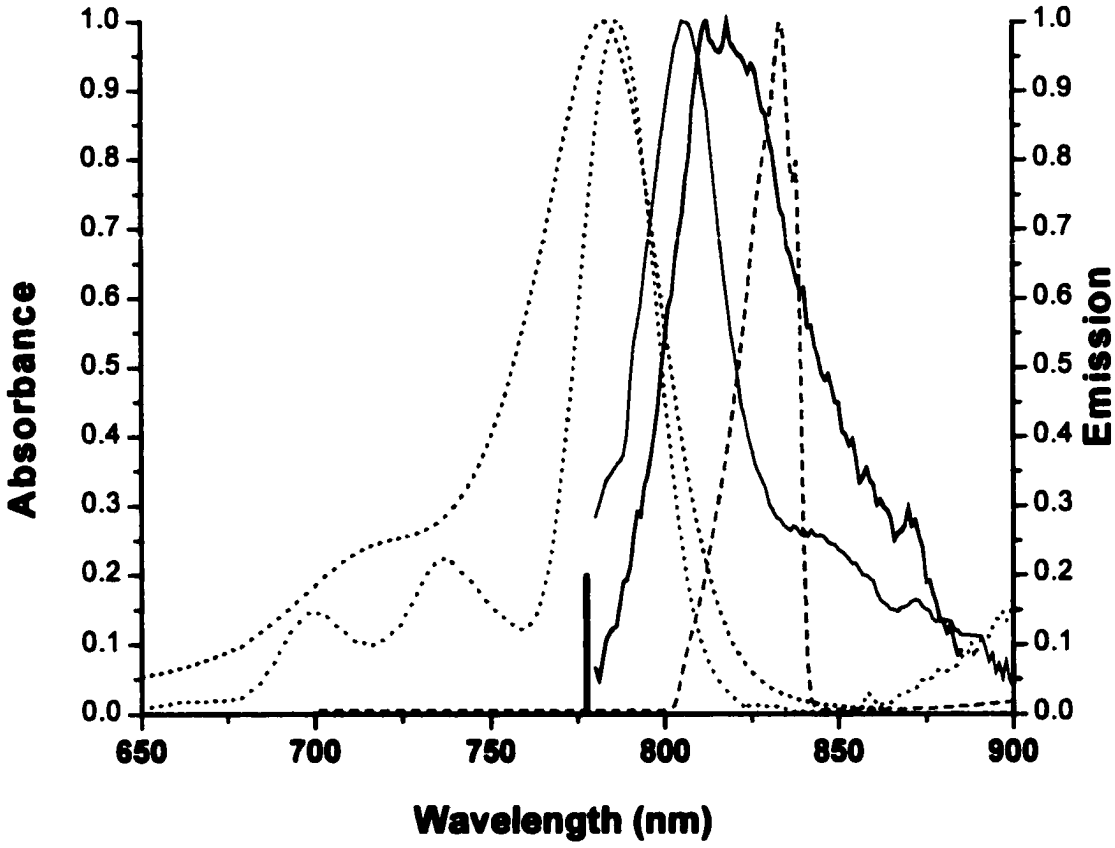

Figure 4.4. Absorption and Emission Spectra of NN382 and Aluminum Naphthalocyanine NIR dyes in DMSO. The blue and black spectra represent Aluminum Naphthalocyanine and NN382, respectively. The red curve represents the transmittance of the spectral filter, which is centered at 825 nm (825RDF30, Omega Optical). The black, solid vertical line represents the excitation wavelength of 780 nm.

laser fluences are used. A comparison of these values demonstrates that the naphthalocyanine dye should produce more than ten times the amount of photons compared to the tricarbocyanine dye. This would indicate that at 780 nm, the limit of detection of the $AlNc(SO_3^-)_4$ should be lower than that of the NN382. However, we did not observe this phenomenon in that as Figure 4.4 illustrates, our filter stack was optimized towards the detection of NN382. (The LOD of NN382 was less than 1.0 pM and the LOD $AlNc(SO_3^-)_4$ was approximately 100 pM).

Additional considerations may be given to the rate of bleaching or photodestruction. This is an intrinsic parameter, which dictates the useful interaction time of a molecule with the laser beam. The lower the rate of photodestruction (or decomposition), the longer a molecule may reside in the illumination volume or in scanning applications the number of passes over a specific area element (on the array surface) may be increased. Literature values for the rate of photodecomposition (or photochemical stability) of $AlNc(SO_3^-)_4$ indicates a value of 3.0×10^{-3} [53] and the value for the tricarbocyanine dyes are 7.0×10^{-3}.[54] The bleaching of both dyes is shown in Figure 4.5. We observed that the NN382 was less photochemically stable than $AlNc(SO_3^-)_4$, consistent with literature values. The rate of photodecomposition was estimated by fitting the linear portion of the bleaching curves in Figure 4.5 to a straight line and determining the slope. The bleaching rate was 9.34×10^{-4} for $AlNc(SO_3^-)_4$ and 3.72×10^{-3} for NN382. We determined this by spotting a PMMA slide with 100nM spots of NN382 and $AlNc(SO_3^-)_4$ and allowing the solution to equilibrate for fifteen minutes. After location

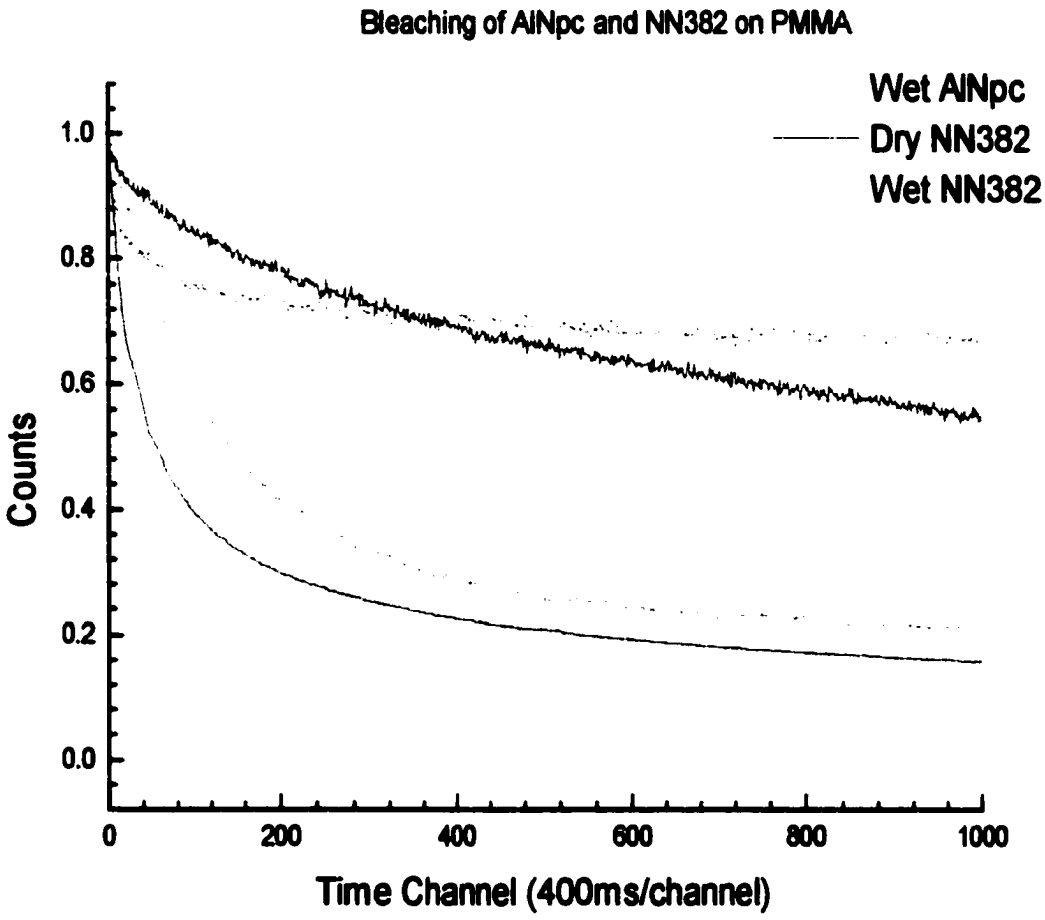

Figure 4.5. Bleaching rates of $AlNc(SO_3^-)_4$ and NN382 on PMMA. Fluorescence was collected under "wet" and "dry" conditions as described in text. Excitation occurred at 780 nm and 1 mW power. The fluorescence intensity has been normalized.

of the spot by the scanning system, the beam was blocked and the slide moved 10 μm. At this point, the beam was unblocked and the fluorescence monitored as a function of time. A series of "dry" experiments were also performed by dropping 10 μL of 100 nM $AlNc(SO_3^-)_4$ on PMMA and allowing the solution to dry under N_2. It was observed that the rate of bleaching was 1.05×10^{-3} and 3.43×10^{-3} for $AlNc(SO_3^-)_4$ and NN382, respectively.

In order to determine the dynamic range and limit of detection of the NIR dyes on PMMA substrates, solutions of NN382 were spotted onto the surface and the fluorescence intensity recorded as a function of the scan position. The drops were 10 μL in volume and covered a circular region approximately 3 mm in diameter. Figure 4.6 provides a plot of the signal-to-noise ratio (SNR) as a function of concentration. The SNR was determined by the following expression;

$$SNR = \frac{T - N}{\sqrt{N}} \qquad (4.1)$$

where T is the total number of counts and N is the noise, which is the number of photons detected by the detection system in the absence of a fluorescent sample. As Figure 4.6 shows, the dynamic range of the device ranges from 1.0 pM to 10 nM, with minimal deviation from linearity (r=0.99213). Additionally, the SNR at 1.0 pM is eight, which is near the limit of detection that is defined as the concentration that yields a SNR of three. The total number of molecules (N) may be determined by the following physical relationship;

$$N=(C \times V \times N_A)/A \qquad (4.2)$$

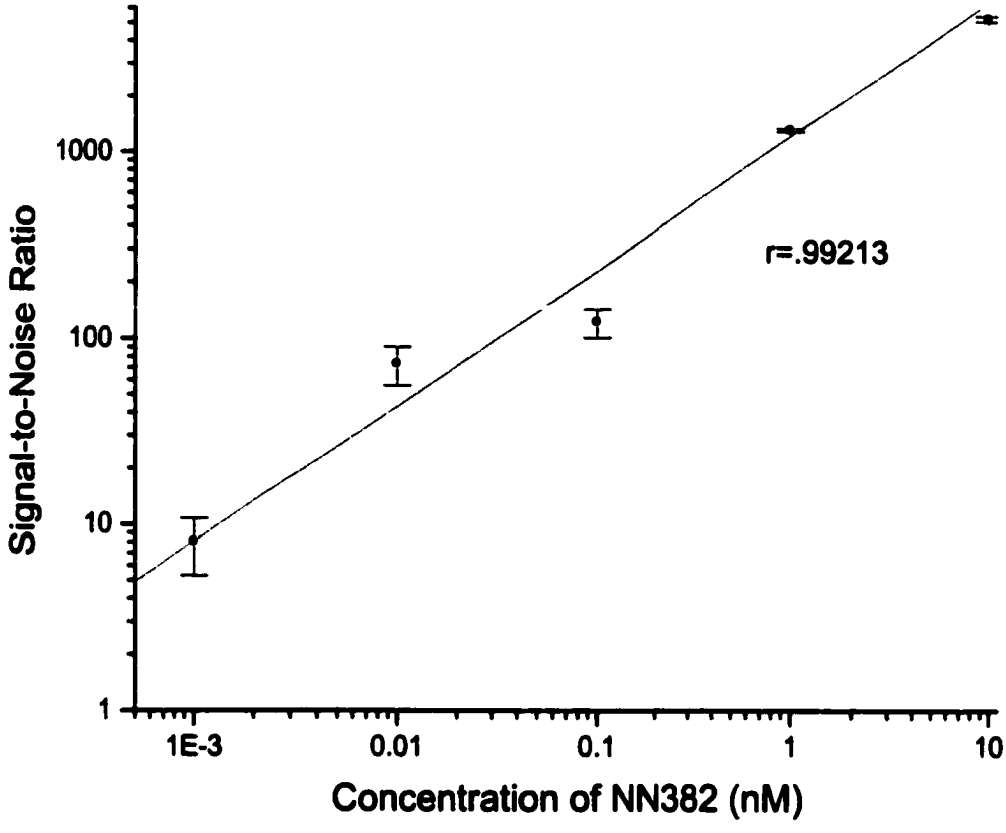

Figure 4.6. Dynamic Range of NIR TCSPC scanning device.

where N is the number of molecules, C is the dye concentration (moles/L), V is the volume of the drop (L), N_A is Avogadro's Number (6.022×10^{23} molecules/mole), and A is the area of the spot (m^2). At 1.0 pM, the surface concentration is 85, 196 molecules per μm^2. However, this value may be recast in terms of the area sampled by the interrogation beam, which has an area of 15 μm^2. Because the spotted dye is evenly distributed across the 3 mm spot the interrogation beam samples a fraction of the total number of molecules, which is given by the following relation;

$$N_{sample} = \frac{A_{sample}}{A_{spot}} N_{total} \qquad (4.3)$$

where N_{sample} is the number of molecules sampled by the scanning device, A_{spot} is the total area the dye covers, A_{sample} is the area sampled by the laser beam, laser beam interrogates, N_{total} is the total number of molecules in determined by equation 4.2. Equation 4.3 yields a value less than one (.18 fluors/μm^2), that may be interpreted as a less than one molecule being present in the sample beam. From an experimental viewpoint, this means that the interrogating beam only sees "part" of a molecule at such a low concentration. This may be exhibited as a variance in the fluorescence as illustrated by three-dimensional plot in Figure 4.3 and the error bars in Figure 4.6.

In order to evaluate the ability of the system to identify analytes through the use of fluorescence lifetimes of the reporter molecules deposited on solid surfaces, a time-resolved analysis of 100 nM $AlNc(SO_3^-)_4$ and NN382 on PMMA was conducted. These experiments were performed by depositing dye solution (in DMSO) on PMMA and allowing it to dry. Fluorescence was then collected for 1 sec so as not to degrade the dye and then analyzed with a non-linear least squares fitting package (FLA-900,

Edinburgh Instruments, Livingston, UK). The resulting decay data indicated that NN382 possessed a lifetime of 791 ps whereas $AlNc(SO_3^-)_4$ possessed a lifetime of 1.904 ns (Figures 4.7 and 4.8 respectively). The lifetime obtained for the $AlNc(SO_3^-)_4$ was much shorter than the value obtained in the literature, which was 2.92 ns (in methanol).[51] The difference between the calculated lifetime and the fluorescence lifetime in the literature may be due to a number of factors. One of these may be the amount of scatter introduced into the calculation because of the geometric arrangement of the system. The increased scatter introduced more scattering photons into earlier time bins, which biased the calculation towards shorter values.[39] In addition, the lack of solvent may affect the measurement also.

In the tricarbocyanine case, a consideration must also be given to the lack of a solvent, which may effectively eliminate the conformational rotation of heteroaromatic fragments during the excited state lifetime, giving rise to a longer lived fluorescence lifetime and time dependent rate of internal conversion.[55] This argument seems to apply here as elucidated by the next paragraph, which studies a "wet" system. However, a more detailed analysis must be completed in order to understand the effects of solvent or lack thereof on the fluorescence lifetime of tricarbocyanine dyes.

In order to evaluate the ability of the NIR scanning device to identify fluorophores in solution we utilized the device to collect fluorescence lifetime information from NN382 and ($AlNc(SO_3^-)_4$) in a channel on a micro-CE chip. In these experiments, solutions of 100 nm NN382 or ($AlNc(SO_3^-)_4$) in 50:50 v/v 1X TAE/methanol buffer were pushed through a channel with the use of a syringe pump.

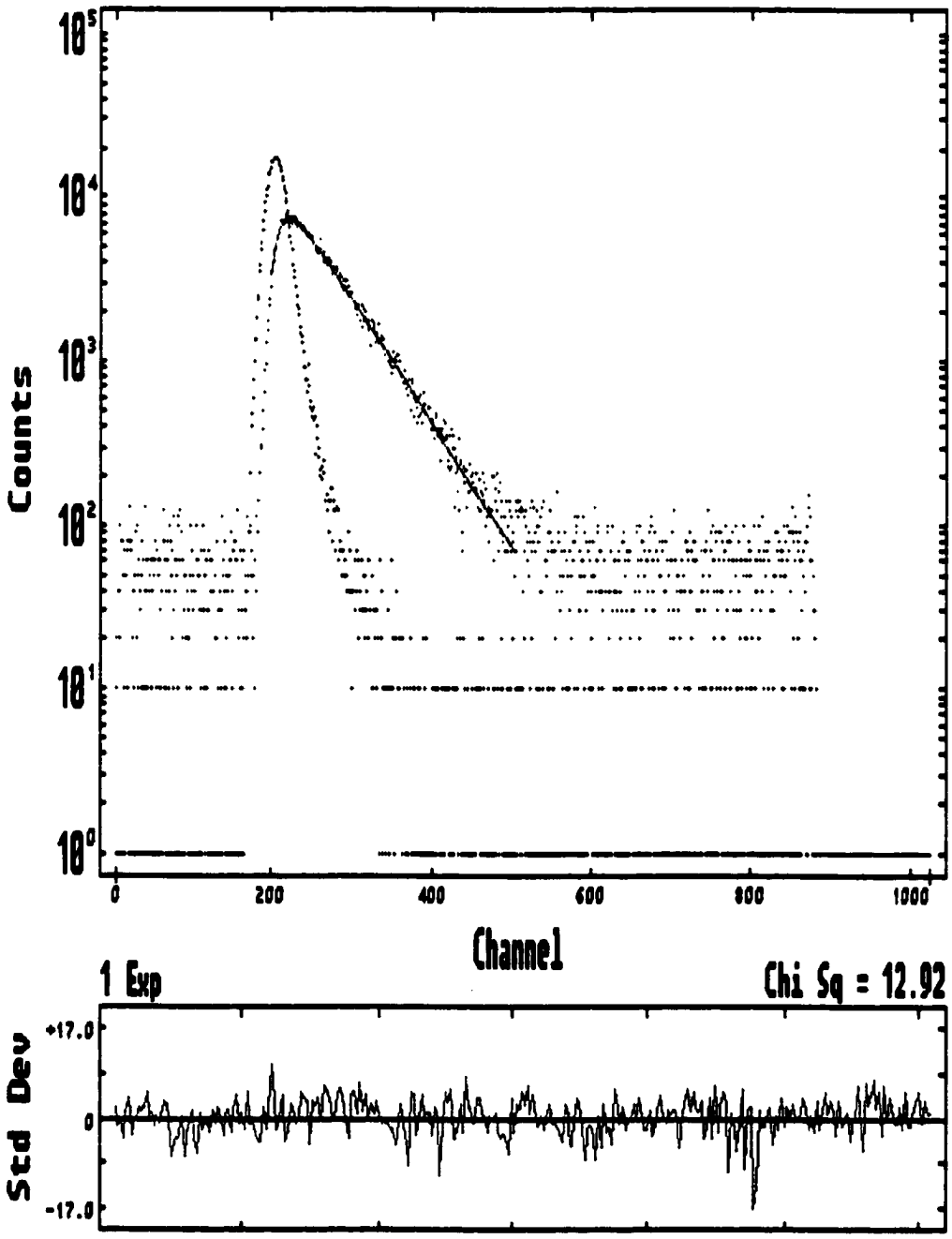

Figure 4.7 Fluorescence Decay profile of NN382 on PMMA under dry conditions.

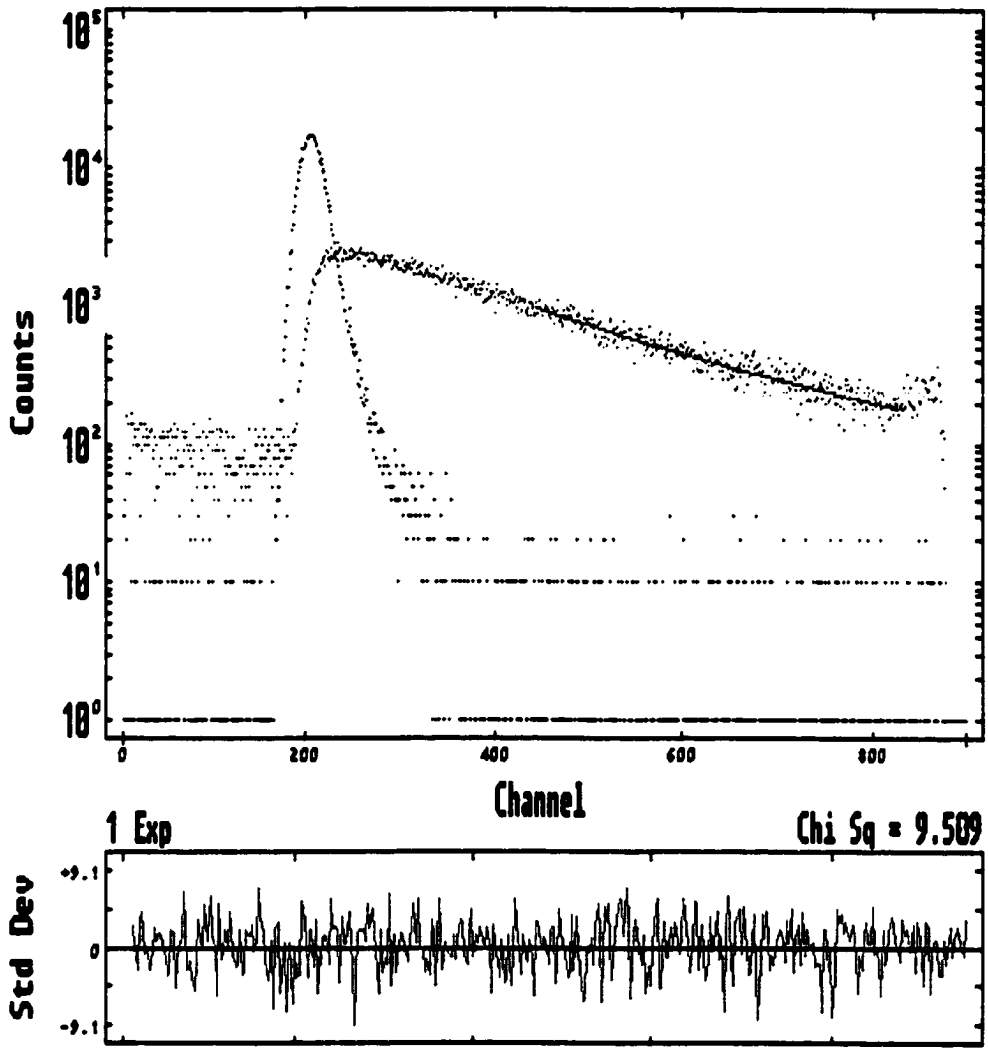

Figure 4.8 Fluorescence decay profile and a ciated residuals of ($AlNc(SO_3^-)_4$) on PMMA under "dry" conditions.

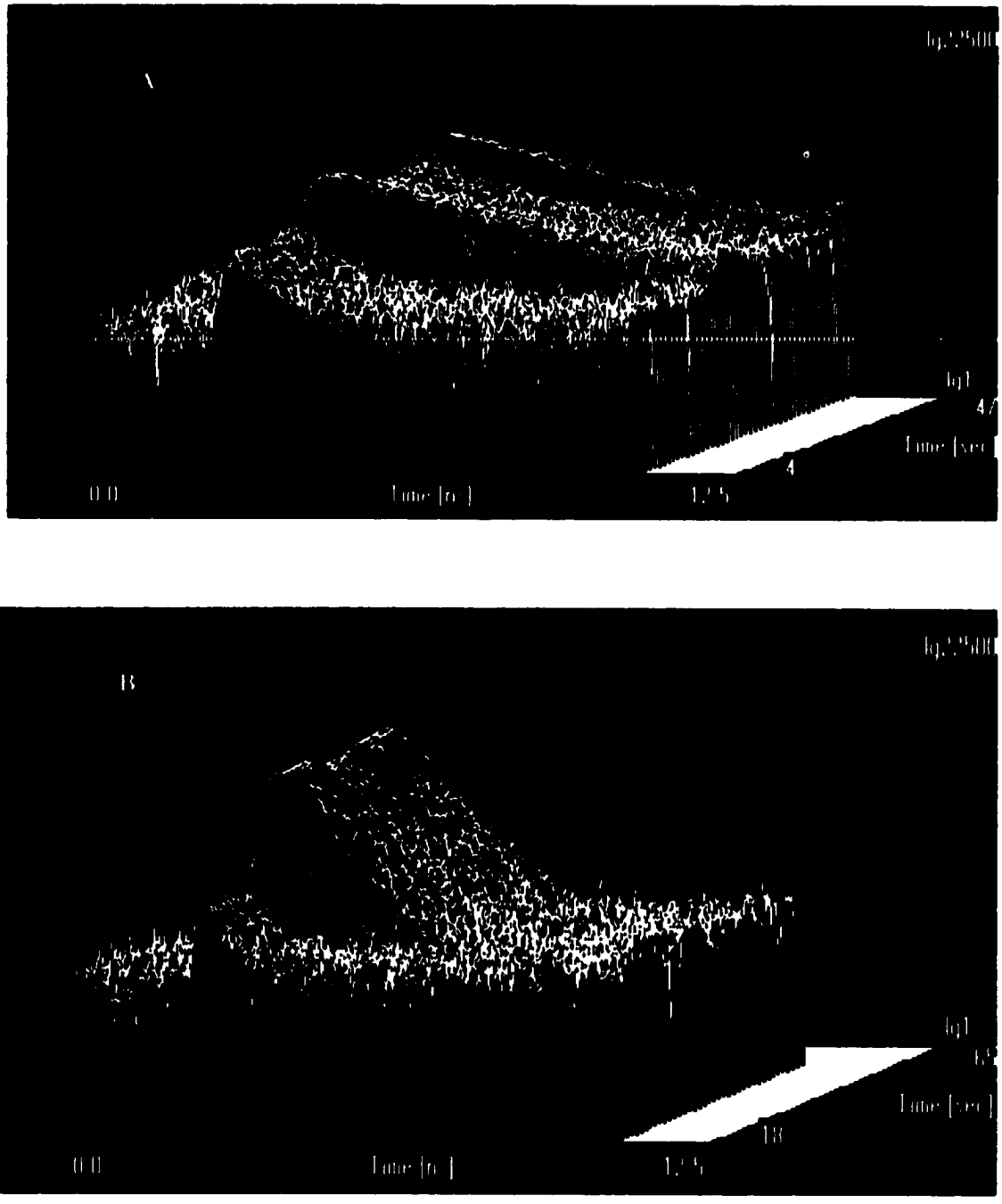

Figure 4.9. Fluorescence Decay Profiles from (A) $AlNc(SO_3^-)_4$ and (B) NN382 from inside a channel in a micro-CE device. Excitation was at 780 nm and the buffer consisted of 1X TAE and 50/50 methanol/water (v/v).

As Figure 4.9 shows, the fluorescence and/or scatter were taken of each NIR dye as well as buffer, which was used to flush out the channel between runs. The lifetime of NN382 was determined to be 684 ps (χ^2=9.5) and that of ($AlNc(SO_3^-)_4$) 2.228 ns (χ^2=12.9). Both of these values vary somewhat from the lifetimes obtained and discussed in the "dry" study. In both cases, this is probably due to the change in the solvent system.[55] Previous studies by our group have demonstrated that as the water content of the solvent system increases the fluorescence lifetimes of tricarbocyanine dyes decrease. The high χ^2 values are contributed to the scatter included in the measurement.

Past chromatographic studies have indicated that one of the primary advantages of time-resolved fluorescence detection is the enhanced signal-to-noise that may result if time gating is implemented.[32-35, 46, 47] Time gating is temporally delaying the collection window to discriminate against short-lived fluorescence and background signals. This temporal technique in conjunction with spectral filtering has proven to be highly successful in discriminating against these background interferences.[35] As a result of these past experiments, a time-gated study was performed in order to determine the effect of time gating on signal to noise ratios in this confocal scanning system.

In this study, 100 nM dye solution was placed on PMMA and allowed to dry overnight. A decay profile of the PMMA as well as fluorescence decay of the dye (NN382 and ($AlNc(SO_3^-)_4$) was obtained. Two analyses were performed for each dye. In the first analysis, signal-to-noise ratios were determined for varying time gates. As Figure 4.10 illustrates, the first time gate included all photons in the decay and with each consecutive time gate the start point of the time bin was shifted 50 channels to the

right (9.77 ps/channel). This forward shifting of the time gate eliminates early arriving photons that are primarily due to scatter from the substrate. However, it is necessary to determine the optimum value of the time gate since too much of an increase in the time delay results in a decrease of the fluorescence intensity and a resulting degradation of the SNR.[32, 34] For example, as the time delay was increased, the SNR increased for the long-lived fluorescence of ($AlNc(SO_3^-)_4$) more than that of the shorter-lived NN382. This occurs because more of the fluorescent photons fall into later time-bins in the case of longer-lived fluorescence as opposed to shorter-lived fluorescence. Consequently, it is easier to discriminate fluorescent photons from scattering photons in systems that contain a long-lived chromophore. For example, the ($AlNc(SO_3^-)_4$) results indicate that there is a two-fold increase in the SNR as a result of this technique; whereas, the SNR for NN382 shows approximately a 50% increase as a result of time gating. In fact, Ishabashi and coworkers observed the SNR increase by an order of magnitude when utilizing this technique with the fluorophores benzo(a)pyrene and benzo(ghi)perylene that possessed fluorescence lifetimes of 53 ns and 110 ns, respectively.[32]

The second analysis involved implementing a sliding gate as depicted in Figure 4.11. In this instance, the signal-to-noise ratio was calculated along different intervals in the histogram. The signal-to-noise ratio was highest in later time bins when the number of scattering photons was minimal and the number of fluorescent photons was not appreciably decreased. In addition, the signal-to-noise ratio was lower for the sliding gate method as opposed to the time delay method. This is due to the accumulation of fluorescent photons in later time bins contributing to the integrated signal, which is not accounted for in the sliding gate method.

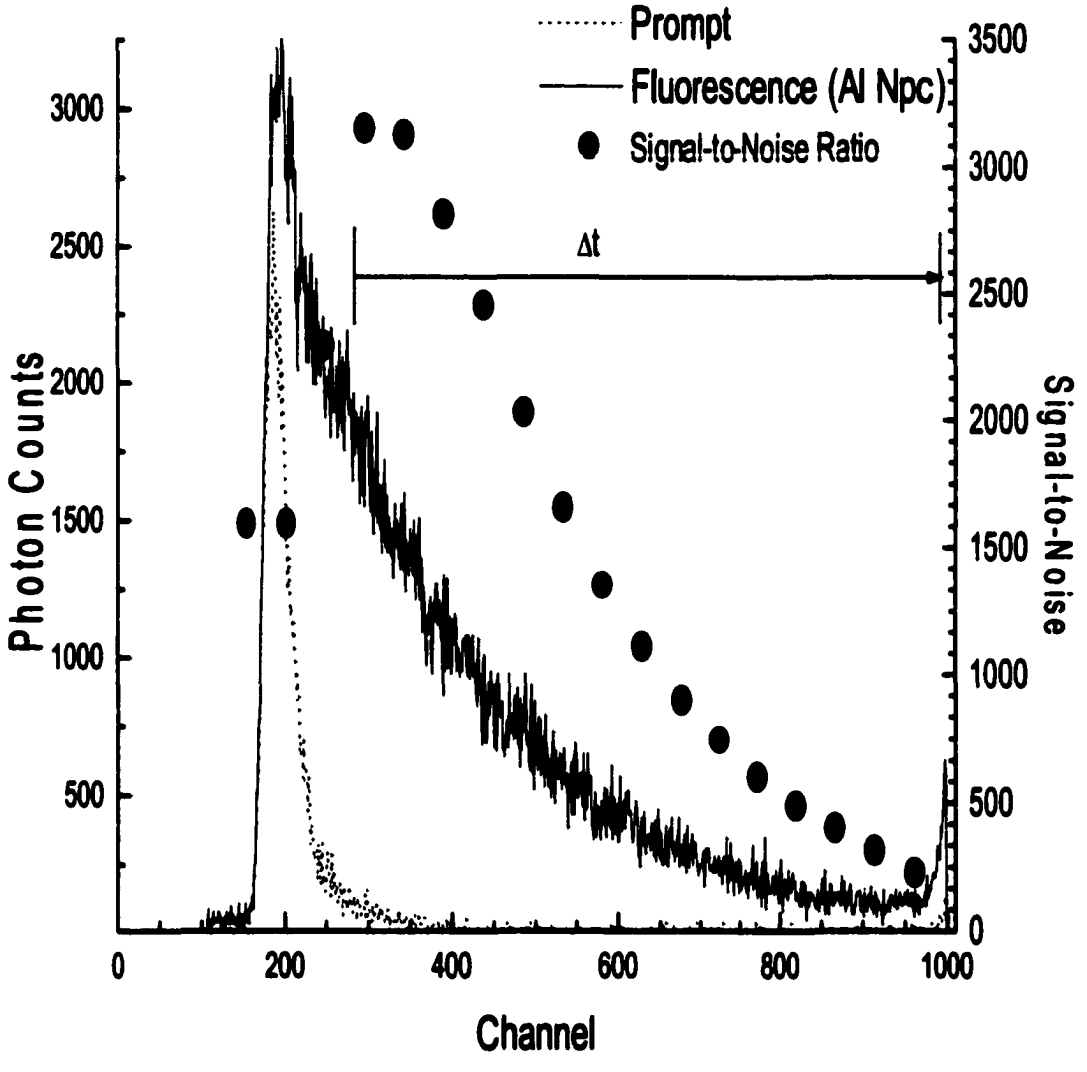

Figure 4.10. Signal-to-Noise Ratio as a function of time delay. The time delay was increased by fifty time channels (9.77 ps/channel) for each successive point in the graph.

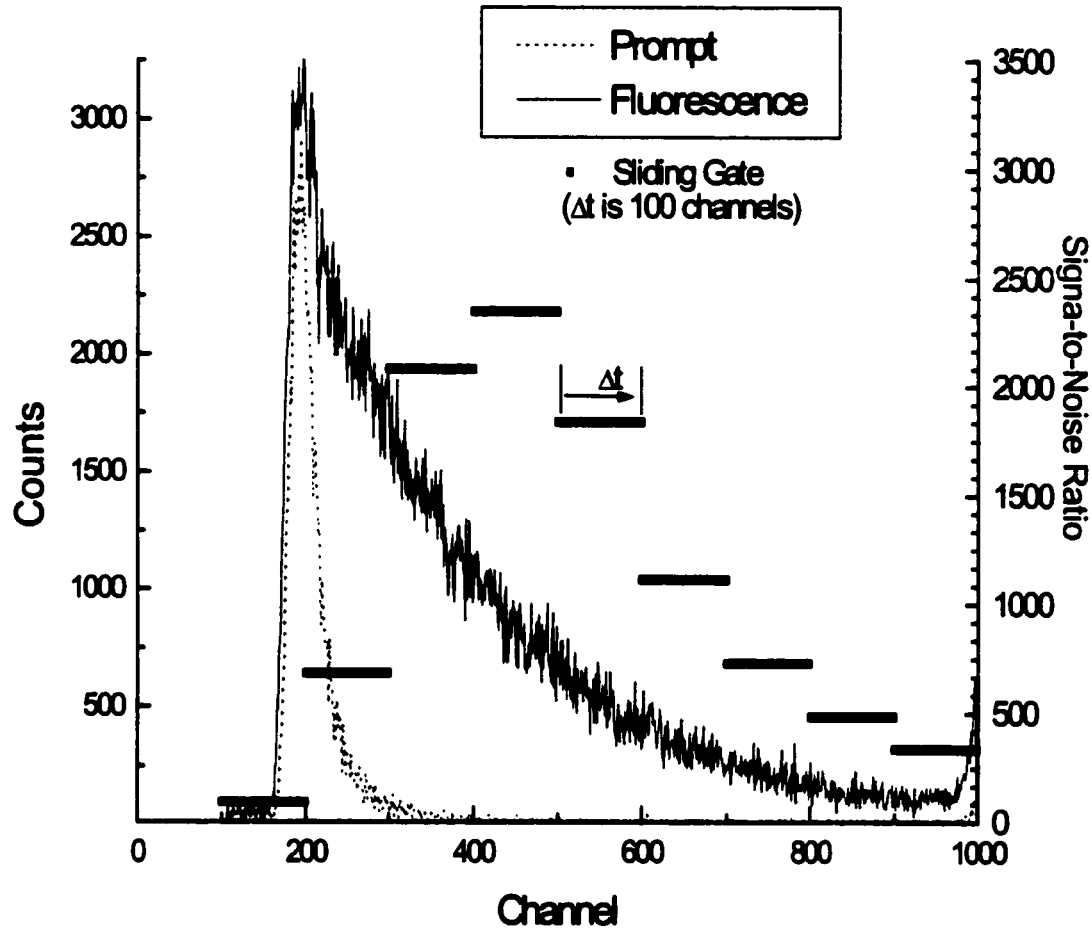

Figure 4.11 Signal-to-Noise Ratio as a function of implementing a 100 channel sliding gate (9.77 ps/channel). The fluorescence was collected with the NIR-TCSPC scanning device from a 100 nm solution of Al(Npc) on PMMA.

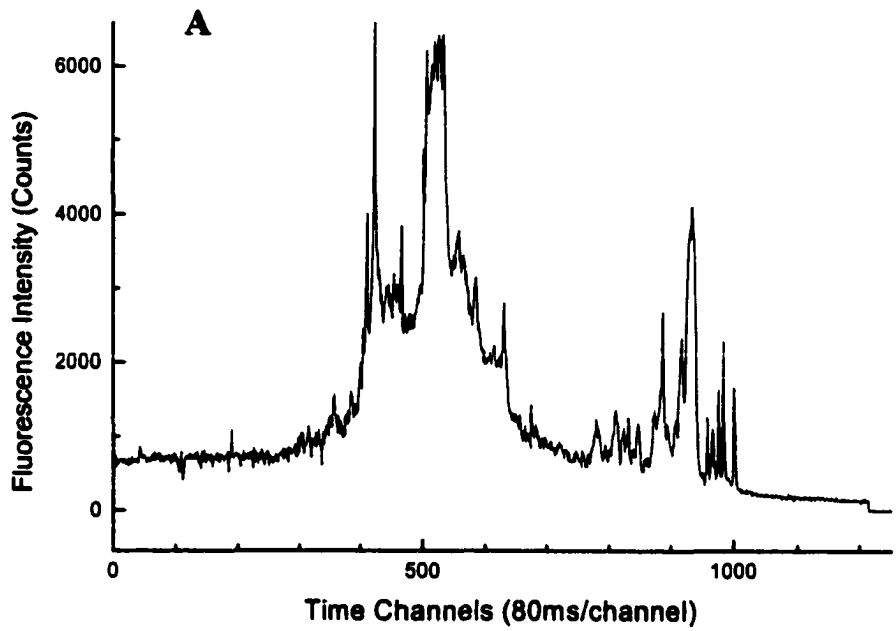

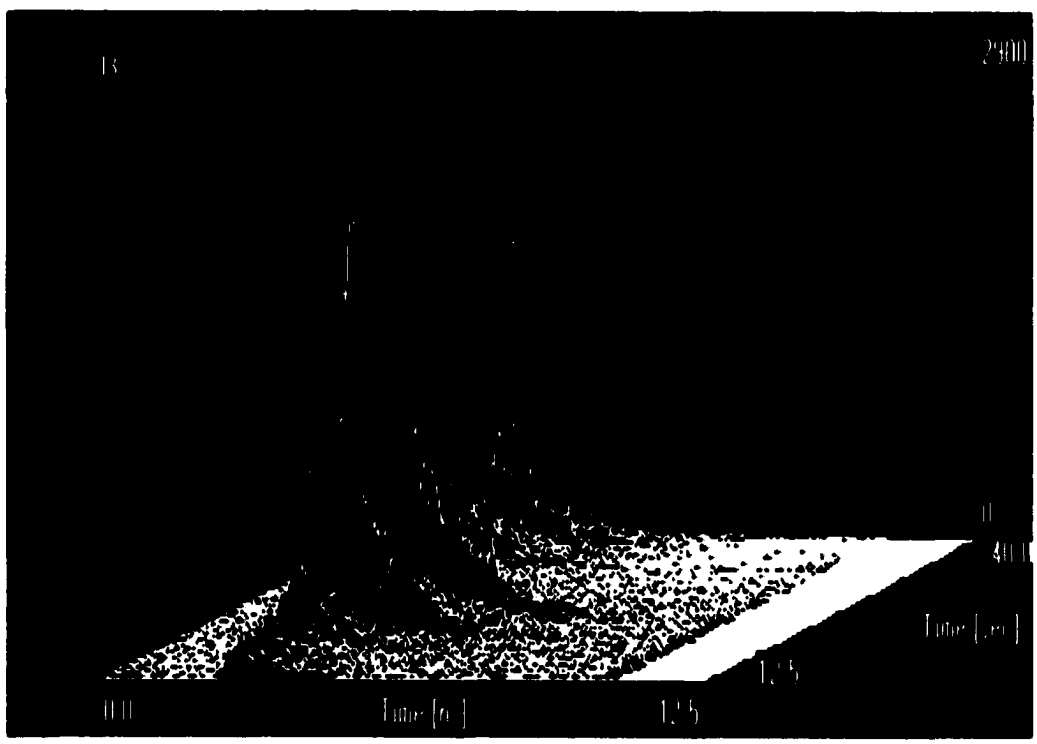

Figure 4.12. (A) Fluorescence Intensity profile of IRD800 labeled oligonucleotides on PMMA. (B) Fluorescence decay profiles of (A).

Traditional DNA microarray analyses utilize either the unique emission wavelength of the reporter dyes to discriminate between different reporter molecules or establish the location of hybridization. In this study, time-resolved fluorescence was analyzed from IRD800 labeled oligonucleotides hybridized to complementary oligonucleotides tethered to the PMMA surface. The oligonucleotide was hybridized to two areas on the PMMA surface. The surface was scanned at a rate of 70 μm/sec and the lasing power at the surface was 0.5 mW. Figure 4.12 depicts the fluorescence intensity and fluorescence lifetime as a function of position. It was determined that the fluorescence lifetime of these dye labeled oligonucleotides was 1.15 ns. The exponential fits yielded high χ^2 values because of the amount of scatter included in the calculation. However, the residuals were randomly distributed about zero and attempts to fit the decay to a double-exponential did not result in an improved goodness of fit.

4.4. Conclusions

We have built and characterized a device for NIR time-resolved fluorescence detection from solid surfaces. This device is lightweight, capable of scanning solid surfaces rapidly, and provides temporal fluorescence information. We have determined that the IRF of this device is 275 ps, which is adequate for determining subnanosecond fluorescence lifetimes. Additionally, we have determined that the LOD of this device is 13 molecules per laser spot. The device is capable of resolving fluorescence lifetimes in the subnanosecond domain and has been applied to the characterization of a hybridized oligonucleotide array. With the confocal scanning device described, it is possible to identify probes by the fluorescence lifetime of the reporter molecule.

Additionally, one detector, filter set, and excitation source is capable of interrogating multiple fluorescent dyes in one experiment.

4.5. References

(1) Covacci, A.; Kennedy, G. C.; Cormack, B.; Rappuoli, R.; Falkow, S. *Drug Development Research* **1997**, *41*, 180-192.

(2) Lemieux, B.; Aharoni, A.; Schena, M. *Molecular Breeding* **1998**, *4*, 277-289.

(3) Pollack, J. R.; Perou, C. M.; Alizadeh, A. A.; Eisen, M. B.; Pergamenschikov, A.; Williams, C. F.; Jeffrey, S. S.; Botstein, D.; Brown, P. O. *Nature Genetics* **1999**, *23*, 41-46.

(4) Plowman, T.; Durstchi, J.; Wang, H.; Christensen, D.; Herron, J.; Reichert, W. *Analytical Chemistry* **1999**, *71*, 4344-4352.

(5) Collins, F. S. *Nature Genetics* **1999**, *21*, 2-2.

(6) Lipshutz, R. J.; Fodor, S. P. A.; Gingeras, T. R.; Lockhart, D. J. *Nature Genetics* **1999**, *21*, 20-24.

(7) Hacia, J. G.; Fan, J. B.; Ryder, O.; Jin, L.; Edgemon, K.; Ghandour, G.; Mayer, R. A.; Sun, B.; Hsie, L.; Robbins, C. M.; Brody, L. C.; Wang, D.; Lander, E. S.; Lipshutz, R.; Fodor, S. P. A.; Collins, F. S. *Nature Genetics* **1999**, *22*, 164-167.

(8) Cargill, M.; Altshuler, D.; Ireland, J.; Sklar, P.; Ardlie, K.; Patil, N.; Lane, C. R.; Lim, E. P.; Kalyanaraman, N.; Nemesh, J.; Ziaugra, L.; Friedland, L.; Rolfe, A.; Warrington, J.; Lipshutz, R.; Daley, G. Q.; Lander, E. S. *Nature Genetics* **1999**, *22*, 231-238.

(9) Guo, Z.; Guilfoyle, R. A.; Thiel, A. J.; Wang, R.; Smith, L. M. *Nucleic Acids Research* **1994**, *22*, 5456-5465.

(10) Herne, T. M.; Tarlov, M. J. *Journal of the American Chemical Society* **1997**, *119*, 3401-3402.

(11) Thiel, A. J.; Frutos, A. G.; Jordan, C. E.; Corn, R. M.; Smith, L. M. *Analytical Chemistry* **1997**, *69*, 4948-4954.

(12) Jordan, C. E.; Frutos, A. G.; Thiel, A. J.; Corn, R. M. *Analytical Chemistry* **1997**, *69*, 4939-4937.

(13) Okahata, Y.; Matsunobu, Y.; Ijiro, K.; Mukae, M.; Murakami, A.; Makino, K. *Journal of the American Chemical Society* **1992**, *114*, 8299-8300.

(14) Gallardo, B. S.; Gupta, V. K.; Eagerton, F. D.; Jong, L. I.; Craig, V. S.; Shah, R. R.; Abbott., N. L. *Science* **1999,** *283*, 57.

(15) S.-Y. Lin, V.; Motesharei, K.; Dancil, K.-P. S.; Sailor, M. J.; Ghadari, M. R. *Science* **1997,** *278*, 840-843.

(16) Cobb, W. T.; McGown, L. B. *Anal. Chem.* **1990,** *62*, 186.

(17) Cobb, W. T.; Mcgown, L. B. *Applied Spectroscopy* **1989,** *43*, 1363-1367.

(18) Bachteler, G.; Drexhage, K. H.; Ardenjacob, J.; Han, K. T.; Kollner, M.; Muller, R.; Sauer, M.; Seeger, S.; Wolfrum, J. *Journal of Luminscence* **1994,** *62*, 101-108.

(19) Soper, S. A.; Legendre, B. L.; Williams, D. C. *Analytical Chemistry* **1995,** *67*, 4358-4365.

(20) Legendre, B. L.; Williams, D. C.; Soper, S. A.; Erdmann, R.; Ortmann, U.; Enderlein, J. *Review of Scientific Instruments* **1996,** *67*, 3984-3989.

(21) Williams, D. C.; Soper, S. A. *Analytical Chemistry* **1995,** *67*, 3427-3432.

(22) Kollner, M.; Fischer, A.; Ardenjacob, J.; Drexhage, K. H.; Muller, R.; Seeger, S.; Wolfrum, J. *Chemical Physics Letters* **1996,** *250*, 355-360.

(23) Li, L. C.; Mcgown, L. B. *Analytical Chemistry* **1996,** *68*, 2737-2743.

(24) Li, L. C.; He, H.; Nunnally, B. K.; Mcgown, L. B. *Journal of Chromatography B* **1997,** *695*, 85-92.

(25) Lieberwirth, U.; Arden-Jacob, J.; Drexhage, K. H.; Herten, D. P.; Muller, R.; Neumann, M.; Schulz, A.; Siebert, S.; Sagner, G.; Klingel, S.; Sauer, M.; Wolfrum, J. *Analytical Chemistry* **1998,** *70*, 4771-4779.

(26) Muller, R.; Zander, C.; Sauer, M.; Deimel, M.; Ko, D. S.; Siebert, S.; Ardenjacob, J.; Deltau, G.; Marx, N. J.; Drexhage, K. H.; Wolfrum, J. *Chemical Physics Letters* **1996,** *262*, 716-722.

(27) Muller, R.; Herten, D. P.; Lieberwirth, U.; Neumann, M.; Sauer, M.; Schulz, A.; Siebert, S.; Drexhage, K. H.; Wolfrum, J. *Chemical Physics Letters* **1997,** *279*, 282-288.

(28) Flanagan, J. H.; Owens, C. V.; Romero, S. E.; Waddell, E.; Kahn, S. H.; Hammer, R. P.; Soper, S. A. *Analytical Chemistry* **1998,** *70*, 2676-2684.

(29) Soper, S. A.; Mattingly, Q., L.; Vegunta, P. *Analytical Chemistry* **1993,** *65*, 740-747.

(30) Imasaka, T.; Ishibashi, K.; Ishibashi, N. *Analytica Chimica Acta* **1982,** *142*, 1-12.

(31) Richardson, J. H.; Larson, K. M.; Haugen, G. R.; Johnson, D. C.; Clarkson, J. E. *Analytica Chimica Acta* **1979,** *116*, 407-411.

(32) Otsuki, A.; Furuta, N. *Analytical Chemistry* **1983,** *555*, 2407-2413.

(33) Miller, K. J.; Lytle, F. E. *Journal of Chromatography* **1993,** *648*, 245-250.

(34) Flanagan, J. H.; Legendre, B. L.; Hammer, R. P.; Soper, S. A. *Analytical Chemistry* **1995,** *67*, 341-347.

(35) Soper, S. A.; Legendre, B. L. *Applied Spectroscopy* **1998,** *52*, 1-6.

(36) Tellinghulsen, J.; Goodwin, P. M.; Ambrose, W. P.; Martin, J. C.; Keller, R. A. *Analytical Chemistry* **1994,** *66*, 64-72.

(37) Soper, S. A.; Legendre, B. L. *Applied Spectroscopy* **1994,** *48*, 400-405.

(38) Li, L.-Q.; Davis, L. *Review of Scientific Instruments* **1993,** *64*, 1524-1529.

(39) Zhang, Y. L.; Soper, S. A.; Middendorf, L. R.; Wurm, J. A.; Erdmann, R.; Wahl, M. *Applied Spectroscopy* **1999,** *53*, 497-504.

(40) Cova, S.; Longoni, A.; Ripamonti, G. *IEEE Transactions on Nuclear Science* **1982,** *NS-29*, 599-601.

(41) Karandikar, B.; Puschett, J.; Matyjaszewski *Polymer Preprints* **1989,** *30*, 250-251.

(42) Duggan, D. J.; Bittner, M.; Chen, Y. D.; Meltzer, P.; Trent, J. M. *Nature Genetics* **1999,** *21*, 10-14.

(43) Soper, S. A.; Legendre, B. L.; Williams, D. C. *Experimental Technique of Physics* **1995,** *41*, 167-182.

(44) Higashijima, T.; Fuchigami, T.; Imasaka, T.; Ishibashi, N. *Analytical Chemistry* **1992,** *64*, 711-714.

(45) Sauda, K.; Imasaka, T.; Ishibashi, N. *Analytica Chimica Acta* **1986,** *187*, 353-356.

(46) Miller, K. J.; Leesong, I. K.; Bao, J. M.; Regnier, F. E.; Lytle, F. E. *Analytical Chemistry* **1993,** *65*, 3267-3270.

(47) Owens, C. V.; Soper, S. A. *Abstracts of Papers of the American Chemical Society* **1998,** *216*, 006-PRES.

(48) Flanagan, J. H.; Khan, S. H.; Menchen, S.; Soper, S. A.; Hammer, R. P. *Bioconjugate Chemistry* **1997,** *8*, 751-756.

(49) Casay, G. A.; Narayanan, N.; Evans III, L.; Czuppon, T.; Patonay, G. *Talanta* **1996,** *43*, 1997-2005.

(50) Lakowicz, J. R. *Topics in Fluorescence Spectroscopy*; Plenum Press: New York, 1992.

(51) McCubbin, I.; Phillips, D. *Journal of Photochemistry* **1986,** *34*, 187-195.

(52) Flanagan, J. H. Doctoral Dissertation, Louisiana State University and Agricultural and Mechanical College, Baton Rouge, LA, 1997.

(53) Soper, S. A.; Mattingly, Q. L. *Journal of the American Chemical Society* **1994,** *116*, 3744-3752.

Chapter 5

Conclusions and Future Work

5.1 Chapter 1 Summary

This dissertation focused on efforts to design, construct, and apply novel near-infrared time correlated single photon counting devices for the detection of analytes in multiplexed systems. These systems are designed to employ capillary electrophoresis and microarray technology towards the identification of dye-labeled DNA fragments or oligonucleotides. It was also demonstrated that fluorescence lifetime analysis could be performed utilizing simple algorithms, which were accurate in the limit of low photocounts.

Chapter 1 outlined the motivation and laid the foundation for discriminating analytical probes by their fluorescent lifetimes as opposed to the spectral wavelength of their emission spectra. The specific problems of sequencing DNA by capillary gel electrophoresis and identifying specific allelic sequences with the use of DNA microarrays were presented.

5.2 Chapter 2 Summary

A detailed explanation of TCSPC was presented in Chapter 2. Fundamental concepts such as the Jablonski Diagram, radiative, and non-radiative pathways were discussed. The phase resolved and the time resolved methods of fluorescence lifetime measurement were discussed. The required instrumentation such as excitation sources, detectors, and timing electronics was presented. Finally, various methods of lifetime analysis were presented. The method of non-linear least squares deconvolves the fluorescence from the instrument response function to determine the correct lifetime of

a fluorescent molecule (including multiexponential decays) whereas; rapid methods such as the maximum likelihood estimator and rapid lifetime determination assume monoexponential decay.[1, 2]

5.3 Chapter 3 Summary and Future Work

In Chapter 3, a multichannel fiber optic-based time correlated single photon counting devices was described. This device used single mode fiber optics to transmit light to and from the experimental stage. The pulse width of light being emitted from a passively mode locked Ti:Sapphire laser was determined to be 148.2 fs and broadened to 198 fs after traveling across ten meters of fiber. We determined that the excitation pulses also undergo spectral spread of 0.2 nm and remained nearly transform limited. It was demonstrated that multichannel TCSPC with subnanosecond resolution could be performed with this system. The average instrument response function of each channel was determined to be 181 ps and the fluorescence lifetime of a representative near-infrared dye, aluminum tetrasulfonated naphthalocyanine was determined to be 3.08 ns.

Presently, the front end of the optical system and the counting electronics described in Chapter 3 are being utilized to characterize NIR dyes and dye primers for DNA sequencing experiments. The system uses the Ti:Sapphire as the excitation source, providing light via the single mode optical fiber system discussed previously. However, the fluorescence emission is collected by a high numerical aperture microscope objective, passed through the appropriate filter set and focused onto a SPAD. The SUN Workstation processes the information to yield a fluorescence intensity electropherogram as well as fluorescence lifetime information for user-defined time windows. The primary emphasis has been to characterize the interaction of the

dyes with replaceable linear polyacrylamide gels and to optimize the composition in order to extend the sequencing reaction to 1 kbp.

Additionally, it would be of interest to perform TCSPC utilizing a single mode fiber for the excitation source and a multimode fiber for the collection of fluorescence. Because the core of a multimode fiber ranges from 50 μm to 250 μm, the collection efficiency would be enhanced and therefore ease the alignment requirements for fluorescence detection. This approach would be especially amenable to fluorescence lifetime analysis of long-lived chromophores such as the naphthalocyanines. Previous researchers have employed the use of multimode fibers for both excitation and emission in phase-resolved experiments towards the identification of analytes by their long-lived fluorescence lifetimes (τ_f>2 ns).[3-7] Of course, one would have to take into consideration the amount of temporal broadening that occurs as the fluorescence transverses the multimode fiber.

An additional extension of this fiber optic work would be the functionalization of the fibers to serve as analytical probes for the detection of metal species in environmental samples[8] or the identification of specific oligonucleotides in biological matrices.[6, 9] This may be accomplished by utilizing individual fibers or arranging the fibers into an array. The primary advantage of this technique would be multiplexed detection and the ability to easily change the excitation wavelength by coupling the fibers to a different excitation source.

5.4 Chapter 4 Summary and Future Work

Chapter 4 presented details on the design, construction, and characterization of a near-infrared time-resolved fluorescence confocal scanning device. This device

consisted of a pulsed diode laser, SPAD, high numerical aperture microscope objective, and the associated filter stack. The instrument response function of this device was determined to be 275 ps, with the spot size of the interrogation beam being 5 μm x 3 μm. It was determined that PMMA was the best substrate for performing time-resolved fluorescence measurements in the NIR because of the reduced amount of scatter coupled into the system. The NIR scanning device was used to interrogate a DNA microarray in which oligonucleotide fragments were hybridized to PMMA. The reporter molecule was the NIR dye IRD800. The molecule was excited with a 780 nm pulsed diode laser and the fluorescence lifetime was 1.15 ns.

The device was also used to obtain fluorescence lifetime information from a micro-CE device. In addition to interrogating one channel, the device is capable if scanning a capillary array electrophoresis (CAE) system on a chip. In conjunction with a parallel effort to completely automate the imaging of a surface, the NIR scanning device will be capable of scanning multiple channels in a repetitive fashion such that a fluorescence intensity and/or lifetime electropherogram is constructed for each channel. Such a system allows for the detection of analytes in microfabricated high-density CAE structures, which is essential for the parallel analysis of multiple samples.[10, 11] The software that has been developed works in tandem with an integrated scanner that utilizes an avalanche photodiode and a pulsed diode laser, which is mounted on an automated stage that moves back-and-forth in two directions. The device has been applied to a slab gel electrophoresis experiment and a fluorescence lifetime as well as fluorescence intensity electropherogram constructed. As Figure 5.1 shows, the data is displayed as a color-coded contour map, with the color representing the fluorescence

intensity or the fluorescence lifetime. The integration of this software package, a completely controlled *x-y* scanning stage, and the NIR scanning device discussed in Chapter 4 will allow researchers to interrogate any surface and obtain fluorescence intensity and lifetime information on-the-fly.

This approach, when applied to a micro-CE device with multiple channels, will have a higher throughput than a single channel device. In addition, the NIR scanning device will be enhanced by the addition of another pulsed diode laser, which lases at a second wavelength, resulting in dual color capabilities. As Figure 5.2 illustrates, this would be accomplished by utilizing a multiband dichroic filter to pass the excitation beams to the sample stage and an additional dichroic to channel fluorescence to the appropriate detector. As the schematic illustrates, two fiber-coupled lasers would be aligned along the same optical path with the use of a single mode fiber optic coupler. The addition of a second excitation line will double the amount of reporter molecules that may be probed in one pass of the device.

An additional area of research that may be of interest is the study of the photophysical characteristics of the NIR dyes as they photobleach. Presently, this is one least understood areas of confocal microscopy.[12] A detailed study of the photophysical characteristics of these dyes would be beneficial towards understanding the optimal conditions to interrogate DNA microarrays as well as micro-CE experiments. For example, the rate of photodestruction dictates the amount of time a fluorophore may be interrogated by a laser beam before it photobleaches. If this parameter is not known, then the intensity of the laser beam may photobleach the fluorophore before any useful information is obtained. Conversely, if the intensity of

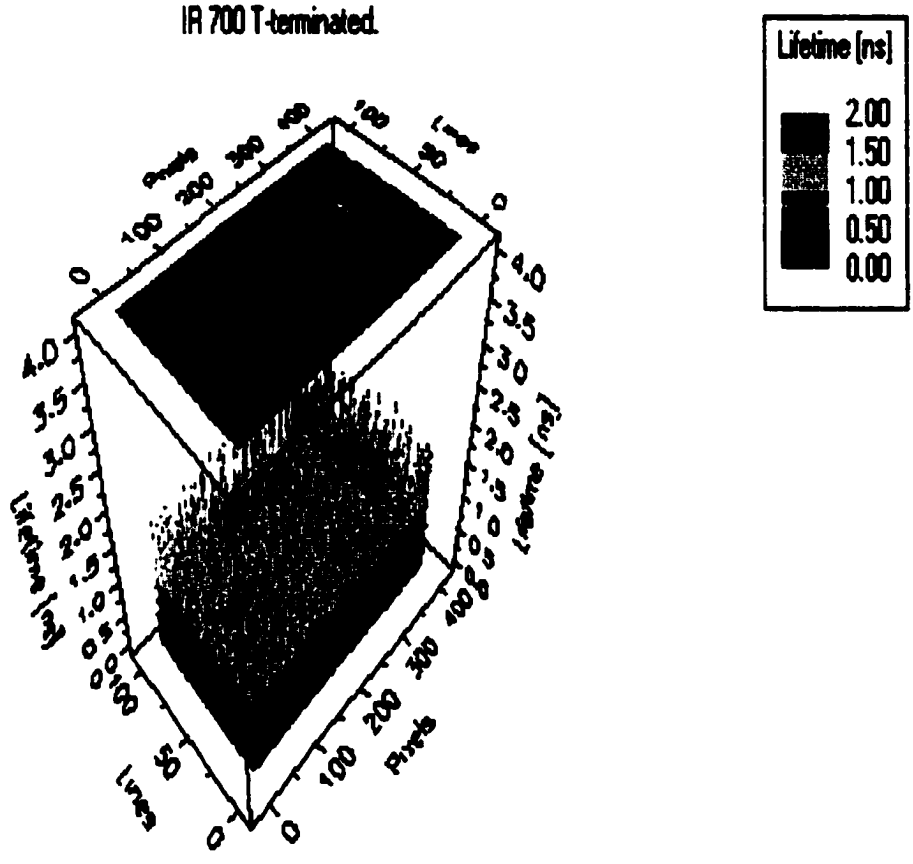

Figure 5.1 Fluorescence lifetime contour map. The fluorescence lifetimes of IR700 primers were obtained with the use of a pulsed diode laser and an avalanche photodiode during a slab gel electrophoresis separation. (Courtesy of Wieslaw Stryjewski)

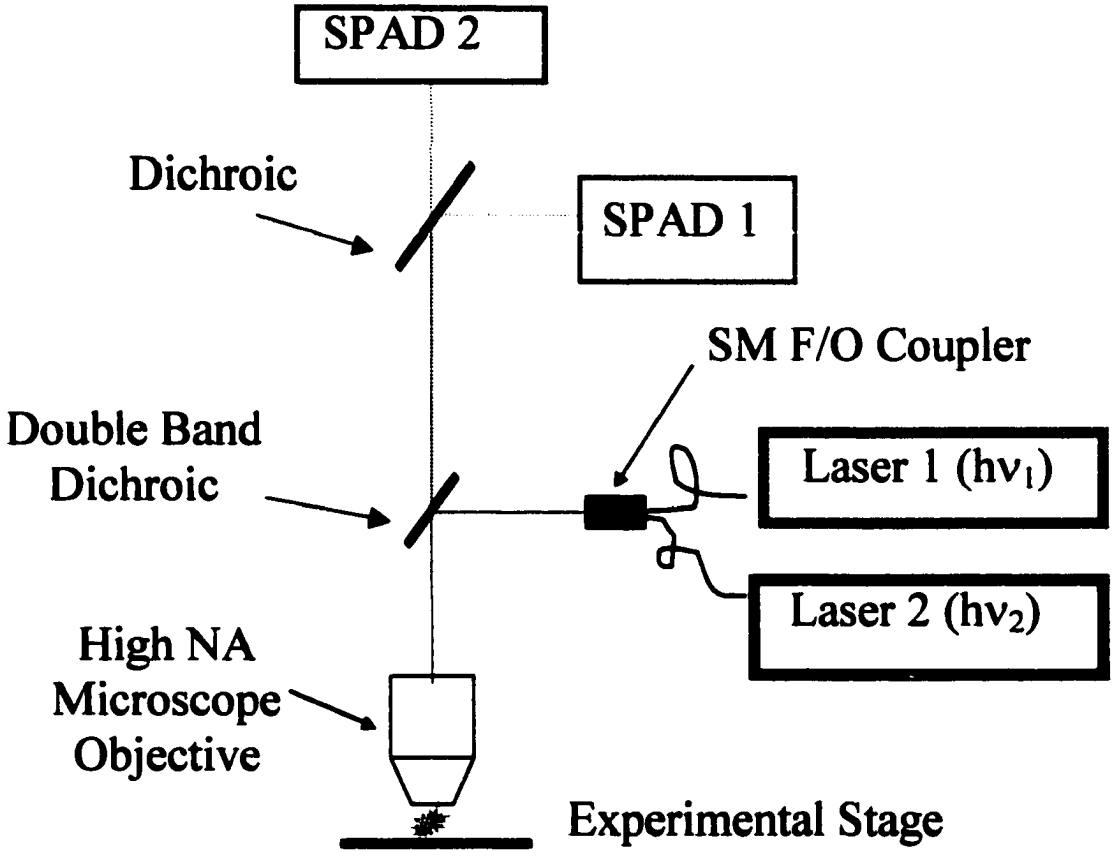

Figure 5.2. Proposed Schematic for a two laser, fiber coupled scanning system. FF, Fluorescence Filter; SM F/O Coupler, Single Mode Fiber Optic Coupler; and SPAD, Single Photon Avalanche Diode.

the beam is too low, the optimal signal-to-noise ratio may not be realized. Typically, studies of the photophysical characteristics of fluorophores in confocal systems take into account the intensity profile as a function of interrogation time, photon density of the excitation source, and intrinsic parameters such as quantum yields and absorption cross-sections. Additional information about the lifetime of the excited state could provide further information about the dynamics of the photobleaching.

5.5 References

(1) Tellinghulsen, J.; Goodwin, P. M.; Ambrose, W. P.; Martin, J. C.; Keller, R. A. *Analytical Chemistry* 1994, *66*, 64-72.

(2) Soper, S. A.; Mattingly, Q. L. *Journal of the American Chemical Society* 1994, *116*, 3744-3752.

(3) Thompson, R. B.; Lakowicz, J. R. *Analytical Chemistry* 1993, *65*, 853-856.

(4) Bright, F. V.; Monnig, C. A.; Hieftje, G. M. *Analytical Chemistry* 1986, *58*, 3139-3144.

(5) Carrol, M. K.; Bright, F. V.; Hieftje, G. M. *Analytical Chemistry* 1989, *61*, 1769-1772.

(6) Petrea, R. D.; Sepaniak, M. J.; Vo-Dinh, T. *Talanta* 1988, *35*, 139-144.

(7) Wyatt, W. A.; Poirer, G. E.; Bright, F. V.; Hieftje, G. M. *Analytical Chemistry* 1986, *59*, 572-576.

(8) Casay, G. A.; Narayanan, N.; Evans III, L.; Czuppon, T.; Patonay, G. *Talanta* 1996, *43*, 1997-2005.

(9) Pilevar, S.; Davis, C. C.; Portugal, F. *Analytical Chemistry* 1998, *70*, 2031-2037.

(10) Mathies, R.; Stryer, L. In *Applications of Fluorescence in the Biomedical Sciences: Proceedings of a meeting held in Pittsburgh, Pennsylvania*; Taylor, D. L., Ed.; Alan R. Liss, Inc.: New York, 1986, pp 129-140.

(11) Zhang, Y. L.; Soper, S. A.; Middendorf, L. R.; Wurm, J. A.; Erdmann, R.; Wahl, M. *Applied Spectroscopy* 1999, *53*, 497-504.

(12) Waggoner, A.; Tsien, R. Y. In *Handbook of Biological Confocal Microscopy*; Pawley, J. P., Ed.; Plenum Press: New York, NY, 1990.

Vita

Emanuel Austin Waddell, Jr. was born in Durham, North Carolina on September 2, 1968. He is the only son of Emanuel Austin Waddell and Evelyn Bedjane and the brother of Athena Michelle Waddell. He is the husband of Karol Coffey Waddell and the father of three sons: Austin, Khalil, and Kendyl Waddell. Emanuel considers himself a product of the Durham City School System and graduated from the North Carolina School of Science and Mathematics in June 1986.

In August 1986, Emanuel enrolled at Morehouse College as a member of the Honors Program under a Full Academic Scholarship. During his academic career at Morehouse, Emanuel co-directed the Frederick Douglass Tutorial Institute for students in the Atlanta area; held offices in the National Society of Black Engineers; and obtained a varsity letter in Track and Field. In May of 1991, Emanuel graduated with an Interdisciplinary Bachelors of Science Degree in Chemistry and Physics.

After graduate study at Clark Atlanta University, Emanuel enrolled at the University of Rochester in Rochester, New York in August of 1993. In May 1995, Emanuel received a Masters Degree in Physical Chemistry. In August of 1996, he enrolled in the Analytical Chemistry doctoral program at Louisiana State University in Baton Rouge, Louisiana. While at LSU, Emanuel held elected positions in the Black Graduate and Professional Student Association, LSU Student Government Association, and the LSU Department of Chemistry Graduate Student Council. Upon completion of his graduation requirements, Emanuel will participate in the National Research Council's Postdoctoral Research Associateship Program at the National Institute of Standards and Technology located in Gaithersburg, Maryland.

DOCTORAL EXAMINATION AND DISSERTATION REPORT

Candidate: Emanuel Austin Waddell, Jr.

Major Field: Chemistry

Title of Dissertation: The Design and Construction of Novel Near-Infrared Time-Correlated Single Photon Counting Devices for the Identification of Analytes in Multiplexed Applications

Approved:

Major Professor and Chairman

Dean of the Graduate School

EXAMINING COMMITTEE:

Date of Examination:

January 24, 2000